SIMULATION OF AEROSOL-CLOUD INTERACTIONS IN THE WRF MODEL AT THE SOUTHERN GREAT PLAINS SITE

A Thesis

by

JONATHAN MICHAEL VOGEL

Submitted to the Office of Graduate Studies of
Texas A&M University
in partial fulfillment of the requirements for the degree of

MASTER OF SCIENCE

Approved by:

Chair of Committee,	Renyi Zhang
Committee Members,	Ramalingam Saravanan
	Courtney Schumacher
	Qi Ying
Head of Department,	Kenneth Bowman

December 2012

Major Subject: Atmospheric Sciences

ABSTRACT

The aerosol direct and indirect effects were investigated for three specific cases during the March 2000 Cloud IOP at the SGP site by using a modified WRF model. The WRF model was previously altered to include a two-moment bulk microphysical scheme for the aerosol indirect effect and a modified Goddard shortwave radiation scheme for the aerosol direct effect. The three cases studied include a developing low pressure system, a low precipitation event of mainly cirrus clouds, and a cold frontal passage. Three different aerosol profiles were used with surface concentrations ranging from 210 cm^{-3} to 12,000 cm^{-3}. In addition, each case and each aerosol profile was run both with and without the aerosol direct effect.

Regardless of the case, increasing the aerosol concentration generally increased cloud water and droplet values while decreasing rain water and droplet values. Increased aerosols also decreased the surface shortwave radiative flux for every case; which was greatest when the aerosol direct effect was included. For convective periods during polluted model runs, the aerosol direct effect lowered the surface temperature and reduced convection leading to a lower cloud fraction. During most convective periods, the changes to cloud, rain, and ice water mixing ratios and number concentrations produced a nonlinear precipitation trend. A balance between these values was achieved for moderate aerosol profiles, which produced the highest convective precipitation rates. In non-convective cases, due to the presence of ice particles, aerosol concentration and precipitation amounts were positively correlated. The aerosol threshold between

precipitation enhancement and suppression should be further studied for specific cloud types as well as for specific synoptic weather patterns to determine its precise values.

DEDICATION

What is a dedication other than some silly words on a page that probably no one cares about? Webster's defines dedication as "a devoting or setting aside for a particular purpose" or "self-sacrificing devotion." The joke remains that as graduate students we sacrifice several years of our life spending long hours on campus working on our research projects. The reasons we put ourselves through this varies, but I'm willing to bet that most of us are here for at least one of a few reasons: (1) to follow an interest we have in atmospheric science, (2) either to further our education or simply to get a graduate degree, or (3) because we either aren't ready to set foot into the real world or the real world isn't ready for us yet (I mean look at the job industry right now). So when trying to answer why I spent the last two years working on this project, the selfish answer would be I did it for myself in the hope that I will be able to better my future. But really, when we try to answer this question, we should look deep down inside and realize the real reason. We probably will never become famous for what we do. They probably will never name a theory, process, or rule after us. The real reason we do this is for the betterment and advancement of science. As scientists, we will devote our entire lives to science.

ACKNOWLEDGEMENTS

I would like to thank my committee for helping me tie this work together down the stretch and especially my advisor, Dr. Renyi Zhang, for giving me the opportunity to work on this project for my Master's Thesis. I would also like to thank Yuan Wang for his assistance early on with getting me starting using the WRF model and helping me fix and debug problems with the model as they arose. At BNL, I would like to thank Dr. Yangang Liu and Dr. Wuyin Lin for their help pertaining to my questions regarding the FASTER project and Tami Toto for compiling the observational datasets.

I would like to thank my family, my parents and my brother, for their continuous support throughout my life thus far. Especially lately, for understanding my stressful and busy schedule while finishing up this project. Finally, I would like to especially thank my girlfriend, Nikki Kinney, for being patient and understanding and keeping me levelheaded and grounded during this stressful time.

This work is funded by the Direct, Office of Science, Office of Basic Energy Sciences, of the U.S. Department of Energy. This work is part of the Brookhaven National Laboratory's Fast-Physics System Testbed and Research Project.

NOMENCLATURE

3DVAR	3-dimensional Variational
ARM	Atmospheric Radiation Measurement
ARW	Advanced Research WRF
BC	Black Carbon
CCN	Cloud Condensation Nuclei
DIE	Direct and Indirect Effect
GCE	Goddard Cloud Ensemble
GCM	General Circulation Model
IN	Ice Nuclei
IEO	Indirect Effect Only
IOP	Intensive Observational Period
IPCC	Intergovernmental Panel on Climate Change
LWC	Liquid Water Content
LWP	Liquid Water Path
MCS	Mesoscale Convective System
METAR	Meteorological Terminal Air Report
MM5	Mesoscale Model version 5.3.6
Nc	Number Concentration
NARR	North American Region Reanalysis
NWP	Numerical Weather Prediction

OLR	Outgoing Longwave Radiation
Qc	Cloud Water Mixing Ratio
Qg	Graupel Water Mixing Ratio
Qi	Ice Water Mixing Ratio
Qr	Rain Water Mixing Ratio
Qs	Snow Water Mixing Ratio
Qtot	Total Water Mixing Ratio: Qc + Qr + Qi + Qs + Qg
SGP	Southern Great Plains
SSR	Surface Shortwave Radiation
TOA	Top-of-Atmosphere
WRF	Weather Research and Forecasting

TABLE OF CONTENTS

Page

LIST OF FIGURES

FIGURE Page

FIGURE Page

LIST OF TABLES

1. INTRODUCTION

Atmospheric aerosols remain one of the most important but least understood aspects of both the climate system and the hydrological cycle. Both natural and anthropogenic aerosols can change the radiative forcing balance via their direct and indirect effects [*Ramanathan et al.*, 2001; *IPCC*, 2007a]. Anthropogenic aerosols have a negative forcing on the earth's radiation budget, which has a net cooling effect on the atmosphere and may offset the warming due to greenhouse gases; however, they also contain the highest level of uncertainty of any of the anthropogenic forcing components [*IPCC*, 2007a] (Figure 1). By acting as cloud condensation nuclei (CCN) and ice nuclei (IN), aerosols can change the microphysical and macrophysical properties of a cloud.

1.1 Aerosol Direct Effect

Through the direct effect, aerosols scatter and absorb incoming solar radiation, which can alter the vertical atmospheric temperature structure, surface and top-of-atmosphere (TOA) radiation fluxes, and cloud fraction [*Coakley et al.*, 1983; *Ackerman et al.*, 2000; *Fan et al.*, 2008]. The direct effect of anthropogenic aerosols has a global mean radiative forcing of -0.5 W m^{-2} (Figure 1); however, large uncertainties are present due to their size and chemical make up. The complexity of anthropogenic aerosols is due primarily to the fact that certain chemical mixtures can lead to a net negative forcing while others can lead to a net positive forcing. Regardless of the aerosol type, all aerosols reduce solar radiation at the surface [*Ramanathan et al.*, 2001].

Sulfate and organic carbon aerosols are two examples of anthropogenic aerosols that have a negative radiative forcing [*Kiehl and Briegleb*, 1993; *Haywood and Ramaswamy*, 1998; *Haywood and Boucher*, 2000; *Ramanathan et al.*, 2001]. Sulfate aerosols have a single scattering albedo of nearly 1 for visible wavelengths meaning that they primarily scatter solar radiation, which leads to a net negative forcing [*Haywood and Boucher*, 2000]. At the TOA, both sulfates and organic carbon also have a negative radiative forcing [*Ramanathan et al.*, 2001]. The global mean radiative forcings for sulfates and organic carbon are -0.4 W m^{-2} and -0.05 W m^{-2}, respectively [*IPCC*, 2007b].

Opposite that of sulfate aerosols, aerosols that contain a mixture of black carbon (BC), or soot, can have a net positive radiative forcing [*Haywood and Ramaswamy*, 1998; *Haywood and Boucher*, 2000; *Jacobson*, 2001; *Ramanathan et al.*, 2001; *Tripathi et al.*, 2005]. At visible wavelengths, BC has a single scattering albedo about 0.2-0.3 [*Bruce et al.,* 1991; *Haywood and Ramaswamy*, 1998]; typically, there is a net positive forcing at the TOA for single scattering albedos < 0.85 [*Ramanathan et al.*, 2001]. While there is reduced solar radiation at the surface due to BC, because BC absorbs solar radiation there is a positive radiative forcing in the atmosphere [*Haywood and Ramaswamy*, 1998; *Ramanathan et al.*, 2001]. The net results in an overall warming caused by BC and a global mean radiative forcing of +0.2 W m^{-2} [*IPCC*, 2007b].

Through the direct effect, absorbing aerosols can have a positive feedback loop that reduces cloud coverage; the term aerosol "semi-direct effect" has been coined to describe this feedback loop [*Hansen et al.*, 1997; *Johnson et al.*, 2004]. In atmospheric layers where absorbing aerosols are present, they work to decrease instability. This

inhibits convection and vertical mixing, thereby hindering the formation of clouds. By inhibiting cloud formation, it reduces TOA radiative cooling that is produced by aerosols and can even lead to positive radiative forcing [*Ackerman et al.*, 2000; *Johnson et al.*, 2004].

1.2 Aerosol Indirect Effect

The aerosol indirect effect is more complicated than the direct effect because it includes a grouping of all the secondary effects that aerosols have on climate due to changes they cause by acting as CCN and IN. The first indirect effect primarily deals with the impact of aerosols on cloud droplet size and number while the second indirect effect deals with the impact aerosols have on cloud size and lifetime [*Twomey*, 1974, 1977; *Albrecht*, 1989; *Pincus and Baker*, 1994; *IPCC*, 2007b] (Figure 2). The indirect effect of anthropogenic aerosols has a global mean radiative forcing of -0.8 W m^{-2} (Figure 1); however, the uncertainties associated with it are much larger than the direct effect. How aerosols effect precipitation is one of the most complex and diverse areas of research with respect to the aerosol indirect effect, specifically the second indirect effect.

It has been widely accepted that through the first indirect effect aerosols that act as CCN and IN lead to a higher amounts of activated CCN and, therefore, cloud droplets in polluted conditions [*Twomey*, 1974, 1977]. For a constant amount of liquid water content (LWC), increasing the number of activated cloud droplets produces more drops at smaller sizes and a narrower size distribution. In a cleaner environment with the same LWC, the amount of activated cloud drops is smaller producing fewer drops; however

drops will grow to larger sizes and have a broader size distribution. Increasing the concentration of cloud drops increases the optical thickness of a cloud leading to a brighter cloud, especially in thin clouds. Optically thicker clouds have a higher albedo meaning they reflect more incoming solar radiation; this leads to a negative forcing on the radiation budget that has a cooling effect on the global climate.

Changing the number and size distribution of cloud droplets also alters the vertical depth and lifetime of clouds as well as precipitation processes [*Albrecht*, 1989; *Pincus and Baker*, 1994] Changes to these cloud features are known as the second indirect effect and contribute to the largest uncertainty in the aerosol indirect effect. By decreasing the size and narrowing the size distribution of cloud droplets, their cross-sectional area decreases and more drops end up having similar fall speeds. This inhibits growth of cloud droplets by collision/coalescence and slows the production of raindrops reducing drizzle and loss of cloud LWC increasing the lifetime of clouds [*Albrecht*, 1989; *Rosenfeld*, 1999]. The largest discrepancies due to the second indirect effect are primarily in the effect aerosols have on precipitation. How aerosols effect precipitation can be broken down into three categories: warm-cloud processes, cold-cloud processes, and mixed-cloud processes.

A warm-cloud, or a warm-cloud process, is one that does not include ice crystals. In a warm-cloud the only way to form a raindrop is either by condensation or by collision/coalescence. Condensational growth requires supersaturation, saturation values greater than 100%, to continue growing a cloud droplet; however, growth by condensation alone takes much longer then growth including collision/coalescence.

Typically, a warm-cloud will have a broader distribution of cloud droplet sizes leading to different cross-sectional areas and fall speeds. The different sizes and fall speeds allow the larger cloud droplets to grow by collecting the smaller drops. Once the cloud droplets reach a radius of 50 μm, they are considered raindrops. The raindrops also continue to grow by collecting smaller raindrops and cloud droplets until they are either too heavy and fall out of the cloud or are too large and breakup due to instability.

In a warm-cloud with higher amounts of aerosols, the number concentration (Nc) of cloud droplets increases. If a similar LWC is present, the resulting distribution of cloud droplet sizes is narrower and centered around smaller sizes. According to the Hocking limit, growth of cloud droplets by collision/coalescence is inefficient while their radius is less than 19 μm [Hocking, 1959]. Since growth by condensation alone is much slower, the aerosols inhibit raindrop formation in warm-clouds leading to a reduction in the precipitation amounts.

A cold-cloud, or cold-cloud process, is one that includes ice crystals. They typically only occur in clouds that reach above the freezing level or clouds that form in the higher latitudes. In cirrus clouds and the upper levels of cumulonimbus clouds, aerosols can also act as IN, which leads to an increased number of ice crystals [*Sassen et al.*, 1995; *Strom and Ohlsson*, 1998]. However, it is unknown if aerosols acting as IN will lead to an increased greenhouse effect that cirrus clouds typically cause or if they will lead to more reflected solar radiation like in brighter warm-clouds [*Sassen et al.*, 1995; *IPCC*, 2007b; *Lee et al.*, 2009a]. An increased number of IN from aerosols could

also increase the probability of cloud glaciation which can impact precipitation [*Cantrell and Heymsfield*, 2005].

A mixed-phase cloud is one that includes both warm-cloud processes and cold-cloud processes. Due to the addition of ice crystals, precipitation formation becomes much more complicated. Two common examples of mixed phase clouds are cumulus congestus and cumulonimbus clouds. Both commonly form in warm, convective environments. In the lower levels of these clouds, warm-cloud processes dominate; however, due to the presence of convection, these clouds can also reach above the freezing level producing a cold-cloud region aloft and a mixed-phase region in the middle. By the Wegener-Bergeron-Findeisen process, in these regions where ice crystals are present, they will grow at the expense of liquid droplets through vapor deposition [*Rogers and Yau*, 1989]. If the number of ice crystals and IN is low, the ice crystals can grow large before falling out of the cloud. This process, as well as growth by riming, aggregation, and accretion, can produce heavy precipitation in convective clouds.

When a mixed-phase cloud is in a region of high aerosol concentration, the aerosols can lead to precipitation enhancement in convective clouds. Because aerosols tend to suppress precipitation due to warm-cloud processes, more cloud droplets can be lifted into the mixed-phase regions of the cloud allowing for more liquid water to be present to enhance the Wegener-Bergeron-Findeisen process. By producing more ice crystals, more latent heat is released aloft leading to enhanced vertical heat transport and convection [*Rosenfeld et al.*, 2008]. These processes increase the instability in the cloud and allow for increased precipitation, known as the aerosol invigoration effect [*Koren et*

al., 2010; *Tao et al.*, 2012]. *Rosenfeld et al.* [2008] also showed that when a convective cloud is present in a clean environment, the opposite effect occurs in that the clouds rain out before mixed-phase processes have a chance to take over.

1.3 Proposed Theories

The impact of aerosols on climate through the direct effect is fairly well understood; it is widely accepted that via the direct effect aerosols produce a net negative radiative forcing and therefore a cooling effect [*IPCC*, 2007a]. Specifically, sulfates, organic carbons, nitrates, and mineral dust have a negative forcing while black carbon and biomass burning have a positive forcing [*IPCC*, 2007b]. The uncertainties in the numerical value of the direct effect come from both a variability in the concentration of each of the components as well as uncertainty in their exact radiative forcing amount. The indirect effect—specifically the effect aerosols have on precipitation—remains one of the largest uncertainties with some cases showing precipitation enhancement while others show precipitation suppression.

Two theories have emerged as to why there is such a variance in how aerosols impact precipitation formation processes. *Khain* [2009] proposed that how aerosols impact precipitation is tied to environmental factors, such as humidity or wind shear, as well as cloud type. These two factors impact whether, in a given case, there is a net production or loss of condensate. If production dominates, then there will be a precipitation enhancement; if loss dominates, then there will be a precipitation suppression. *Li et al.* [2011] proposes that the impact on precipitation is tied more

closely to mixed-phase processes and liquid water content. They show that mixed-phase clouds with warm bases lead to an increase in both precipitation and thickness, while clouds with either no ice or cool bases had no change.

1.4 Previous Studies

The following is a brief literature review of a few studies that are relevant to this study. *Fan et al.* [2008] studied how aerosols impact radiative forcing as well as deep convective cloud properties using a spectral bin cloud resolving model the Goddard Cloud Ensemble (GCE) model, with a single scattering albedo of 0.85. Including the aerosol radiative effects led to a decrease in cloud amount, optical depth, ice Nc, liquid and ice water path, and droplet size. In addition, a net surface cooling was observed while a net warming was present in the lower troposphere. Black carbon led to negative forcing at the surface and positive forcing at the TOA while the semi-direct effect contributed to positive forcing at both heights. For deep convection, a net negative forcing was noted primarily due to the aerosol indirect effect. By increasing atmospheric aerosol absorption, the surface cooling and warming aloft increases stability in the atmosphere inhibiting convective development.

While the direct effect of aerosols scatter incoming solar radiation, the impact of aerosols on clouds can also affect outgoing longwave radiation (OLR). *Lee et al.* [2009b] conducted a sensitivity study on how aerosols affect radiation balances in both a deep convective system and a warm stratiform system using a two-moment scheme employed in the Weather Research and Forecasting (WRF) model. In the convective case,

shortwave forcing was offset by about 45% in the polluted case and 80% in the clean case by longwave forcing. In the stratiform case, the offset was less than 20%. In both cases, higher aerosol concentrations led to increased shortwave and longwave forcing; however, the shortwave forcing appears to increase faster than longwave forcing. Their results also show that ice clouds as well as differing cloud type can impact the strength of the shortwave and longwave forcing.

Looking at the same cold front case from 17-20 March 2000 that is presented later in this study, *Cheng et al.* [2007] used a warm-cloud microphysics scheme in the PSU/NCAR mesoscale model version 5.3.6 (MM5) to study both the microphysical and radiative impacts of aerosols. In their study they used three aerosol profiles with surface concentrations ranging from 800 to 32000 cm^{-3}. Microphysically, increasing the aerosol concentration led to increased cloud droplet concentration but at smaller sizes and decreased in the raindrop concentration. Cloud albedo and water path also increased while surface precipitation and short wave radiation decreased, each with increasing aerosol concentration.

Tao et al. [2007] studied the effects of aerosols on three deep convective cases: a mesoscale convective system (MCS) in the tropical Pacific, a MCS in Oklahoma, and a sea breeze front in Florida. Using the GCE model, they employed two aerosol profiles: an idealized clean profile (100 cm^{-3} for clean maritime and 600 cm^{-3} for clean continental) and an idealized polluted profile of 2500 cm^{-3}. In all three cases, under clean conditions precipitation begins sooner while under polluted conditions rain suppression is noticeable. This rain suppression is only uniformly evident in the early stages of each

case. In the latter stages, the results diverge: for the Oklahoma case rain suppression continues throughout, for the Florida case no changes to precipitation are evident, and in the Pacific case precipitation enhancement occurs. Their results show that in the Pacific case, evaporative cooling is enhanced which strengthens the cold pool and leads to stronger convection and increased precipitation. In the Oklahoma case, an increase in smaller ice particles suppresses the cold pool and convective precipitation processes leaving only warm rain to dominate.

Li et al. [2008] performed a sensitivity study on a cumulus cloud event by implementing a two-moment bulk microphysics scheme into the WRF model that accounts for warm and mixed-phase cloud processes. The surface aerosol Nc ranged from 200 to 50,000 cm^{-3}. While cloud droplet concentration increased and cloud droplet radius decreased with increasing aerosol concentration, they found that the precipitation, cloud coverage, and updraft did were not linearly related to aerosol concentration. For maritime and continental aerosol concentrations, all three values increased with increasing aerosol concentrations. For very polluted aerosol concentrations, these three values rapidly decreased. The nonlinearity in the results is likely due to the complexities in cloud microphysics; specifically, how the aerosols impact warm rain and ice nucleation processes.

1.5 Objectives

The primary objective of this study is to investigate how changes to aerosol concentrations directly and indirectly impact clouds from three different weather

systems that occur during March 2000 at the Southern Great Plains (SGP) site. The specific tasks include: (1) Determine the effects aerosols have on precipitation rates and total precipitation; (2) Analyze the effects aerosols have on other microphysical and cloud properties such as droplet concentration, mixing ratio, and liquid water path (LWP); (3) Analyze the effects aerosols have on surface and TOA radiative fluxes; (4) Observe any changes to the physical properties of clouds such as cloud fraction and depth due to aerosols; (5) Quantify any changes to surface meteorological variables such as temperature, pressure, horizontal wind, etc. (6) Compare relative changes between each model run due to aerosol concentrations, direct and indirect effect, and in relation to observational values.

2. EXPERIMENT SETUP

To study aerosol-cloud interactions, a modified version of the WRF model is used. The WRF model implements modifications to a two-moment bulk microphysical scheme as well as a shortwave radiation scheme. Three aerosol profiles are used to observe changes due to varying the aerosol concentration. Three time periods (case studies) at the SGP site from March 2000 are used to observe changes that occur due to different weather events and environmental factors. Finally, the cases are run including the direct and indirect effect (DIE) as well as the indirect effect only (IEO) to observe how the different aerosol effects change the results. The combination of each of these variations leads to six individual model runs for each time period. The description of the model setup, aerosol profiles, and case studies follow. In addition, statistical methods are included to ensure the significance of the results.

2.1 WRF Model

The WRF model is a next-general mesoscale numerical weather prediction (NWP) model designed for use both operationally and for research purposes. It includes multiple dynamical cores, a 3-dimensional variational (3DVAR) data assimilation system, and software architecture that allows for parallelism. The Advanced Research WRF (ARW) can be utilized for several applications including: idealized simulations, parameterization research, data assimilation research, forecast research, real-time NWP, hurricane research, regional climate research and coupled-model applications.

The WRF is a fully compressible, nonhydrostatic model, with a hydrostatic option. It uses terrain-following hydrostatic pressure vertical coordinates, grid staggering by the Arakwa C-grid, Runge-Kutta 2nd and 3rd order time integration schemes, 2nd and 6th order advection schemes in both the horizontal and the vertical, time-split small steps for acoustic and gravity-wave modes, and the dynamics conserve scalar variables.

For this study, a modified version of WRF version 3.1.1 is used. The modifications implemented include a two-moment bulk microphysical scheme as well as a modified Goddard shortwave radiation scheme. The microphysical scheme was implemented by *Li et al.* [2008] and includes the mass mixing ratio and Nc for five hydrometeor types including: cloud droplets, raindrops, ice crystals, snow, and graupel, as well as including the mass mixing ratio of water vapor. The cloud droplets are included because of their significant impacts on aerosol effects as well as radiative properties. The size distribution for each of the five hydrometeors is determined via the gamma function. Among these five hydrometeors, thirty-two microphysical processes between them are included in the two-moment microphysical scheme (Figure 3). The primary purpose of implementing the two-moment bulk microphysical scheme is to include the aerosol indirect effect.

The radiative effects of aerosols on clouds pertain to their optical depth, single scattering albedo, and asymmetry factor. Modifications to the Goddard radiation scheme were implemented by *Fan et al.* [2008] to include radiative forcing by the aerosol direct effect. To replace using fixed aerosol radiative properties, the aerosol module was implemented to determine aerosol radiative properties as a function of wavelength,

aerosol composition, mixing state, and relative humidity. To avoid repeated calculations, once the aerosol radiative properties are determined, a lookup table is calculated for the optical properties for all size ranges.

For each model run, three nested domains are setup with two-way feedback (Figure 4). The outer, middle, and inner domains have spatial resolutions of 18, 6, and 2 km each with a temporal resolution of 180 seconds and file output at 15-minute intervals. The innermost domain is 3.5° by 3.5° and centered at (36.5934°N, 97.5113°W); it roughly covers the same domain as the ARM SGP site near Ponca City, OK and is where all model data and calculations presented in this study are from. The North American Region Reanalysis (NARR) data is used to produce the input forcing files for the WRF.

2.2 Aerosol Profiles

To study the impact of varying aerosol concentrations have on the direct and indirect effects, three different aerosol profiles are utilized in this study (Figure 5). The clean cases (green profile, Figure 5) use a relatively clean background continental profile with an initial surface Nc of 210 cm^{-3}, as used by *Li et al*. [2009] from the TexAQS 2000 campaign. The moderate cases, referred to herein as SGP cases, (yellow profile, Figure 5) are based on aerosol measurements taken at the SGP site during the 2003 Aerosol IOP campaign. The SGP cases have an initial surface concentration of $1.2e^{3}$ cm^{-3}. The polluted cases (red profile, Figure 5) are ten times the SGP profile with an initial surface concentration of $1.2e^{4}$ cm^{-3}; which is similar in magnitude to the urban case used by

Cheng et al. [2007]. For all three profiles, the aerosol concentration is assumed to decrease roughly exponentially with height above about 5 km [*Cheng et al.*, 2007; *Fan et al.*, 2007; *Li et al.*, 2009]. For each case, the aerosol profile is horizontally distributed homogenously across all three domains.

For each case, the aerosol profile is initialized with a homogenous horizontal distribution across all three domains. There are no aerosol sources in the model and the profile is not fixed; it is allowed to evolve and change with time as aerosols become activated to form cloud droplets. However, more aerosols can be advected into the domain from across the boundaries due to the boundary conditions. For the microphysical scheme, the profile represents sulfate aerosols. When the direct effect is included, the radiation scheme assumes a 95% to 5% ratio by mass of sulfate to black carbon aerosols.

2.3 Case Studies

From March 1 to March 26, 2000, the March 2000 Cloud IOP campaign was conducted at the ARM SGP site. The goal of the campaign was to collect 3-dimensional cloud properties from observational data including the standard set of ARM SGP instruments, radar and lidar observations, and aircraft instrumentation, which included a total of 12 flights during the period. This cloud data has been broken down into six sub-periods that contain different synoptic and cloud properties (Figure 6) and has been extensively studied regarding cloud-climate feedback in atmospheric general circulation

models (GCMs) [*Zhang et al.*, 2005]. For this study, aerosol-cloud interactions will be studied for three of these six cases: Cases A, D, and E from Figure 6.

Case A pertains to clouds to the north of a developing low pressure system from March 1-4, 2000 (Figure 7a). About 12 hours prior to the start of this case, a cold front moved through the domain at about 0430Z on March 1. Clouds begin to move into the domain from a low pressure system that forms in the Four Corners region around 2000Z on March 1. By 2000Z on March 2, the low pressure system is entering the southwest corner of the domain while a thick layer of clouds covers the region. Between March 2-3, the center of the low moves along the Oklahoma-Texas boarder with cloud development primarily to its north. By 1330Z on March 3, the system is leaving the region with the skies mainly clearing up by 1200Z on March 4 as high pressure filters in.

Case D pertains to a collection of non-precipitating clouds from March 12-15, 2000 (Figure 7b). Prior to the start of this case, there was a stationary front to the south draped across central Texas from the Louisiana-Missouri boarder across to New Mexico, with a high pressure center behind it located centrally over the domain. During March 13, a cold front passes to the north of the domain which also moves the high pressure center out of the region. During March 14, a weak low pressure system passes through southern Texas, bringing some high level clouds and light precipitation through the domain.

Case E pertains to clouds associated with the genesis of a cold front that move through the domain from March 15-19, 2000 (Figure 4c). The cold front approaches from the north-northwest and arrives in the domain at about 0100Z on March 16.

Satellite imagery shows convective development nearly directly over the SGP central facility from 0000Z to 0300Z. By 1300Z the cold front had moved south into Texas and out of the domain where it stalls out. Behind the cold front, mainly lower level clouds persist over the domain. On March 18, another low pressure system passes to the south of the domain right long the Oklahoma-Texas boarder. The region finally clears out by about 2000Z on March 19.

2.4 Statistical Methods

To evaluate the response of model derived variables due to changes in the aerosol direct and indirect effects by changes in aerosol concentrations, the mean value over a given x-y domain over a given time period is more meaningful than an instantaneous distribution of a given variable. For a four-dimensional variable, the mean is calculated by Equation (1), where *m* is the given variable of interest and N is the total number of points over which the mean is calculated. For a three-dimensional variable (often surface variables), the z-component is ignored. Using the mean and the standard deviation, a confidence interval is calculated with a two-sided student's t-distribution, by Equation (2), where *S* is the sample standard deviation, *n* is equal to *N-1*, and *A* is the corresponding value from t-distribution table for a given probability.

3. RESULTS AND DISCUSSION

In the following section, how aerosols impact cloud properties is analyzed for three different weather events: a low pressure system that passes south of the domain, low precipitating clouds, and a cold front. The modeled data are compared to observational data, when available, to determine consistency of the model data with the trend of observations. Obtaining consistency with the exact magnitude of the observations is not the goal here; rather, it is that the trends are consistent—eg. consistency in determining when the maximum rainfall rates occurred is more important than obtaining exactly similar rainfall rates. For point location observations, such as surface radiation, data was observed from different instruments at the SGP Central Facility. For domain average observations, such as precipitation, data was compiled from various data sources over the entire domain. Specific observational data sources will be specified in the following sections when the variables are first introduced (Table 1).

Once consistency is determined between the model and observations, changes due to the aerosol effects are investigated. First, how varying the aerosol concentration impacts cloud properties. Second, how including or removing the aerosol direct effect also impacts the results. For each case, three aerosol profiles are used as outlined in the previous section: clean, SGP (moderate), and polluted. Then, each profile is used twice once with the DIE and once with the IEO, for a total of six runs per case. In the end,

changes between each of the six model runs due to aerosols and the DIE/IEO are more important than differences between observed and modeled data.

3.1 Case A: March 1-4, 2000

From March 1-4, 2000, the center of a developing low pressure system passes to the south of the domain along the Oklahoma-Texas boarder. As this system is developing, several cloud types are experienced at the SGP site. Initially, cirrus clouds filter into the region, followed by a period of convection and cumulus clouds, and finally ending with a layer of stratus clouds before clearing up (Figure 8d). This case allows for the observation of three different types of cloud events in a single case.

3.1.1 Case A Results

In Figure 8d, the observed cloud fraction is the fractional area percentage of clouds in an atmospheric layer taken at the SGP Central Facility using the Active Remote Sensing of Clouds Value-Added Product. For Figures 8abc and 8efg, the modeled cloud fraction is the percentage of the 25 nearest grid points (a five-by-five horizontal box around the SGP Central Facility) with a total water mixing ratio (Qtot) greater than 10^{-6} kg kg^{-1} [*Cohen and Craig*, 2006], where Qtot is the sum of cloud (Qc), rain (Qr), ice (Qi), snow (Qs), and graupel (Qg) mixing ratios.

In each of the six model runs, cirrus cloud formation is consistent with respect to approximate occurrence time; however, the depth and thickness of each cirrus cloud is much larger than observed. The same is true for the modeled cumulus and stratus clouds throughout the event. While small variances exist in cloud extent from case to case in

Figure 8, the average cloud fraction over the entire time series shows statistically significant increases or decreases with respect to aerosol concentration depending on whether it is the a DIE or an IEO case (Figure 9). For the DIE cases, increasing the aerosol concentration led to an increase in cloud fraction by 6.9%, while for the IEO cases, increased aerosol concentrations decreased the cloud fraction by 8.1%. The physical interpretation of these trends is discussed in Section 3.1.2.

In Figure 10, the observed rain rate and accumulated rain were compiled based on rain gauge data from the Arkansas Red-Basin River Forecast Center. The modeled rain rate and accumulated rain were determined from finding the domain average of the accumulated total grid scale precipitation. Observational data showed two local maxima in precipitation rates, while modeled data had three local maxima (Figure 10a). The first local maxima in rain rate corresponded to the tallest and thickest cloud concentration over the entire time period. Beginning with this maximum and continuing for about 9 hours after, increased aerosols led to a precipitation enhancement; however, the modeled rate was about half the observed rate. In the modeled data, a second local maximum occurred at the beginning of Julian day 63 and continued for about two hours. During this local maximum, both SGP profiles had the highest rainfall rates while the DIE clean and polluted profiles had the lowest rainfall rates. The higher than observed rainfall rates during this maximum likely were due to the higher cloud fraction values at this time in all model runs. During the final local maxima in rainfall rates, for about a four hour period, increased aerosols led to a precipitation reduction. However, during this period, the modeled rate was about twice the observed rate but the observed rates were likely

due to a combination of cumulus and stratiform rain whereas the modeled results appear to be primarily due to stratiform.

Despite the discrepancies in precipitation maxima, the accumulated rainfall during this time period was similar to the observed rainfall (Figure 10b). Averaged over the entire time period, for the development of this low pressure system, increased aerosols led to a precipitation enhancement of about 0.01 mm hr^{-1} and between a 0.9 and 1.0 mm increase in accumulated rain, about a 3% increase (Figure 11). For both the clean and polluted aerosol profiles, the IEO case had statistically significantly more precipitation than the DIE case.

Figures 12-17 display domain averages for the modeled values of the mixing ratio for cloud, rain, and ice water as well as Nc for the cloud, rain, and ice drops. As expected, as the aerosol concentration increased the number of activated cloud droplets (Figure 12), and therefore the amount of cloud water also increased (Figure 13). Figures 18a and 18d show that for the SGP and polluted cases there were significantly more activated cloud droplets for the DIE runs than for the IEO runs. Since the amount of water vapor available in each case is roughly the same, increasing the number of activated cloud droplets meant more droplets at smaller sizes. As a result of this, Figures 14 and 15 show a decrease in the number of raindrops and the rain water mixing ratio with increased aerosol concentration. Despite the number of activated cloud drops being consistently larger for DIE cases (Figure 18d), the number of raindrops is not consistently larger for all IEO cases (Figure 18e). For the total ice, Figures 16 and 17 show the average mixing ratio and Nc for all ice particles: Qi, Qs, and Qg. Their number

increases with increasing aerosol concentrations while their mixing ratio decreases (Figures 16 and 17); however, there is no consistent difference in mixing ratio nor Nc with respect to the DIE and IEO cases (Figures 18c and 18f).

For vertical velocity, instead of using the vertical velocity from every grid point, what is called the "core" vertical velocity was used. *Wang* [2005] defined the core as a region with an absolute vertical wind speed > 1 m s^{-1} and total condensed water mixing ratio > 10^{-5} kg kg^{-1}. For this study, the core was assumed to be any region previously defined as a cloudy region, i.e. with a Qtot > 10^{-6} kg kg^{-1}. Figure 19b suggests that for the IEO cases, the mean vertical velocity increases with increasing aerosols while the opposite is true for the DIE cases. However, looking at Figure 20 shows that in both the DIE and IEO cases, the extent of the strongest updraft and downdraft regions increases in both cases, specifically around 0000Z (updraft area) and 1400Z (downdraft area) on day 63. Throughout day 62, both the maximum updraft and downdraft speeds increased (Figure 21); however, their peak values came around 0000Z on day 63, which was about 12 hours after the tallest clouds were observed at the SGP site (Figure 8). Time averages of both the maximum updraft and downdraft proved to be inconclusive between each case (Figures 19a and 19b).

The Broadband Heating Rate Profile Project was used for the observed downwelling surface shortwave radiation (SSR) flux and upwelling OLR fluxes; the modeled data is averaged from the 121 nearest grid points (an 11-by-11 horizontal box around the SGP Central Facility). For the shortwave radiation, the model correctly captured the diurnal cycle; however, when clouds were present the model over predicted

the amount of downwelling SSR (Figure 22a). Despite the over prediction, a decrease in downwelling SSR was observed (Figure 23a). Both the DIE and IEO cases had similar values for the clean and SGP profiles; the polluted profile showed a more significant decrease for the DIE case. When the direct effect was included, the DIE case showed a decrease of 37 W m^{-2} from the clean to polluted case. The IEO case, which did not included the direct effect, only showed a decrease of about 14 W m^{-2}. Regarding OLR, no overly significant differences were noted between each of the six cases (Figure 22b), Statistically the DIE cases showed a decrease in OLR while the IEO cases showed an increase (Figure 23a), consistent with the change in cloud fraction (Figure 9).

Figure 22c includes two types of surface temperature observations: Merged Sounding Value Added Product from the SGP Central Facility (black line on Figure 22c) and METAR observations from Ponca City Regional Airport, OK (blue-purple line on Figure 22c); the modeled data is averaged from the 121 nearest grid points (an 11-by-11 horizontal box around the SGP Central Facility). Since there was a net reduction in radiative fluxes of between 16 and 34 W m^{-2} for the IEO and DIE cases respectively, the surface temperature also decreased. While the temperature decrease was not statistically significant in the DIE nor the IEO cases, changes from the clean to polluted profiles produced a decrease of 0.56 K and 0.15 K for the DIE and IEO cases, respectively (Figure 23c).

The observed LWP from Microwave Radiometer Retrievals at the SGP Central Facility were compared to the average LWP from the 25 nearest grid points (a five-by-five horizontal box around the SGP Central Facility). The modeled LWP values showed

a positive correlation to the aerosol concentration while overall maintaining a similar magnitude to that of the observed LWP values. The effect of aerosols on surface pressure and surface horizontal wind speed were also studied; neither showed any changes with respect to changes in aerosols.

3.1.2 Case A Discussion

For this developing low pressure system which contained at least three different types of clouds—cirrus, cumulus, and stratus—overall, in both the DIE and the IEO cases, increased aerosol concentration had two main impacts: a net reduction in the total radiative fluxes and precipitation enhancement. While having several cloud types at once can add to the complexity for each individual cloud event, the overall trend for the low pressure system as whole can be observed.

The reduction in downwelling SSR is as expected; the DIE cases included both direct and indirect and correctly has the highest reduction. The IEO cases only include the aerosol indirect effect; however, the increase in the liquid water path caused by the aerosols does lead to some reduction in downwelling SSR. In both the DIE and IEO cases, the aerosols lead to a, albeit statistically insignificant, reduction in surface temperature of up to 0.55 K. By increasing cloud thickness and lifetime, indirectly, aerosols could also increase temeperature. A change in the cloud properties could lead to a change in the OLR which is seen in the correlation between changes in cloud fraction and changes in OLR.

As presented in the previous section, the average cloud coverage increased in the DIE cases and decreased in the IEO cases with respect to increasing aerosol

concentration. Despite these trends, the model consistently had thicker and often taller clouds when compared to the observational data. The higher modeled amounts could be due to data sources since the observational data is based on cloud optical properties while the modeled data is based on mixing ratios. The difference may be due to the Qtot threshold being set too low when counting cloudy cells or the problem could be from using Qtot instead of another quantity such as Qc alone or Qc and Qi together. For example, in the modeled data, the cloud coverage is often higher below the cloud and near the surface. In determining cloud fraction using Qtot, it may be counting a collection of raindrops that have fallen out of the cloud as part of the cloud itself. Based on Figures 12, 14, and 16, rain water mixing ratio is the likely culprit for increased cloud fraction, especially at the surface. Regardless of how the clouds are counted, they do not impact the radiative and microphysical processes, as they are based on the actual the mixing ratios and Nc, not derived products like cloud fraction.

As revealed from many previous studies, increasing the aerosol concentration leads to an increase in the number of cloud droplets, producing more cloud droplets at smaller sizes. Most previous studies assume a fixed LWP in the clouds, but, in this model, the LWP was not fixed. The LWP increased during this case with increasing aerosol concentration but the increase was not significant. So the assumption could be made that the LWP is roughly constant for this case. As aerosol concentration increased, the cloud droplet concentration and mixing ratio also increased while the raindrop concentration and mixing ratio decreased. If this were a warm-cloud only case or a warm-cloud microphysical model, precipitation suppression would be expected. Since

this model includes mixed-phase microphysics, cloud type and ice amounts will influence the effect of aerosols on precipitation.

For this case, the total ice has an inverse relationship: as the concentration of aerosols increase, the total ice concentration increases while the mixing ratio decreases. However, despite the lower amounts of ice water, increasing the concentration of total ice can help enhance precipitation if ice particles grow at the expense of liquid drops. The enhancement of precipitation due to ice particles can be seen from 1200Z to 1800Z on day 62 (Figure 10a). While this period has a lower than observed rain rate, during this time the number of raindrops is lowest while the number of ice particles is highest for polluted cases (Figures 15 and 17). Despite the lowest concentrations of raindrops, the polluted cases had the highest rainfall rate on day 62 out of all the model runs. Around 0700Z on day 63, raindrop concentration shows the same trend as before but ice particle concentration is approximately uniform over all six model runs. During this time period, warm-rain dominates and precipitation suppression is observed. Averaged over the entire time period, the enhancement due to the mixed-phase period dominates the suppression during the warm-phase period, leading to a net increase in precipitation in both the DIE and IEO cases.

Because this is not primarily a convective case, core vertical velocity data can be difficult to judge. For the mean vertical velocity data, two trends are present. Mean vertical velocity decreases in the DIE cases while it increases for the IEO cases for increasing aerosol concentration. In the DIE cases, the inclusion of some black carbon aerosols can absorb solar radiation warming an atmospheric layer. At the same time, this

will decrease the amount of solar radiation reaching the surface leading the surface cooling (Figure 22c). This can stabilize the atmosphere leading to an overall reduction in vertical velocity. In the IEO case, aerosol direct effect is not included and all aerosols are assumed to be sulfate. Therefore, warming an atmospheric layer is reduced in these cases and aerosols can invigorate vertical velocity values. While Figure 19a shows an overall reduction in updraft speed in both DIE and IEO cases, looking at individual events in Figure 20 suggests a broadening of the updraft core around 0000Z on day 63 and of the downdraft core around 1700Z on day 63. Again, these discrepancies are likely caused due to this case including several cloud types and not being primarily a convective event.

3.2 Case D: March 12-15, 2000

From March 12-15, 2000, most clouds that pass through the region are associated with weather systems that do not directly pass through the center of the domain. As a cold front passes to the north, some midlevel clouds pass through the region. Later, as a low pressure center passes far to the south some cirrus and stratus clouds move through the region. Most of these clouds produce little precipitation over the domain. The most significant rain comes near the end of the time period when a few cumulus clouds formed in Oklahoma to the south of the SGP Central Facility due to a low pressure system to the south. All observed and model averaged quantities in the following section were calculated by the same methods as presented in Section 3.1 unless otherwise noted.

3.2.1 Case D Results

Figure 24d shows that early on there are only a few non-precipitating mid to upper level clouds that pass over the SGP Central Facility. Lower level clouds, primarily stratus with a few cumulus clouds mixed in, are not observed at the SGP Central Facility until later during day 74. The modeled data for all six cases are fairly uniform capturing the timing and the approximate cloud base well (Figures 24abc and 24efg). The only differences in the modeled data are slightly larger and thicker clouds are present throughout: the clouds that from around 0400Z on day 73 reach close to the ground and the low level clouds from around 1900Z on day 74 develop more convection than is observed. Figure 25 shows that during the IEO cases, the cloud coverage is practically uniform between all three aerosol profiles, while for the DIE cases the only reason there is a decrease in cloud coverage is due to the reduction of the cumulus cloud on day 74.

Since most of the clouds during this time period are primarily non-precipitating, the only observed major precipitation event is during the low level clouds after 1200Z on day 74 (Figure 26a). Because the modeled data presents larger and thicker clouds throughout the entire period, several short periods of precipitation are also present in the model; however, with regards to the final precipitation event, all six cases capture it but delay it by about two hours. During the extra modeled precipitation events, at times the clean cases show the lowest rain rates and for several hours the DIE polluted case showed the lowest overall rain, but generally no one aerosol profile showed a uniform dominance consistently nor for any significant amount of time. It is, however, during the final precipitation maximum that a trend in rain rates can be observed.

After 1200Z on day 74, precipitation from some cumulus clouds is present over the domain. The IEO SGP case had the highest precipitation and the DIE polluted case had the lowest precipitation, the other four cases had similar rain rates. This event produced the spreading of accumulated precipitation seen in Figure 26b. For the DIE and IEO cases, the SGP profiles resulted in the most accumulated precipitation. Because most of the precipitation during this period came from a brief shallow convective event at the end, the trend related to aerosol concentration is similar to most convective cases. A primarily convective case, with deep convection, will be discussed in further detail in Section 3.3. In general the rainfall increased from clean to SGP cases, but then decreased from SGP to the polluted cases (Figure 27). For the DIE cases, the accumulated rainfall ranges from a maximum of 3.9 mm to a minimum of 2.3 mm. For the IEO cases, the accumulated rainfall ranges from a maximum of 4.5 mm to a minimum of 3.3 mm. Overall, the IEO cases generally averaged more precipitation than the DIE cases.

During this case, the aerosol concentration increased cloud droplet concentration and water mixing ratio also increased. The cloud water mixing ratio nearly doubles in the IEO cases (Figure 34a), while in the DIE cases the droplet concentration increases by two orders of magnitude (Figure 34d). Despite these overall increases during that entire time period, looking only at the brief convective instance after 1200Z on day 74 shows the cloud water has a small decrease in the DIE cases from the SGP to the polluted case while in the IEO cases it stayed roughly the same (Figure 28). Regardless, the number of cloud droplets continued to increase with increasing aerosols (Figure 29).

Because the LWP for all six cases is not significantly different from one another and due to the activation of more cloud droplets, the Nc and mixing ratio of raindrops should decrease. Figures 30 and 31 support this notion, showing a negative correlation between aerosol concentration and raindrops. The number of raindrops decreases by between 200 kg^{-1} and 300 kg^{-1} for the DIE and IEO cases, respectively, while the mixing ratio decreases by about $4.0x10^{-7}$ kg kg^{-1}.

During this period, all clouds had high mixing ratio values for the total ice particles (Figure 34). The two times when total ice mixing ratio is at its maximum are around 1400Z on day 72 and 1600Z on day 74. On day 74, aerosol concentration and total ice water mixing ratio were inversely proportional (Figure 32); however, the average over the entire time period shows that the IEO SGP case had the most, the DIE polluted case had the least, and the other four cases had similar mixing ratios (Figure 34c). For the Nc, the IEO cases showed a positive correlation to aerosol concentration. The DIE cases showed a parallel to the rain rate trend—largest total ice Nc during the SGP case while the polluted case had the lowest (Figures 27b and 34f).

The core vertical velocity values for time averaged maximum, minimum, and mean speeds had nearly identical trends to the total ice Nc (Figure 35). For the strongest updrafts and downdrafts, the IEO cases were positively correlated while the DIE cases had highest values for the SGP and lowest for the polluted. Other than a slight decrease in the IEO polluted case, the mean vertical velocity had a similar trend. The slight dip is likely due to the downdraft increasing faster than the updraft. Because most of this case consisted of non-precipitating clouds, the domain averaged core vertical velocity is

mostly uniform for all six cases; however, the convective clouds just prior to 0000Z on day 75 show differences in vertical velocity (Figure 36). After 1500Z on day 74, the updraft area and speed varies between each case, the same is true for the downdraft area and speed after 0000Z on day 75. For both of these events, the strongest speeds and the most coverage is present for both SGP cases.

Because there were very few clouds throughout the entire time period, their effects on the downwelling SSR as well as the OLR were only minor. The most significant differences were during the brief convective period during the daytime of day 74 (Figures 38a and 38b). Generally, there was not much difference in the SSR nor the OLR for the IEO cases, but with the inclusion of the aerosol direct effects, the OLR increased by about 3 W m^{-2} while the SSR decreased by about 24 W m^{-2} for a net of decrease of 27 W m^{-2} in the local radiative fluxes (Figures 39a and 39b). This decrease in radiation caused a corresponding decrease in surface temperature of about 0.27 K, though it was not statistically significant (Figure 39c). For the IEO cases, there was only a slight SSR reduction which was offset by a slightly greater OLR reduction producing a small temperature increase.

For this case, the observed and modeled LWP were similar in magnitude, but the LWP had a trend similar to that of the rain rates where the SGP cases had the highest LWP in both the DIE and IEO cases. Horizontal wind speed and surface pressure were also studied, but showed no signification changes with respect to aerosol concentration.

3.2.2 Case D Discussion

For this case, the SGP Central Facility experienced mainly clear skies for greater than 80% of the period. When clouds were present, they were primarily non-precipitating clouds; however, at the end of the time period a few cumulus clouds were present from a low pressure system that was far to the south. In both the DIE and the IEO cases, the cloud fraction associated with the cirrus clouds was mainly consistent. The only changes to cloud fraction occurred during the cumulus clouds after 1200Z on day 74. The IEO case shows no change in their amount while the DIE cases show a decrease in their amount.

The changes in cloud fraction can be linked directly to Qtot. For both the DIE and IEO cases, the increase in Qc is directly offset by the decrease in Qr. However, the total Qi is relatively consistent across all aerosol profiles for IEO while it decreases with increasing aerosols in the DIE cases. The differences in Qi in the DIE cases occur only during day 74.

For the IEO cases, while the precipitation rates show a nonlinear trend, all other quantities show a relatively linear relationship to aerosol concentration. As aerosols increase, so does cloud droplets, updraft speed, and downdraft speed. However, adding the aerosol direct effect allows the cumulus case to show the nonlinear trend that was experienced by *Li et al.* [2008]. This is manifested in the DIE cases with nonlinearities in rainfall, total Qi, total ice particle Nc, and vertical velocities—the aerosols initially increase these values from clean to SGP profiles but then result in a decrease from SGP to polluted profiles. It is difficult to determine which is the primary driver but all

mentioned variables appear to be interconnected. For this case, the likely cause appears to be the aerosol direct effect.

Regarding radiation fluxes, for the IEO cases when the aerosol direct effect is not included changes to radiation are caused primarily to LWP. For this case, the LWP only increases slightly, hence only the small changed to SSR and OLR and, by association, surface temperature (Figure 39). For the DIE cases, the aerosol direct effects are included in the model results. In this case, the increased aerosols led to a reduction in SSR primarily during the cumulus clouds at the end of the case. However, due to lower amounts of water in the atmosphere as well as activated aerosols in this case, the amount of OLR increases. The combination of these two fluxes leads to a slight surface cooling. And while typically activated IN and cirrus clouds lead to reduction in the OLR, the total amount of ice particles in this case was generally low thereby reducing, even negating, this effect.

3.3 Case E: March 15-19, 2000

From March 15-19, 2000, the domain experiences almost continuous cloud cover. Initially, a cold front passes through bringing mainly convective based clouds and precipitation. Throughout the remainder of the period, mainly low-level stratiform clouds are present during an upper level low pressure and then to the north of a surface low pressure system that moves along the Oklahoma-Texas border. The cold front brings the strongest convection of any of the three cases and is the most ideal for studying aerosols effects on deep convective events. The stratiform events that follow are the

longest period during the three cases for continuous stratus clouds. As in Section 3.2, all observed and model averaged quantities in the following section were calculated by the same methods as presented in Section 3.1 unless otherwise noted.

3.3.1 Case E Results

From the cloud observations (Figure 40d), clouds are present at the SGP Central Facility consistently throughout the entire case. Deep cumulus clouds are only present during the first third of day 76; after the cold front passes, low-level stratiform clouds remain continuously for over three days. Figures 40abc and 40efg show that the model reproduces the length and thickness of cloud coverage well during this case, unlike the previous cases. However, at the SGP Central Facility, the model exhibits two differences from observations: (1) The cumulus clouds occur about nine hours later and (2) The cloud event centered around 0000Z on day 79, becomes much more vertically developed in the model cases than what was actually observed. Overall, the cloud coverage is generally consistent between the six modeled; the only significant instantaneous differences are in the cloud fraction around 0700Z on day 77 and 0200Z on day 78. Averages over the entire time period show practically no change in cloud fraction in the DIE cases, while for the IEO cases the cloud fraction increases from 24.0% to 25.3% (Figure 41).

During this case, observations show there are approximately three times of local precipitation maxima (Figure 42a). The first observed maximum is convectively driven during the passage of the cold front. The second maximum is primarily stratiform based due to the upper level low. The third maximum is mainly stratiform based, but

convective precipitation cannot be ruled out as some cumuliform clouds were also present in the domain as the low pressure system passed to the south. As opposed to having more of a consistent trend in precipitation rates like the observed data, the modeled data have several local maxima (Figure 42a). Instead of focusing on them all, only the three that correspond with the observations as well as the fourth one that occurs during day 29 will be covered.

During the first maximum, the polluted cases resulted in the lowest precipitation while the SGP cases had the highest precipitation. This may be an example of where the polluted profiles have too many aerosols and inhibit precipitation whereas the SGP profiles have the right amount to enhance precipitation. Throughout the remaining data precipitation primarily comes from stratiform sources from about 1700Z on day 76 to about 1900Z on day 78. During this period, the IEO polluted profile has the highest precipitation rates followed by both SGP and then both clean profiles. The anomaly in this trend is the DIE polluted profile, which remains the lowest precipitation case during the first three-fourths of the entire time period. The final maxima in the modeled data occurs after 0000Z on day 79 and corresponds to a modeled cumuliform event that is much stronger and lasts longer than any of the observations show. During this peak, the DIE polluted case shows a sudden increase in precipitation rates, while a trend from the other five is difficult to determine.

The average domain accumulations for all six model runs are below the average observed domain accumulations (Figure 42b). Averaging over the entire time period shows a nonlinear relationship between aerosol concentration and rainfall (Figure 43).

This suggests that, for this case, initially aerosols lead to invigoration before reaching a certain aerosol concentration at which they begin to reduce the precipitation. For the DIE cases, the rain rate varies by 0.012 mm hr^{-1} being as high as 0.259 mm hr^{-1} in the SGP profile to as low as 0.247 mm hr^{-1} for the clean profile. For the IEO cases, the rain rates are significantly higher than the DIE cases being as high as 0.268 mm hr^{-1} in the SGP case to as low as 0.249 mm hr^{-1} for the clean case.

As was the norm in the previous two cases, increasing the concentration of aerosols leads to an increase in the Nc and the mixing ratio for cloud droplets (Figures 44 and 45). Both the DIE and IEO cases showed similar values and increased for Nc by an order of magnitude, while mixing ratio increased by about $6x10^{-6}$ kg kg^{-1} (Figures 50a and 50d). As expected, due to the increase in cloud droplets, the Nc and mixing ratio of raindrops decreased (Figures 50b and 50e), especially during convective periods (Figures 46 and 47). The Nc decreases by about 800 kg^{-1} and while the mixing ratio decreases by $5x10^{-7}$ and $9x10^{-7}$ kg kg^{-1} for the IEO and DIE cases, respectively (Figures 50b and 50e). However, despite the steady increase in cloud water mixing ratio, this is not the case from clean to SGP cases for rain water. In the DIE cases, the rain water only decrease slightly; while in the IEO cases, the rain water actually increases from clean the SGP cases (Figure 50b). As also noted in the previous cases, total ice water mixing ratio decreased while the Nc of total ice particles increased with increasing aerosol concentration (Figures 48 and 49). The total ice water mixing ratio decreased by about 4-$5x10^{-6}$ kg kg^{-1} for the IEO and the DIE cases while the total ice particle Nc increased by about 8000 kg^{-1} for both cases (Figures 50c and 50f).

During the strongest convective event, when the cold front passed through during day 76, Figure 52 shows that with increasing amounts of aerosols, the average vertical velocity decreases. This is further supported by a reduction the updraft and downdraft speeds around 0200Z on day 76 in Figure 53b. Averaged over the entire case, the opposite trend is observed where more aerosols generally led to an enhancement in both the updraft and the downdraft (Figures 51a and 51c). This increase is primarily due to the increased updraft and downdraft speeds during the stratiform periods (Figure 53). While only small, the overall vertical velocity decreases with increasing aerosol concentration suggesting that the magnitude of the downdraft increases faster than that of the updraft.

As in the previous two cases, for the model properly captured diurnal variations in downwelling SSR while still over predicting the amount. Despite the overprediction, an inverse relationship is present between the downwelling SSR and aerosol concentration (Figure 54a); the same is also seen for the OLR (Figure 54b). Both the DIE and IEO cases showed similar reductions in both shortwave and longwave radiation at about 45 W m^{-2} and 2.5 W m^{-2}, respectively (Figures 55a and 55b). Due to a net reduction in the radiation budget of about 42.5 W m^{-2}, the surface temperature also decreased (Figure 54c); however, the this decrease in surface temperature not statistically significant at 0.8 K and 0.6 K for the DIE and IEO cases, respectively (Figure 55c).

As in Case A, the modeled LWP showed a positive correlation to the aerosol concentration (Figure 55d). Horizontal wind speed and surface pressure were also studied, again showing no significant changes with respect to aerosol concentration.

3.3.2 Case E Discussion

During the time period for this case, nearly continuous cloud coverage was experienced over the SGP domain with two cloud types primarily present—cumuliform and stratus. Since the cumuliform clouds produced over half of the accumulated precipitation, this case can be considered primarily a convective case. Generally, in both the DIE and the IEO cases, aerosols had two main impacts: a decrease in the downwelling SSR and, due to the convective nature of this event, a nonlinear impact on precipitation.

Increasing the amount of aerosols generally leads to a reduction in shortwave radiation at the surface both through the direct scattering by aerosols and indirectly through increasing the cloud LWP. This can also lead to a reduction in the OLR at the TOA. In this model, the direct effects of aerosols are only included in the DIE cases, so the expectation is that the reduction in downwelling SSR should be greater for the DIE cases than the IEO cases; however, Figure 55 shows this is not the case. Instead, both the OLR and downwelling SSR show similar reductions for both the DIE and the IEO cases. suggesting that during this time period the radiative effects are primarily due to changes in the LWP rather than those from the aerosol direct effect. Overall, the changes to both radiative fluxes in the DIE and IEO cases led to a decrease in surface temperature of over 0.5 K; however, that decrease is not statistically significant.

The amount of cloud coverage is also linked to the radiative fluxes. In general, all six model runs were similar to the observed cloud fraction in both coverage time as well as cloud depth and thickness. The most significant differences in cloud fraction between the model and the observations were in regards to the timing of the convective events. The cumulus clouds associated with the cold front arrived at the SGP Central Facility later than observed and the model produced stronger convection and taller clouds on day 79. While these differences can change the timing of values based on the SGP Central Facility, they will not impact domain averaged values such as rainfall.

Averaged over the entire time period, for the IEO cases cloud fraction and aerosol concentration were positively correlated, as expected. However, the DIE cases showed practically no change in cloud fraction. The difference can be tied to two specific times: about 0700Z on day 77 and about 0000Z on day 79. In the DIE cases, cloud fraction was negatively correlated during low-level stratus clouds on day 77 and positively correlated during shallow cumulus on day 79, with respect to aerosol concentration. These differences offset each other producing no net change in cloud fraction. For the IEO cases, the cloud fraction for both day 77 and day 79 were positively correlated leading to a net increase in cloud fraction.

Cloud fraction, as previously stated, is determined from the total water mixing ratio of all the hydrometeors, Qtot. As expected, cloud droplet Nc and mixing ratio are positively correlated to aerosol concentration. In an environment where LWP is constant, this would cause a reduction in raindrop water mixing ratio; however, LWP is allowed to vary in this model. While LWP increases with more aerosols, it is not large enough to

offset the additional cloud droplets, producing a reduction in raindrops. Because this is a mixed-phase case, and this model includes mixed-phase processes, the total ice amount is also significant. Like in Case A, more aerosols led to more ice particles but a lower ice water mixing ratio.

Because most of the precipitation associated with this case is of convective origin, the changes in all three drops/particles are important. Like *Li et al.* [2008] showed, for a deep convective case the relationship between aerosol concentration and rainfall is nonlinear. Figure 43 shows that initially a precipitation enhancement is present; however, after a certain threshold a reduction of precipitation is noticed. The reduction in precipitation is more prevalent in the DIE case than in the IEO case. While both total ice water mixing ratio and total ice particle Nc were at their peak values during both convective events, they do not explain the highest rainfall amounts during the SGP aerosol profiles. The most reasonable explanation incorporates the cloud, rain, and ice values. As cloud water and droplet values linearly increase, one would expect the inverse to be true of rain water and drops. Despite this expectation, the decrease in rain values from clean to SGP aerosol profiles is not as steep as expected, and in the IEO SGP case the rain water mixing ratio values increase. In the SGP aerosol profile, this could be due to an ideal concentration of all three values that leads to a precipitation enhancement.

There is a similar expectation with regards to vertical velocity—increased amounts of aerosols should enhance the updraft and downdraft speeds. Averaged over the entire time period this is the case as shown in Figure 51a; however, Figure 55 shows

that during both convective periods, the polluted cases have some of the weakest updrafts and downdrafts. Because the updraft and downdraft are weakened, this can also contribute to a decrease in precipitation. *Li et al.* [2008] showed a similar trend where initially aerosols increased updraft speeds; however, at highly polluted conditions, the updraft was weakened.

During the stratiform precipitation period of this case, despite having less vertical structure, the presence of some remaining ice particles may invalidate the typical warm rain assumption. In this case, it appears to have led to increased precipitation in the IEO polluted case. This can also be seen from about 1000Z on day 77 to 1200Z on day 78 when raindrop Nc is similar between all six cases. Cleaner atmospheric conditions due to the cold frontal passage may also explain the enhancement during the low-level startiform period. The DIE polluted case continuously has among the lowest precipitation rates for over three-halves of the time period despite rain and ice Nc as well as updraft velocities suggesting otherwise. It is not until day 79 that some of this precipitation is released with rainfall rates 0.2 mm hr^{-1} higher than all other cases at that time.

3.4 Intercomparison and Discussion

The synoptic weather setup was unique for each of the three cases. For Case A, a low pressure system developed nearby to the domain which allowed several cloud types to pass through as the system grew and matured. For Case D, a few different weather systems passed by the domain, but not directly through it. This primarily caused only

non-precipitating clouds from the far reaches of each system to pass through the domain. It was only at the end that a few shallow cumulus clouds reached the domain from a low pressure system far to the south. For Case E, initially a cold front passed through the domain providing the deepest convection of any case. After its passage, an upper-level low hung around keeping low-level stratiform clouds over the domain for an extended period of time. Despite the differences between the forcing mechanisms in each, there were similarities between which cloud types formed over the domain as well as similar trends between certain variables.

For each case, averaged over the entire time period, there was no uniformity on how aerosol concentration or which radiation scheme was used impacted the cloud coverage. In some cases, the cloud fraction increased while in others it decreased. For each individual event, it appears that the cloud fraction for DIE and the IEO cases trended opposite one another—for instance if the DIE generally increased then the IEO generally decreased. For Cases D and E, during periods of cumuliform clouds, the polluted DIE cases showed a decrease in cloud fraction when compared to the polluted IEO cloud fraction. This decrease is likely due to reduced convection caused by a reduction in surface warming by the SSR, which was influenced by the inclusion of the aerosol direct effect. For other periods of clouds, several factors likely caused the lack of similarity such as: differences in the amount of activated aerosols, cloud type, or the type of forcing mechanism that formed the clouds.

Despite some inconsistencies in cloud fraction between similar cloud types in different cases, rain rates did show similarities. In all three cases there was at least one

convectively forced rain rate maxima. Of these convectively forced maxima, in each case at least one showed a nonlinear trend in precipitation which includes: 0000Z on day 63, 1600Z on day 74, and 0300Z on day 76. Each of these convective events showed that initially, increasing aerosol concentration can enhance precipitation but at some point a certain aerosol concentration will instead reduce precipitation. Since most of the accumulated precipitation is primarily of convective origin in cases D and E, this same trend can be seen in the time averaged precipitation values (Figures 27 and 43). In Case A, however, the total precipitation comes from several different sources and ice particles are also present throughout the entire time rain is occurring. Typically, during a stratiform period only warm-rain processes take place so a reduction in precipitation will occur; however, due to the ice particles throughout, Case A experiences a net precipitation enhancement.

As has been shown in many previous studies, as the concentration of aerosols increases so too does the concentration of cloud droplets and Qc. The increase in cloud Nc reduces the cloud droplet effective radius making raindrop formation more difficult thereby reducing raindrop Nc and Qr. Many previous studies have assumed that the LWP remained constant, but this model allows LWP to vary. The LWP in most cases was positively correlated to aerosol concentration, but in some cases this increase was not significant. Regardless, the Qr did not decrease as quickly as the Qc from clean to SGP aerosol profiles in every case. The raindrop Nc also did not decrease as quickly as the cloud droplet Nc increased from clean the SGP aerosol profiles in most cases. The largest decreases in Qr and raindrop Nc occurred from the SGP to polluted aerosol

profiles. This combination of the steady increase in cloud water and droplets with the only gradual decrease in rain water and droplets could be why the SGP aerosol profiles often had the most rainfall. The sharper decrease in in rain water and drops from SGP to polluted aerosol profiles could also explain the decrease in precipitation for the polluted cases.

Changes to the cloud and rain water and drop quantities are not the only hydrometeors to impact precipitation, because most clouds in these cases were mixed-phase clouds the presence of ice is also important. In most cases, increased amounts of aerosols lead to an increase in the total ice Nc, which is expected due to aerosols acting as IN. However, in most cases, as the total ice Nc increased, the total ice water mixing ratio decreased meaning more ice particles at smaller sizes. Generally, having more ice particles is beneficial as they will grow at the expense of cloud droplets and eventually become large enough to fall out and produce rain.

In this modeling study, while the precipitation maxima often occurred at the same time as local total ice particle Nc maxima, the model runs with the most ice particles—generally polluted cases—did not have the highest rainfall rates. This would suggest a delicate balance between cloud, rain, and ice drop Nc is more relevant to precipitation increases than any one hydrometeor. It also explains why the SGP has the highest rainfall rates, as it is the closest of the three aerosol profiles used in this study to that equilibrium point.

Previous studies have also suggested that the presence of more ice particles can aid in vertical heat transport and invigorate the updraft. While not a one-to-one

relationship, model results from this study suggest that maximum updraft and downdraft values appear to be related to the total ice particle Nc. In Cases D and E, the vertical velocities were also almost directly related to the amount of accumulated precipitation. So, in addition to a delicate balance in hydrometeors, the changes to vertical velocity can influence precipitation, especially in convective cases. Often the increase in updraft and downdraft speeds were either equally balanced or the updraft grew faster; however, for the polluted cases in Cases D and E, the downdraft outweighed the updraft leading to a reduction in the overall average core vertical velocity. The reduction in mean vertical velocity also corresponded with a reduction in precipitation rates for the polluted cases.

In addition to the effects on precipitation, the aerosol concentration almost uniformly altered radiative fluxes. In both the DIE and IEO cases, the aerosol concentration and LWP were generally positively correlated. Changes to the LWP alters the optical depth of clouds impacting SSR while changes to the amount of water vapor in the atmosphere can change the OLR. As expected, both the DIE and IEO cases showed at least some decrease in SSR with respect to increased aerosol concentration. By including the direct effects of aerosols in the DIE cases, the SSR reduction was significantly greater. Over all three cases, for the DIE cases, the SSR reduction was between 20 – 40 W m^{-2}. Despite the uniformity in the SSR across all three cases, the same is not present for the OLR regardless of if it was a DIE or IEO case. In some cases the OLR increased while in others it decreased; however, in spite of the differences between each case, the change in OLR was never greater than about 5 W m^{-2}. So, for all three cases when using the DIE, a net reduction in the radiative fluxes was always

present. Pertaining to surface temperature, the IEO cases showed generally no change. But for the DIE cases, the surface temperature decreased for all three cases but with little to no statistical significance.

4. SUMMARY AND CONCLUSIONS

A modified version of the WRF model was used to investigate the direct and indirect effects of aerosols on three specific cases at the SGP Central Facility during the March 2000 Cloud IOP campaign. The WRF model was previously adapted to incorporate a two-moment bulk microphysical scheme and a modified Goddard shortwave radiation scheme. The microphysical scheme was implemented to include the mass mixing ratio as well as Nc for five hydrometeors as well as thirty-two microphysical processes between them allowing for inclusion of the aerosol indirect effect. The radiation scheme was implemented to include radiative forcing by the aerosol direct effect.

Three cases from the March 2000 Cloud IOP campaign were used in this study. Case A, March 1-4, 2000, primarily experiences clouds to the north of a developing low pressure system. Case D, March 12-15, 2000, is a low precipitation event consisting of mainly cirrus clouds. Case E, March 15-19, 2000, pertains to the clouds associated before and after a cold front passes through the domain. For each case, three different aerosol profiles were used: a clean background continental profile, a profile based on observations from the 2003 Aerosol IOP campaign at the SGP site, and a polluted profile which is has a concentration of aerosols ten times larger than the SGP profile. For each aerosol profile, two separate model runs were used: one including only the aerosol indirect effect and one including both the aerosol direct and indirect effects. This give a

total of six model runs per case and a total of eighteen different model for the whole study.

Over the entire study, aerosols had the largest impacts on SSR, precipitation amounts, and microphysical properties. Aerosols did change the overall cloud fraction between each model run, but the only significant trends were a reduction in cumulus clouds for polluted cases. For OLR, trends were related to the overall cloud fractions where some events experienced an increase while others experienced a decrease. For the SSR, increased aerosol concentration led to a greater reduction in the DIE cases than in the IEO cases. This follows expectations as both cases showed similar increases in LWP but only the DIE cases included the added SSR reductions due to aerosol direct effect. While the SSR as well as net radiative fluxes decreased over all cases, the surface temperature only showed slight decreases, which were mainly statistically insignificant. Even though a small decrease in temperature is seen, this data suggests that an extremely polluted case with much more aerosol loading is likely needed for significant global cooling.

Cloud type, the inclusion of ice into the microphysical processes, and the variation of vertical velocity all with respect to the aerosol concentration led to significant, often nonlinear, changes to precipitation amounts. Each case had at least one period of convective precipitation with nonlinear precipitation changes. During the convective periods, from clean to SGP profiles precipitation was enhances but from SGP to polluted profiles precipitation was suppressed. Only Case A, which contained several

cloud type precipitation sources but always included some ice particles, saw a positive correlation between aerosol concentration and precipitation.

The data from this study suggests that instead of any linear relationship between water mixing ratio and particle Nc, a delicate balance between cloud, rain, and total ice drop and water mixing ratio changes the maximum precipitation, especially in convective cases. Often the SGP aerosol profile experienced this perfect balance. For this profile, cloud droplet and total ice particle Nc were elevated while raindrop Nc was diminished but all three were not elevated or diminished substantially enough to destroy the balance.

For the convective cases, vertical velocity also influences precipitation amounts. When precipitation rates are positively correlated to aerosol concentration, the updraft increased either equally or more than the downdraft; however, when the precipitation rates decreased with more aerosols, the mean vertical velocity also decreased implying either stronger downdrafts or weakening updrafts. The relationship to the vertical velocity also explains how Case A, a case that had several precipitation sources, showed a linear precipitation trend.

In summary, for the direct effect, more aerosols will reduce the SSR, but for a significant temperature reduction a highly polluted event is required. For the indirect effect, a delicate balance is necessary for precipitation enhancement between the cloud, rain, and ice drop Nc as well as their water mixing ratios. If the precipitation is convectively driven, then the balance between the updraft and downdraft is also necessary. These balances need to be studied in further detail to determine what their

exact thresholds are, specifically between different cloud types and different synoptically driven cases. If the thresholds can be found for most cases, they can be extremely useful for present areas of research such as weather modification.

REFERENCES

Ackerman, A. S., O. B. Toon, D. E. Stevens, A. J. Heymsfield, V. Ramanathan, and E. J. Welton (2000), Reduction of tropical cloudiness by soot, *Science*, *288*, 1042-1047, doi: 10.1126/science.288.5468.1042.

Albrecht, B. A. (1989), Aerosols, cloud microphysics, and fractional cloudiness, *Science*, *245*, 1227-1230.

Bruce, C. W., T. F. Stromberg, K. P. Gurton, and J. B. Mozer (1991), Trans-spectral absorption and scattering of electromagnetic radiation by diesel soot, *App. Opt.*, *30*, 1537-1546.

Cantrell, C. and A. Heymsfield (2005), Production of ice in tropospheric clouds, *Bull. Amer. Meteor. Soc.*, *86*, 795-807, doi: 10.1175/BAMS-86-6-795.

Cheng, C.-T., W.-C. Wang, and J.-P. Chen (2007), A modeling study of aerosol impacts on cloud microphysics and radiative properties, *Q. J. R. Meteorol. Soc.*, *133*, 283-297, doi: 10.1002/qj.25.

Coakley, J. A., Jr., R. D. Cess, and F. D. Yurevich (1983), The effect of tropospheric aerosols on the Earth's radiation budget: a parameterization for climate models, *J. Atmos. Sci.*, *40*, 116-138.

Cohen, B. G. and G. C. Craig (2006), Fluctuations in an equilibrium convective ensemble. Part II: numerical experiments, *J. Atmos. Sci.*, *63*, 2005-2015.

Fan, J., R. Zhang, G. Li, W.-K. Tao, and X. Li (2007), Simulations of cumulus clouds using a spectral microphysics cloud-resolving model, *J. Geophys. Res.*, *112*, D04201, doi: 10.1029/2006JD007688.

Fan, J., R. Zhang, W.-K. Tao, and K. I. Mohr (2008), Effects of aerosol optical properties on deep convective clouds and radiative forcing, *J. Geophys. Res.*, *113*, D08209, doi: 10.1029/2007JD009257.

Hansen, J., M. Sato, and R. Ruedy (1997), Radiative forcing and climate response, *J. Geophys. Res.*, *102*, 6831-6864.

Haywood, J. and O. Boucher (2000), Estimates of the direct and indirect radiative forcing due to tropospheric aerosols: a review, *Rev. Geophys.*, *38*, 513-543.

Haywood, J. M. and V. Ramaswamy (1998), Global sensitivity of the direct radiative forcing due to anthropogenic sulfate and black carbon aerosols, *J. Geophys. Res.*, *103*, 6043-6058.

Hocking, L. M. (1959), The collision efficiency of small drops, *Q. J. R. Meteorol. Soc.*, *85*, 44-50, doi: 10.1002/qj.49708536305.

Intergovernmental Panel on Climate Change (IPCC) (2007a), *Climate Change 2007: Synthesis Report.* Contribution of working groups I, II, and III to the Fourth Assessment Report of the Intergovernmental Panel on Climate Change [Core Writing Team, R. K. Pachauri, and A. Reisinger (eds.)]. IPCC, Geneva, Switzerland, 104pp.

Intergovernmental Panel on Climate Change (IPCC) (2007b), *Climate Change 2007: The Physical Science Basis.* Contribution of working group I to the Fourth Assessment Report of the Intergovernmental Panel on Climate Change [edited by S. Solomon et al.], Cambridge University Press, Cambridge, United Kingdom and New York, NY, USA.

Jacobson, M. Z. (2001), Strong radiative heating due to the mixing state of black carbon in atmospheric aerosols, *Nature*, *409*, 695-697.

Johnson, B. T., K. P. Shine, and P. M. Forster (2004), The semi-direct aerosol effect: impact of absorbing aerosols on marine stratocumulus, *Q. J. R. Meteorol. Soc.*, *130*, 1407-1422, doi: 10.1256/qj.03.61.

Khain, A. P. (2009), Notes on state-of-the-art investigations of aerosol effects on precipitation: a critical review, *Environ. Res. Lett.*, *4*, doi: 10.1088/1748-9326/4/1/015004.

Kiehl, J. T. and B. P. Briegleb (1993), The relative roles of sulfate aerosols and greenhouse gases in climate forcing, *Science*, *260*, 311-314.

Koren, I., G. Feingold, and L. A. Remer (2010), The invigoration of deep convective clouds over the Atlantic: aerosol effect, meteorology or retrieval artifact? *Atmos. Chem. Phys.*, *10*, 8855-8872, doi: 10.5194/acp-10-885-2010.

Lee, J., P. Yang, A. E. Dessler, B.-C. Gao, and S. Platnick (2009a), Distribution of radiative forcing of tropical thin cirrus clouds, *J. Atmos. Sci.*, *66*, 3721-3731, doi: 10.1175/2009JAS3183.1

Lee, S. S., L. J. Donner, and V. T. J. Phillips (2009b), Sensitivity of aerosol and cloud effects on radiation to cloud types: comparison between deep convective clouds and warm stratiform clouds over one-day period, *Atmos. Chem. Phys.*, *9*, 2555-2575.

Li, G., Y. Wang, and R. Zhang (2008), Implementation of a two-moment bulk microphysics scheme to the WRF model to investigate aerosol-cloud interaction, *J. Geophys. Res.*, *113*, doi: 10.1029/2007JD009361.

Li, G., Y. Wang, K.-H. Lee, Y. Diao, and R. Zhang (2009), Impacts of aerosols on the development and precipitation of a mesoscale squall line, *J. Geophys. Res.*, *114*, doi: 10.1029/2008JD011581.

Li, Z., F. Niu, J. Fan, Y. Liu, D. Rosenfeld, and Y. Ding (2011), Long-term impacts of aerosols on the vertical development of clouds and precipitation, *Nature Geosci.*, *4*, 888-894, doi: 10.1038/ngeo1313.

Pincus, R. and m. B. Baker (1994), Effect of precipitation on the albedo susceptibility of clouds in the marine boundary layer, *Nature*, *372*, 250-252.

Ramanathan, V., P. J. Crutzen, J. T. Kiehl, and D. Rosenfeld (2001), Aerosols, climate, and the hydrological cycle, *Science*, *294*, 2119-2124.

Rogers, R. R. and M. K. Yau (1989), A short course in cloud physics, *Pergamon Press*, Oxford, New York, NY, USA.

Rosenfeld, D. (1999), TRMM observed first direct evidence of smoke from forest fires inhibiting rainfall, *Geophys. Res. Lett.*, *26*, 3105-3108.

Rosenfeld, D., U. Lohmann, G. B. Raga, C. D. O'Dowd, M. Kulmala, S. Fuzzi, A. Reissell, and M. O. Andreae (2008), Flood or drought: how do aerosols affect precipitation? *Science*, *321*, 1309-1313, doi: 10.1126/science.1160606.

Sassen, K., D. O'C. Starr, G. G. Mace, M. R. Poellot, S. H. Melfi, W. L. Eberhard, J. D. Spinhirne, E. W. Eloranta, D. E. Hagen, and J. Hallet (1995), The 5-6 December

19991 FIRE IFO II jet stream cirrus case study: possible influences of volcanic aerosols, *J. Atmos. Sci.*, *52*, 97-123.

Strom, J. and S. Ohlsson (1998), In situ measurements of enhanced crystal number densities in cirrus clouds caused by aircraft exhaust, *J. Geophys. Res.*, *103*, 11355-11361.

Tao, W.-K., X. Li, A. Khain, T. Matsui, S. Lang, and J. Simpson (2007), Role of atmospheric aerosol concentration on deep convective precipitation: cloud-resolving model simulations, *J. Geophys. Res.*, *112*, doi: 10.1029/2007JD008728.

Tao, W.-K., J-P. Chen, Z. Li, C. Wang, and C. Zhang (2012), Impact of aerosols on convective clouds and precipitation, *Rev. Geophys.*, *50*, RG2001, doi: 10.1029/2011RG000369.

Tripathi, S. N., S. Dey, and V. Tare (2005), Aerosol black carbon radiative forcing at an industrial city in northern India, *Geophys. Res. Lett.*, *32*, L08802, doi: 10.1029/2005GL022515.

Twomey, S. (1974), Pollution and the planetary albedo, *Atmos. Eniron.*, *8*, 1251-1256.

Twomey, S. (1977), The influence of pollution on the shortwave albedo of clouds, *J. Atmos. Sci.*, *34*, 1149-1152.

Wang, C. (2005), A modeling study of the response of tropical deep convection to the increase of cloud condensation nuclei concentration: 1. Dynamics and microphysics, *J. Geophys. Res.*, *110*, D21211, doi: 1029/2004JD005720.

Zhang, M., S. Klein, D. Randall, R. Cederwall, and A. Del Genio (2005), Introduction to special section on toward reduction cloud-climate feedback uncertainties in

atmospheric general circulation models, *J. Geophys. Res.*, *110*, D15S01, doi: 10.1029/2005JD005923.

APPENDIX A

EQUATIONS

$$\overline{M} = \frac{1}{N(x,y,z,t)} \sum m(x,y,z,t) \quad (1)$$

$$C = \overline{M} \pm A\frac{S}{\sqrt{n}} \quad (2)$$

APPENDIX B

TABLES

Table 1. Observed and modeled variables and their sources.

Variable Name	*Observation*	*Model*
Cloud Fraction	ARSCL (SGP Central Facility)	5x5 centralized box
Rain Rate / Acc. Rain	ARBRFC (SGP Domain)	SGP Domain
Qc, Qr, Qi	None	SGP Domain
Nc: Cloud, Rain, Ice	None	SGP Domain
W Core	None	SGP Domain
LWP	MWRRET (SGP Central Facility)	5x5 centralized box & SGP Domain
SSR, OLR	BBHRP (SGP Central Facility)	11x11 centralized box
Surface Temperature	Merged Sounding VAP & KPNC METAR (SGP Central Facility)	11x11 centralized box

APPENDIX C

FIGURES

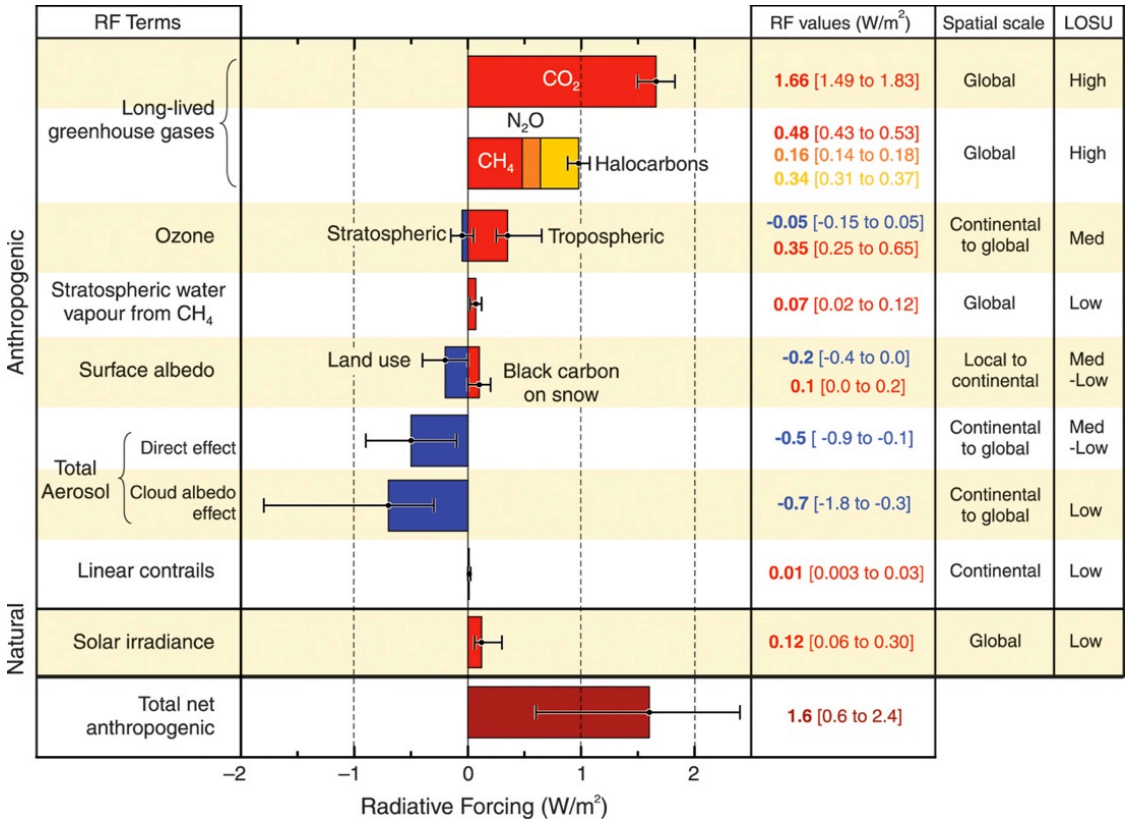

Figure 1. Estimated global average radiative forcing values for 2005 and uncertainty ranges [FAQ 2.1, Figure 2. from *IPCC*, 2007b].

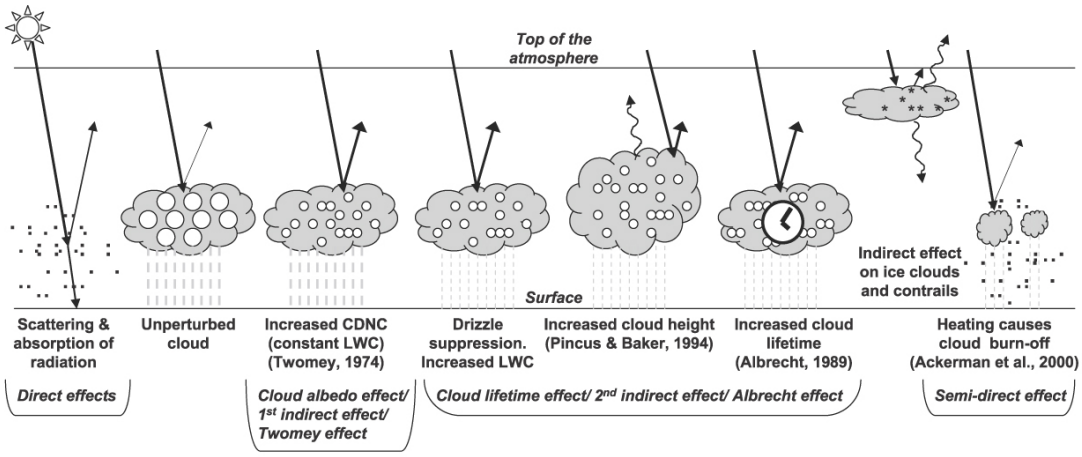

Figure 2. Diagram of the different ways aerosols can impact the global radiation budget [Figure 2.10. from *IPCC*, 2007b].

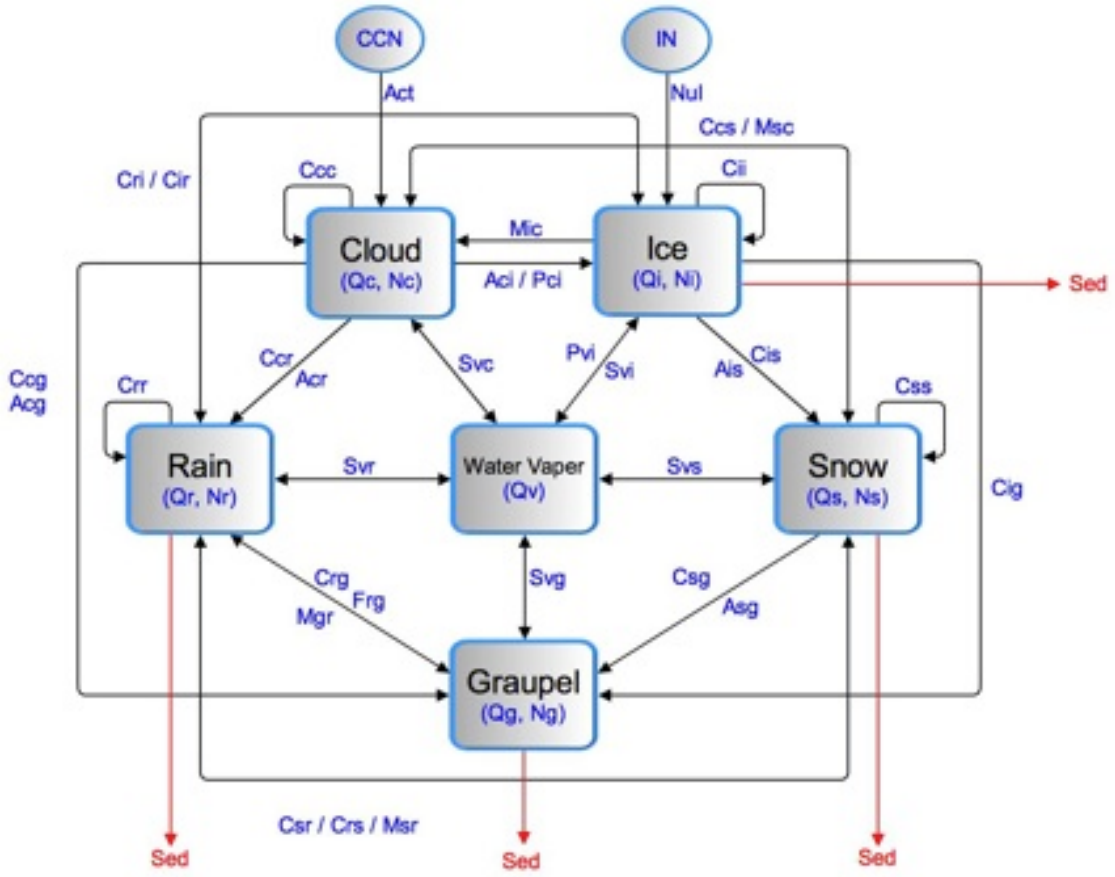

Figure 3. Schematic diagram of the microphysical interactions between the five hydrometeors and the CCN/IN included in the model microphysics scheme.

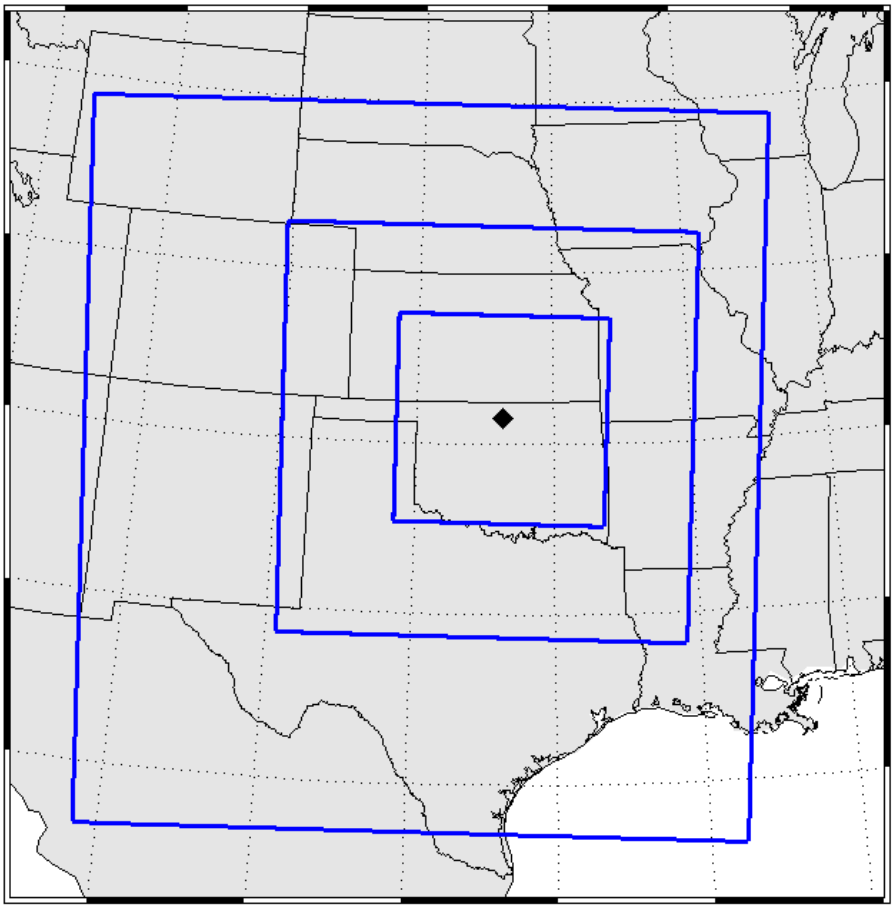

Figure 4. The three nested domains used in the WRF model in this study. The innermost domain has 2 km spatial resolution and is centered at (36.5934°N, 97.5113°W). The diamond represents the SGP Central Facility.

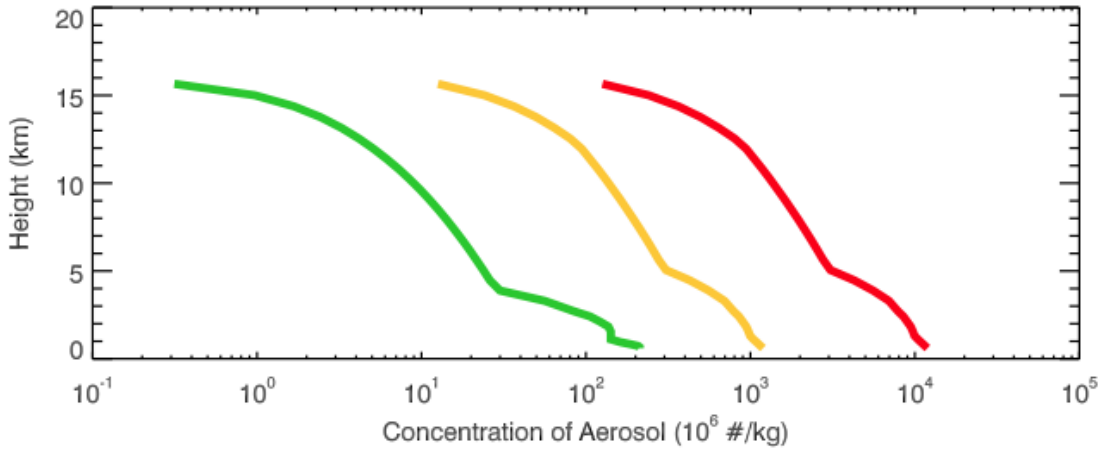

Figure 5. The three vertical aerosol profiles used in this study. Colored profiles correspond to: clean (green), SGP (yellow), and polluted (red).

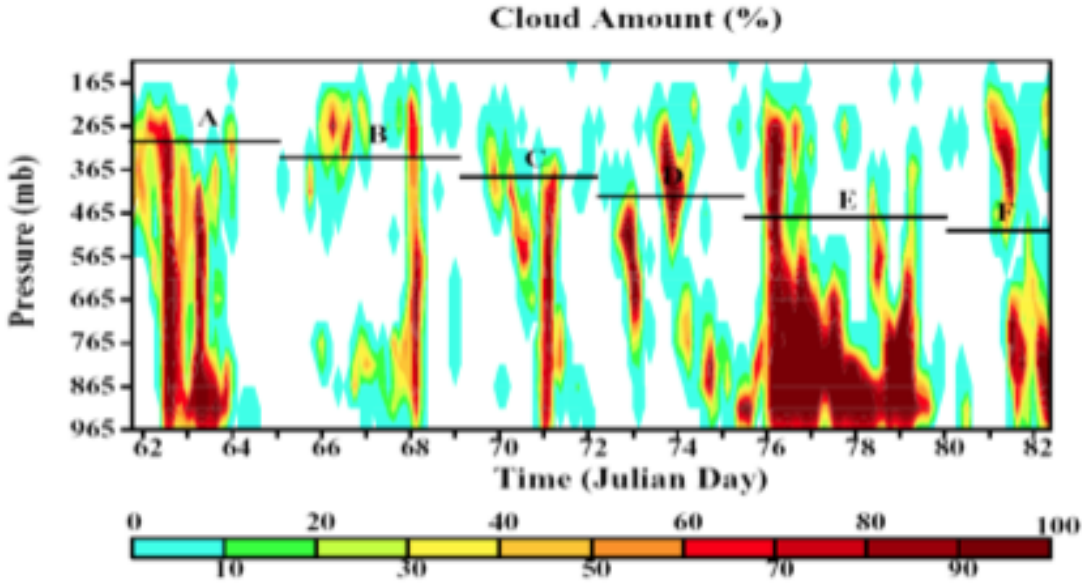

Figure 6. Observed vertical cloud amount profiles from the ARSCL during the March 2000 Cloud IOP campaign showing the six different case periods.

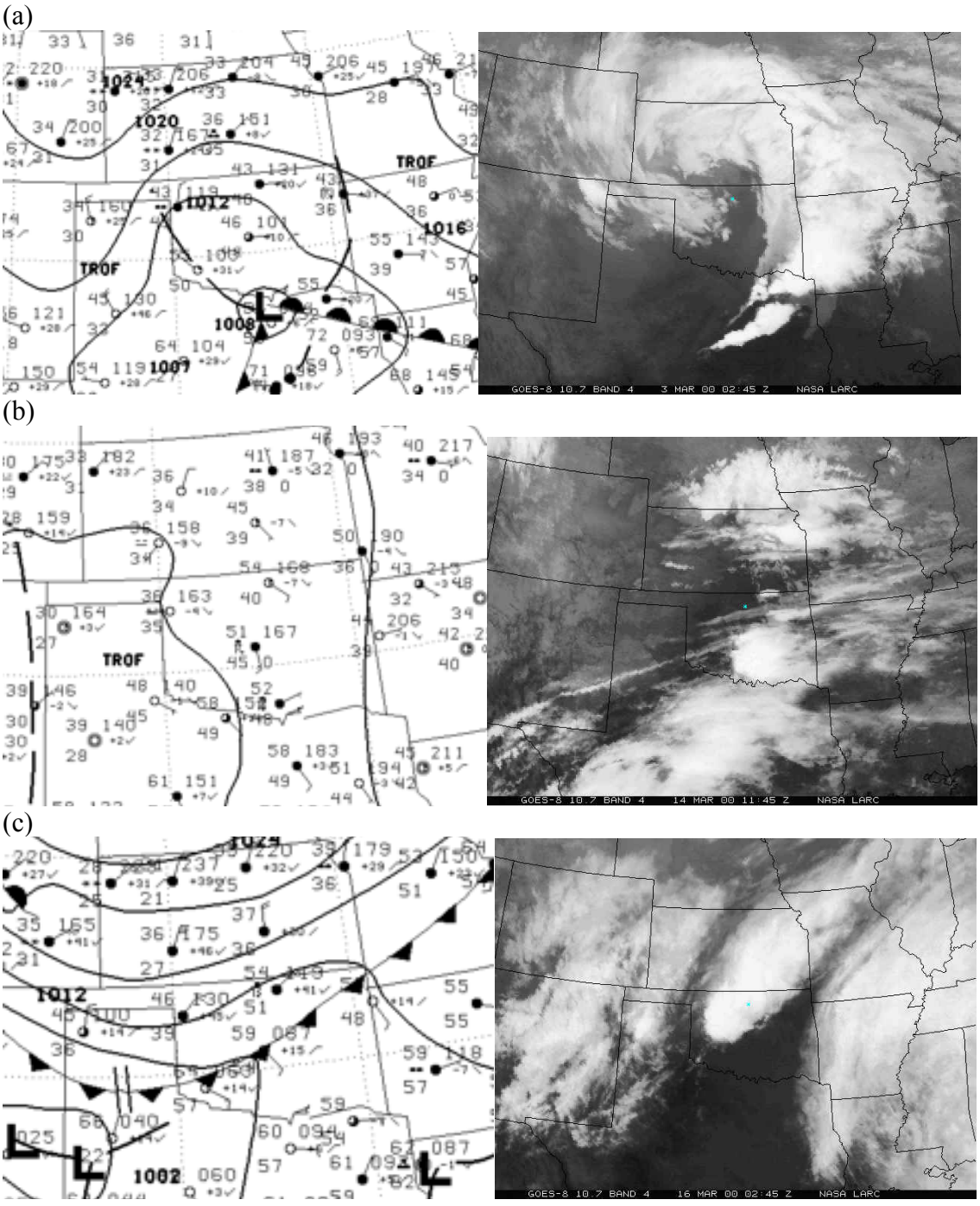

Figure 7. Surface maps (left) and satellite images (right) for each of the three cases in this study. Time and date for each image are: (a) 0300Z on March 3, 2000; (b) 1200Z on March 14, 2000; (c) 0300Z on March 16, 2000. Satellite images were taken 15 minutes before the listed times.

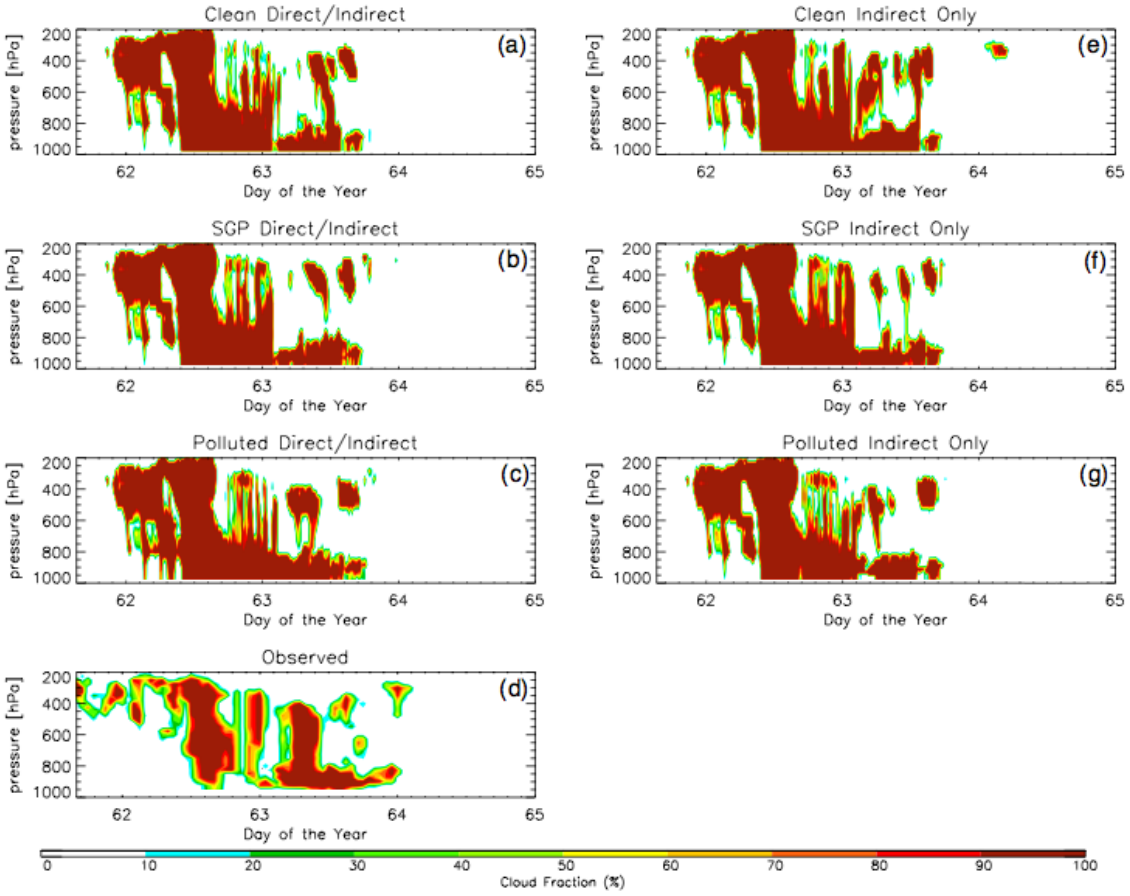

Figure 8. Cloud fraction values for Case A. The figures are for (a), (b), and (c), clean, SGP, and polluted DIE cases, respectively; (d) observations; (e), (f), and (g) clean, SGP, and polluted IEO cases, respectively.

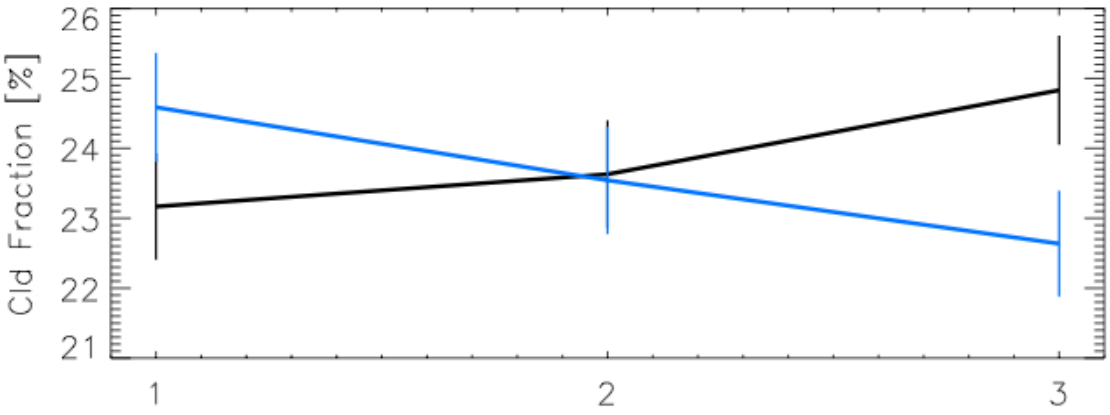

Figure 9. Average cloud fraction for Case A over the entire time period with 95% confidence intervals. The black line is the DIE cases; the blue line is the IEO cases. With 1, 2, and 3 coinciding with clean, SGP, and polluted aerosol profiles.

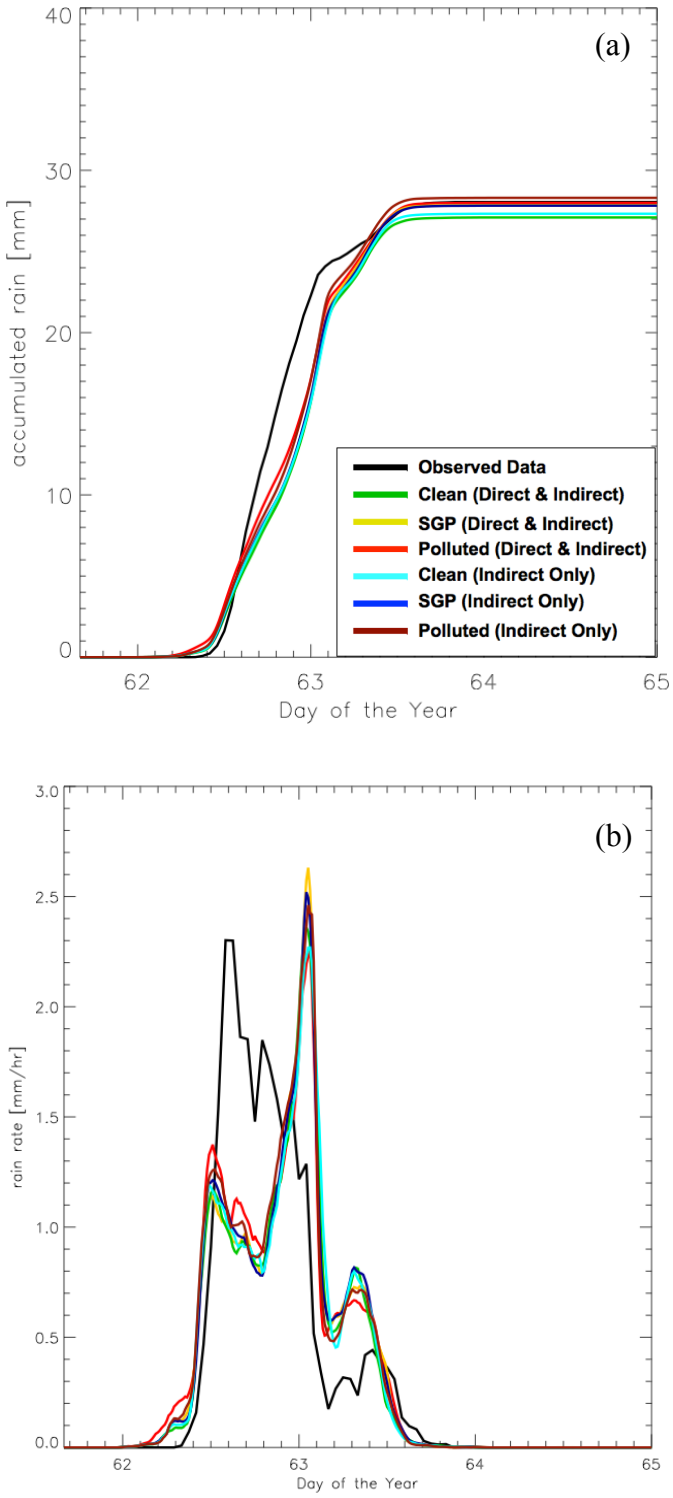

Figure 10. Domain average rainfall rates (a) and domain average accumulated rainfall (b) for Case A.

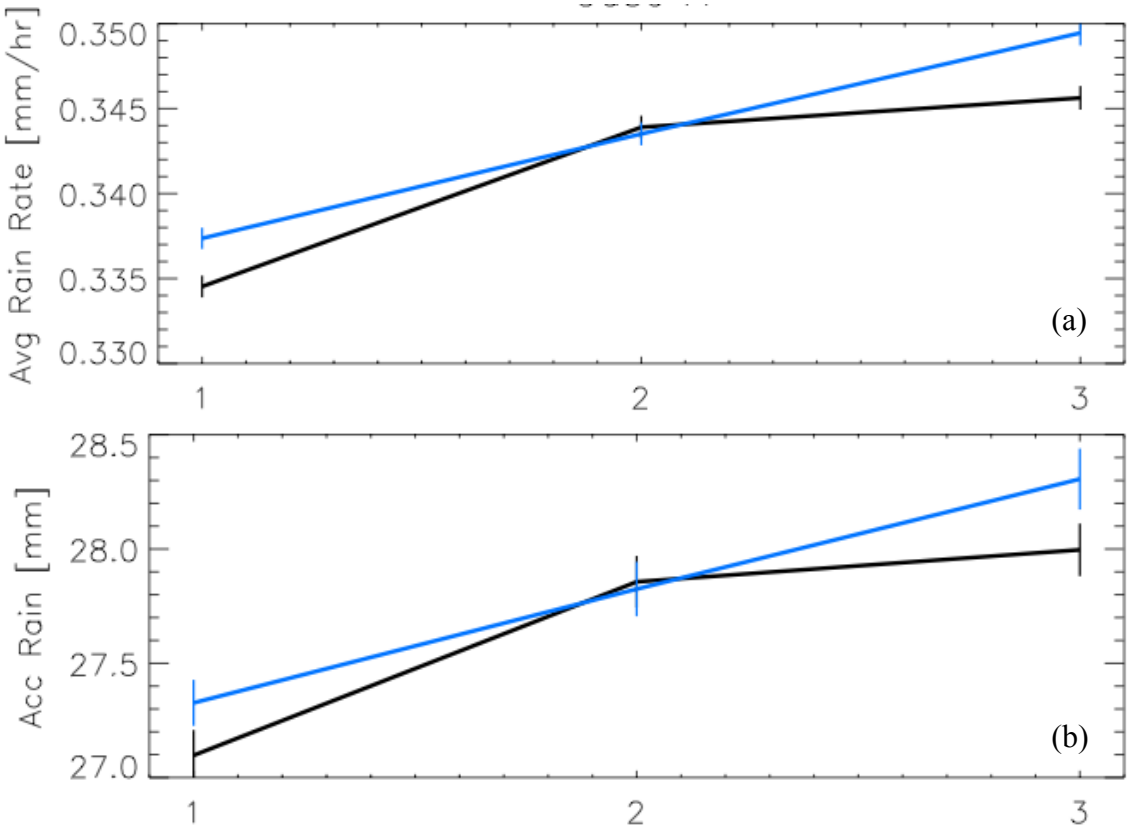

Figure 11. Average rainfall (a) and average accumulated rainfall (b) over the entire time period with 95% confidence intervals for Case A. The black lines are the DIE cases; the blue lines are the IEO cases. With 1, 2, and 3 coinciding with clean, SGP, and polluted aerosol profiles.

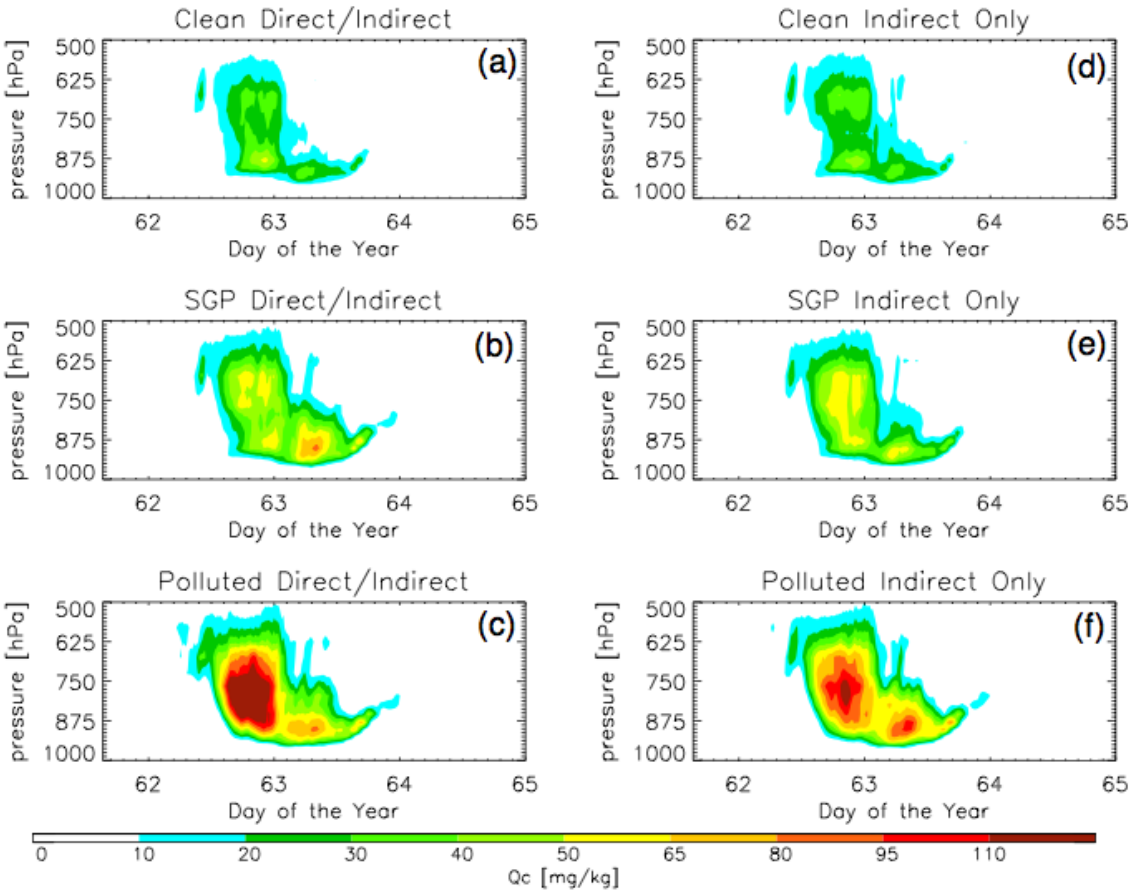

Figure 12. Domain average cloud water mixing ratio for Case A. The figures are for (a), (b), and (c) clean, SGP, and polluted DIE cases, respectively; (d), (e), and (f) clean, SGP, and polluted IEO cases, respectively.

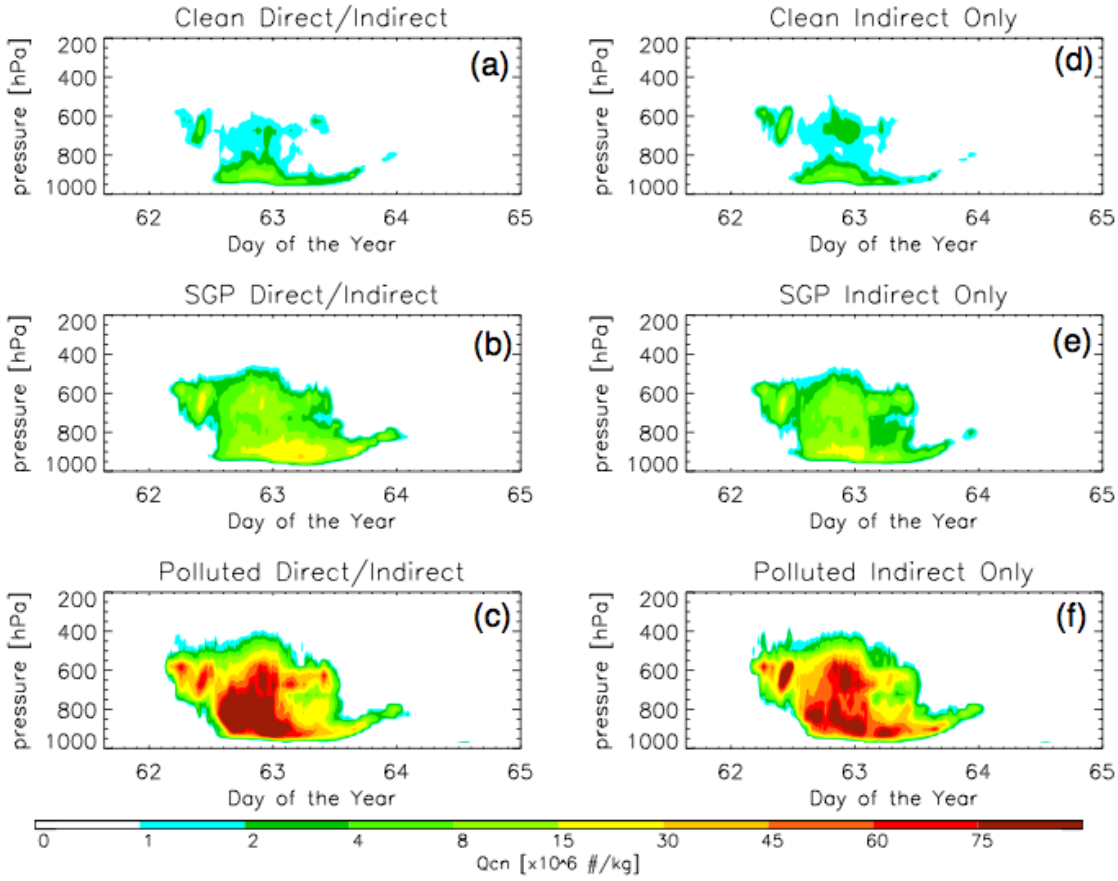

Figure 13. Domain average cloud droplet number concentration for Case A. The figures are for (a), (b), and (c) clean, SGP, and polluted DIE cases, respectively; (d), (e), and (f) clean, SGP, and polluted IEO cases, respectively.

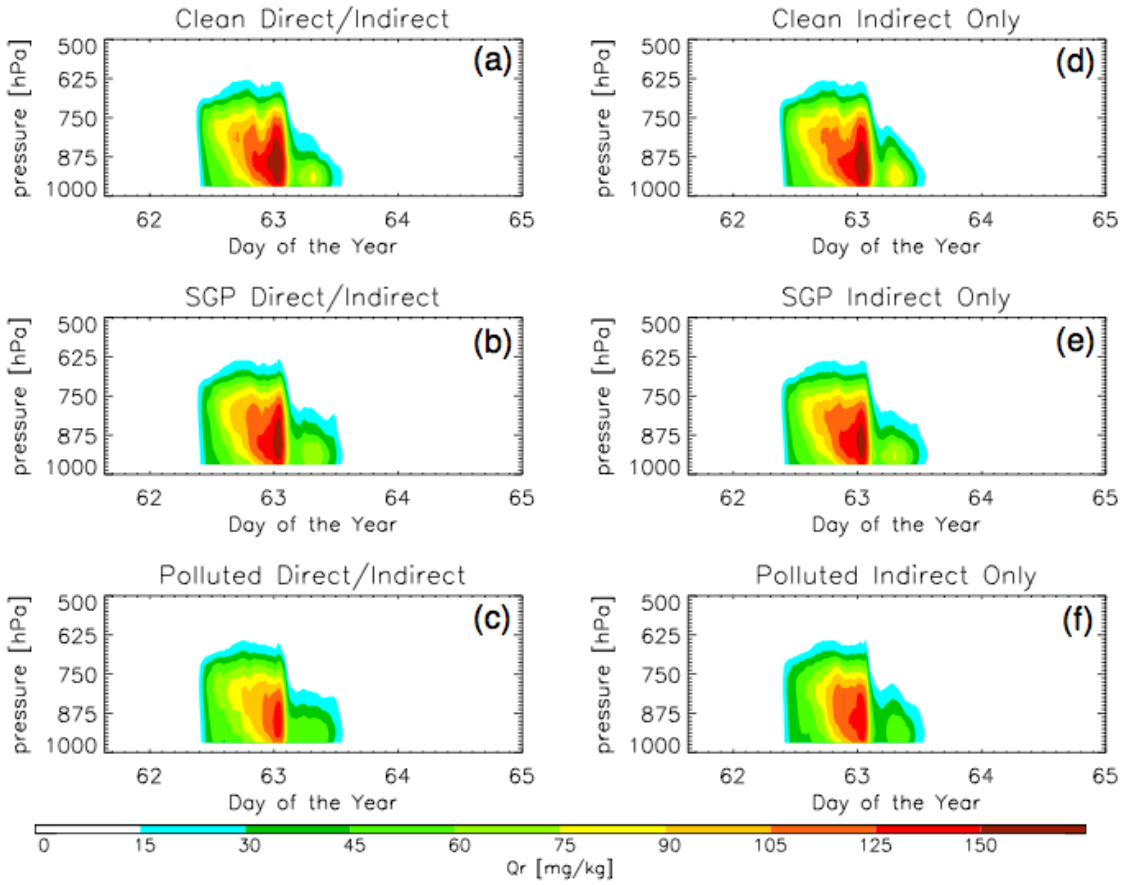

Figure 14. Domain average rain water mixing ratio for Case A. The figures are for (a), (b), and (c) clean, SGP, and polluted DIE cases, respectively; (d), (e), and (f) clean, SGP, and polluted IEO cases, respectively.

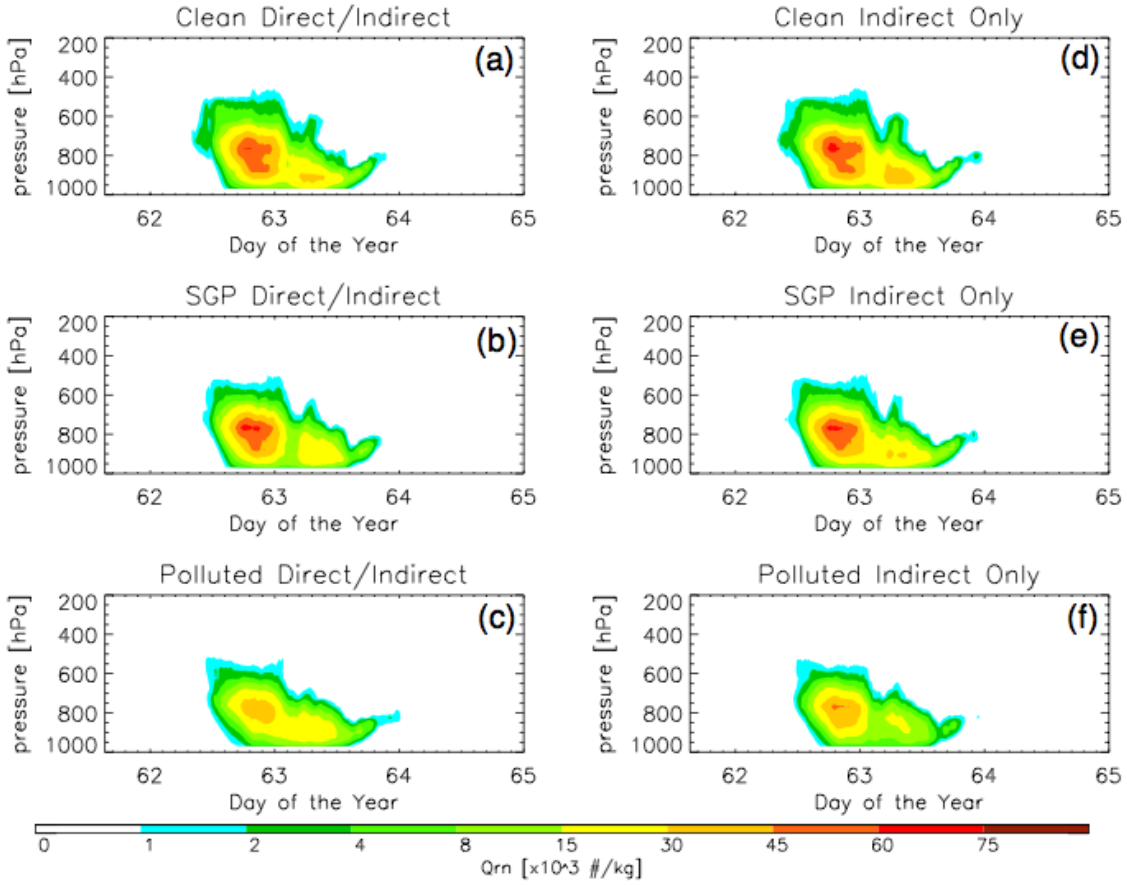

Figure 15. Domain average raindrop number concentration for Case A. The figures are for (a), (b), and (c) clean, SGP, and polluted DIE cases, respectively; (d), (e), and (f) clean, SGP, and polluted IEO cases, respectively.

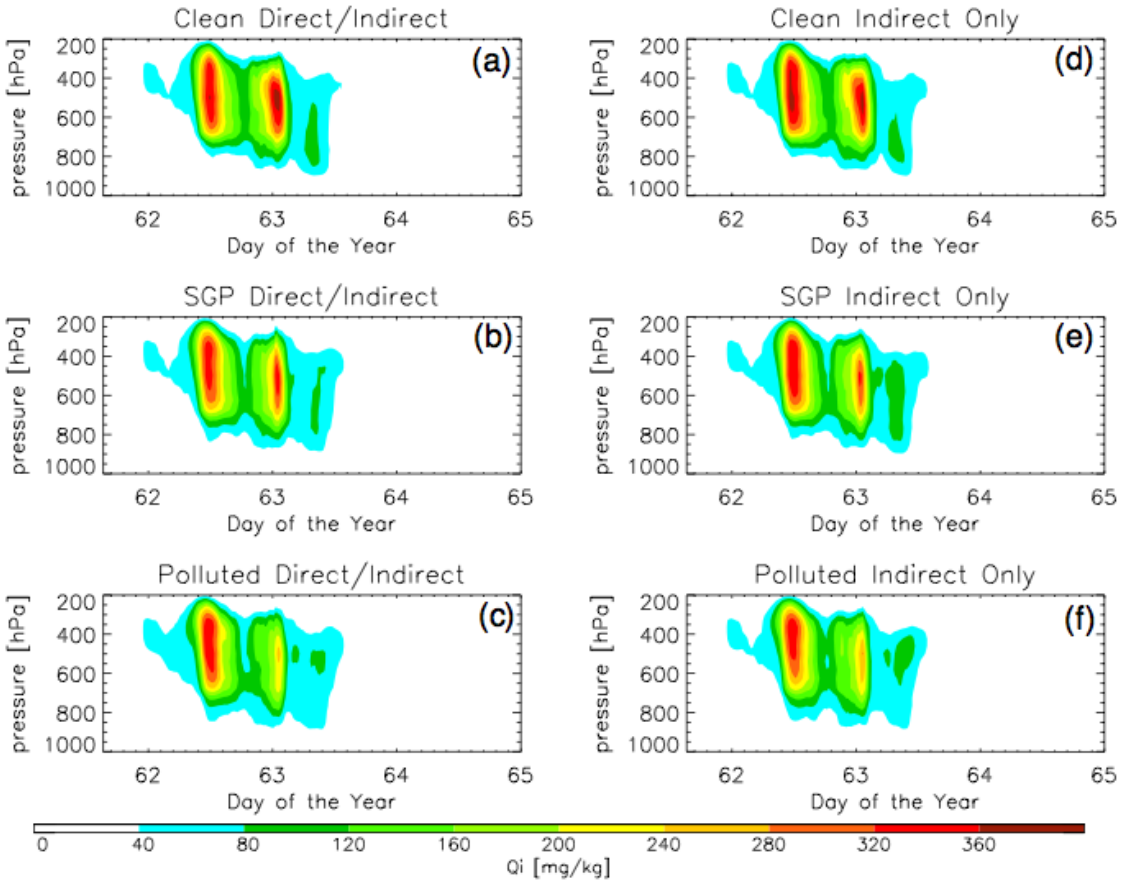

Figure 16. Domain average ice water mixing ratio for Case A. The figures are for (a), (b), and (c) clean, SGP, and polluted DIE cases, respectively; (d), (e), and (f) clean, SGP, and polluted IEO cases, respectively.

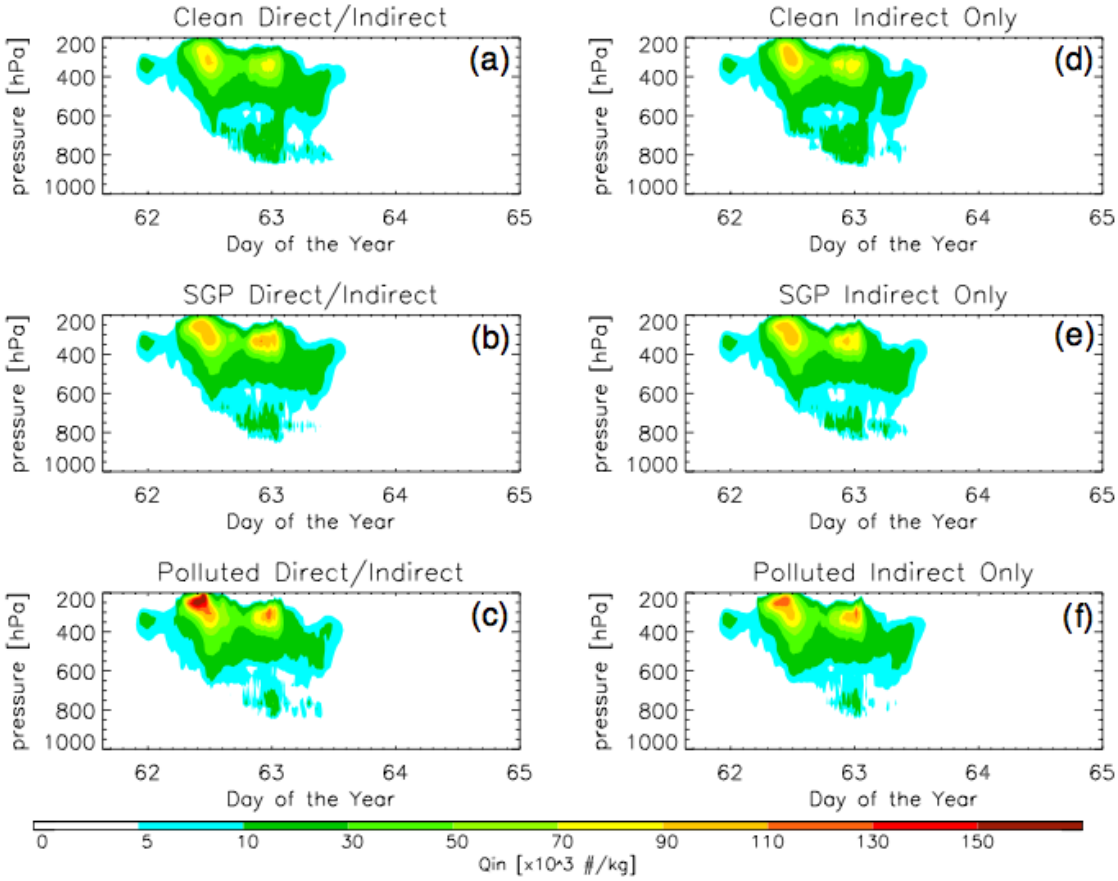

Figure 17. Domain average ice particle number concentration for Case A. The figures are for (a), (b), and (c) clean, SGP, and polluted DIE cases, respectively; (d), (e), and (f) clean, SGP, and polluted IEO cases, respectively.

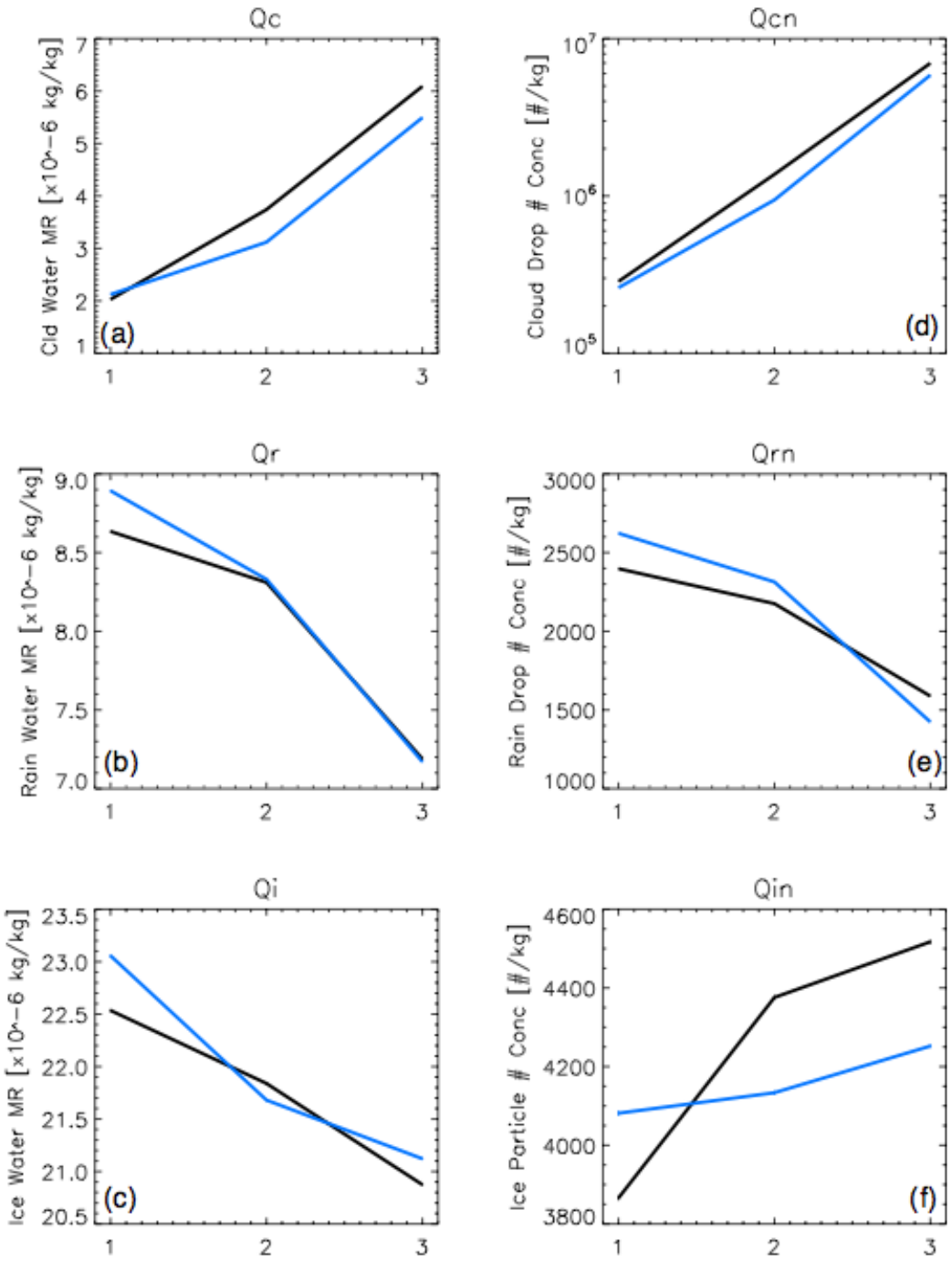

Figure 18. Average mixing ratio over the entire time period for Case A with 95% confidence intervals for cloud (a), rain (b), and ice (c) water. Average number concentration over the entire time period for Case A with 95% confidence intervals for cloud (d), rain (e), and ice (f) drops. The black lines are the DIE cases; the blue lines are the IEO cases. With 1, 2, and 3 coinciding with clean, SGP, and polluted aerosol profiles.

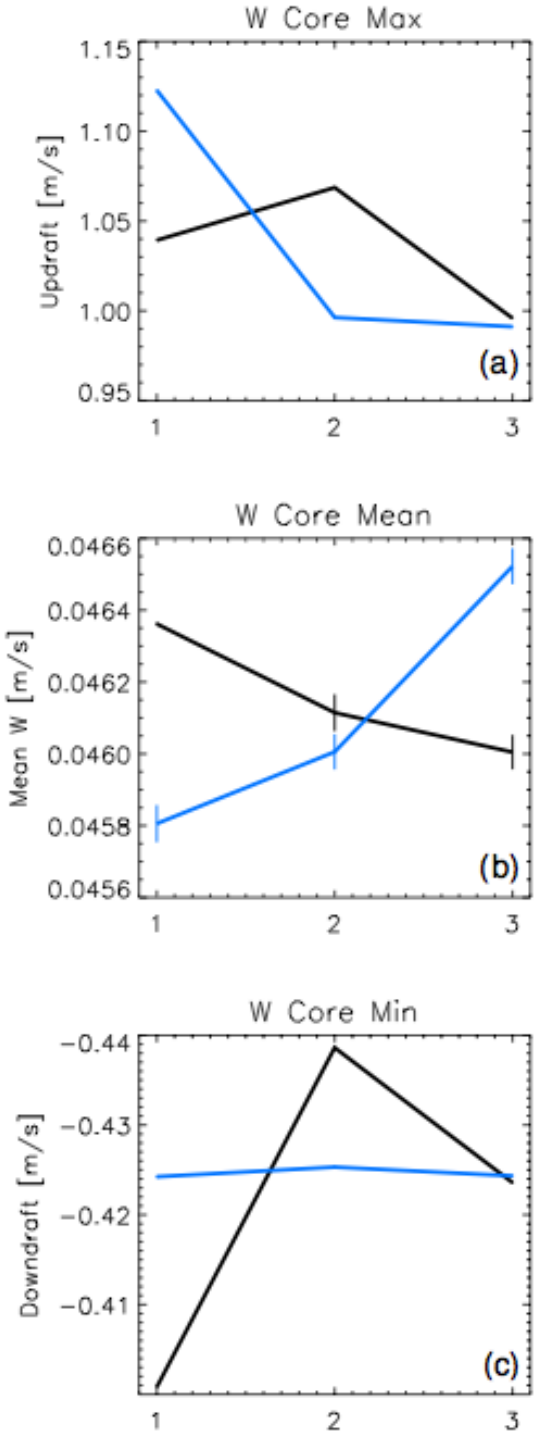

Figure 19. Average vertical velocity in cloudy regions over the entire time period for Case A with 95% confidence intervals for the strongest updraft (a), average velocity (b), and strongest downdraft (c). The black lines are the DIE cases; the blue lines are the IEO cases. With 1, 2, and 3 coinciding with clean, SGP, and polluted aerosol profiles.

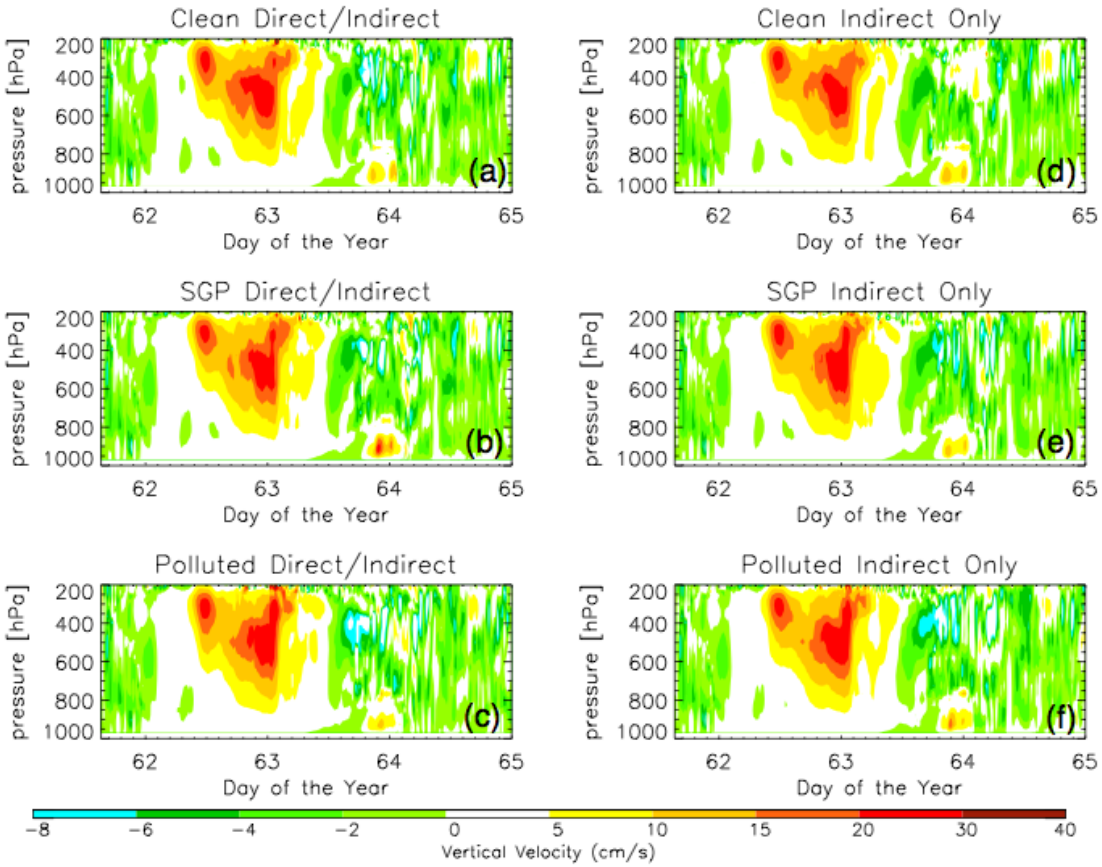

Figure 20. Average vertical velocity in cloudy regions for Case A. The figures are for (a), (b), and (c) clean, SGP, and polluted DIE cases, respectively; (d), (e), and (f) clean, SGP, and polluted IEO cases, respectively.

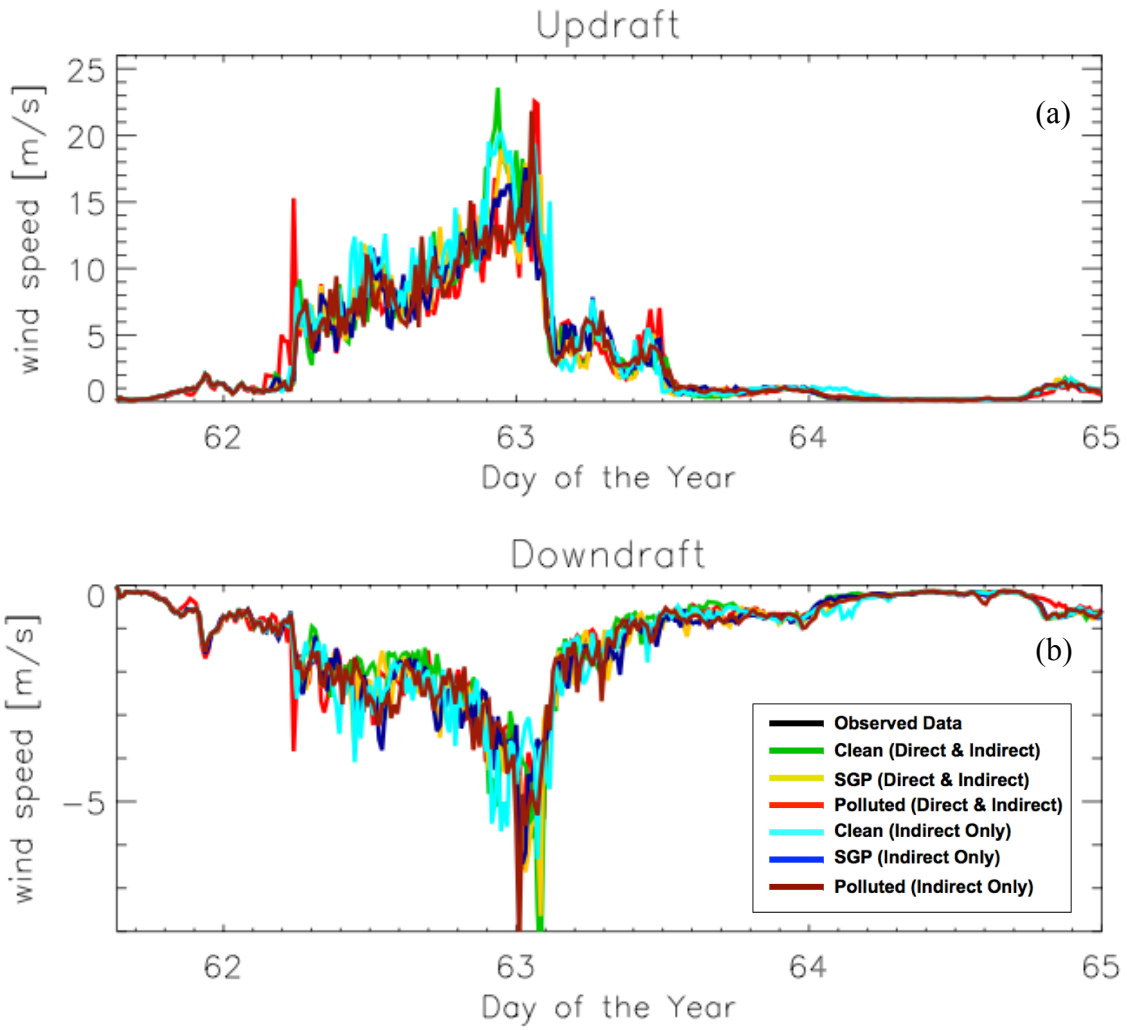

Figure 21. Time evolution of the maximum updrafts (a) and downdrafts (b) in the cloudy regions for Case A.

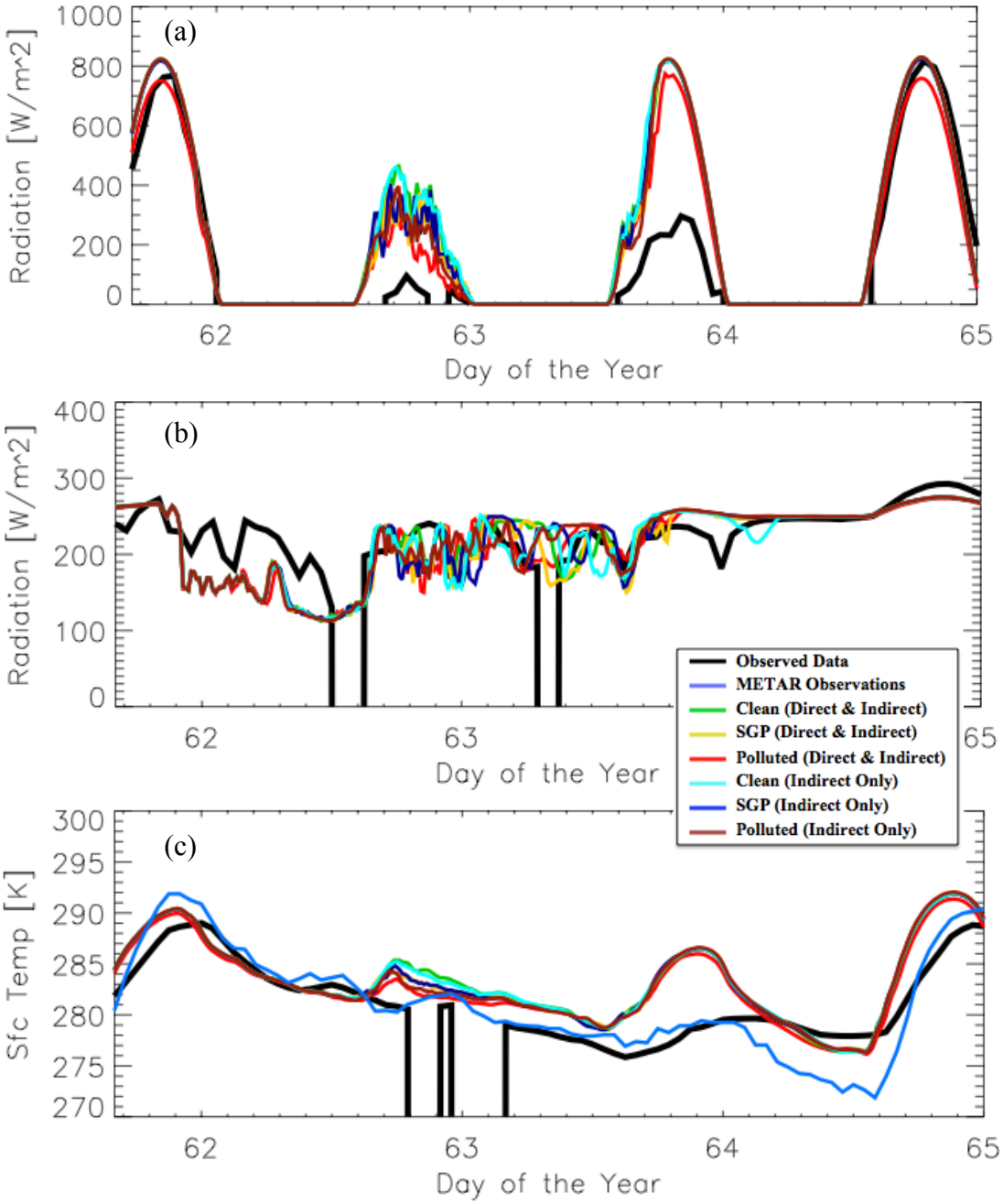

Figure 22. Averaged values of surface shortwave radiative fluxes (a), outgoing longwave radiative fluxes (b), and surface temperatures (c).

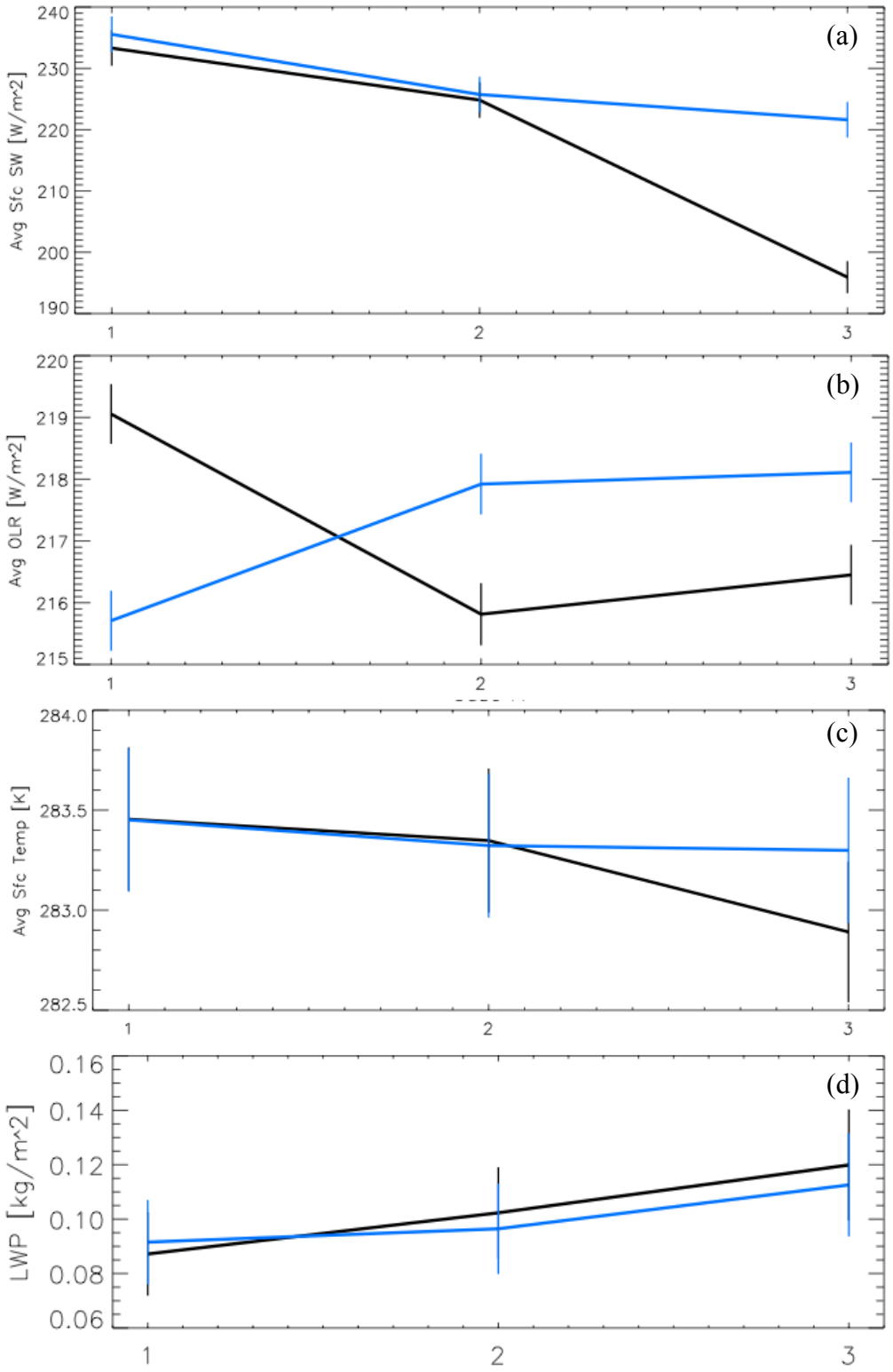

Figure 23. Time averaged values for Case A with 95% confidence intervals for surface shortwave radiative fluxes (a), outgoing longwave radiative fluxes (b), surface

temperatures (c), and domain averaged LWP (d). The black lines are the DIE cases; the blue lines are the IEO cases. With 1, 2, and 3 coinciding with clean, SGP, and polluted aerosol profiles.

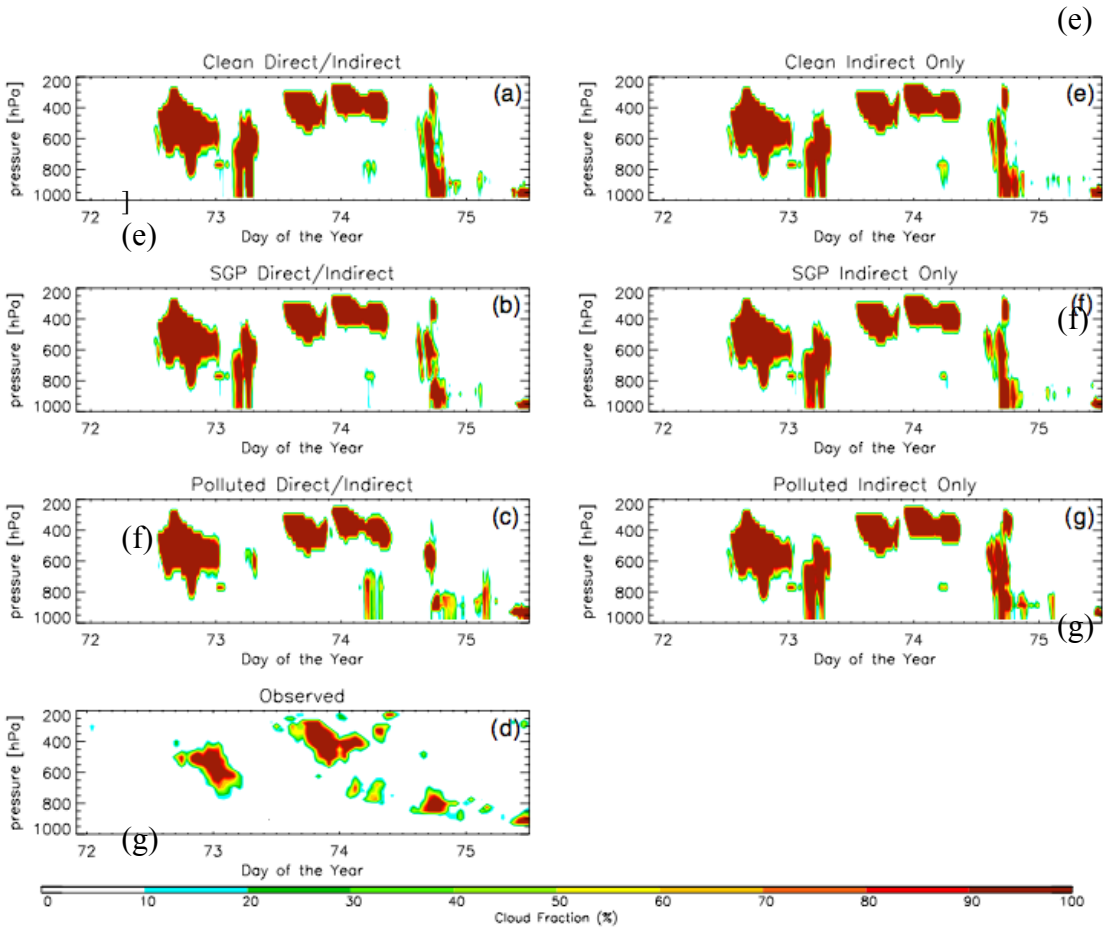

Figure 24. Cloud fraction values for Case D. The figures are for (a), (b), and (c) clean, SGP, and polluted DIE cases, respectively; (d) observations; (e), (f), and (g) clean, SGP, and polluted IEO cases, respectively.

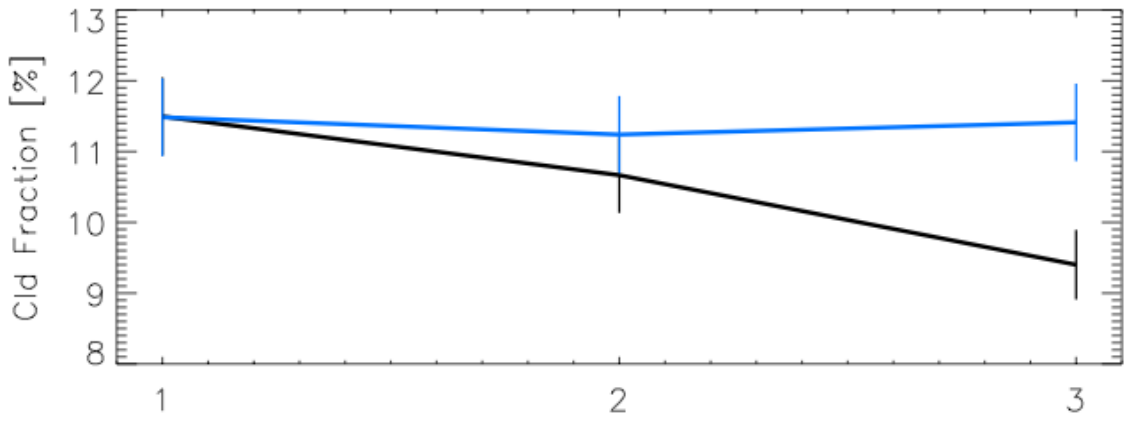

Figure 25. Average cloud fraction for Case D over the entire time period with 95% confidence intervals. The black line is the DIE cases; the blue line is the IEO cases. With 1, 2, and 3 coinciding with clean, SGP, and polluted aerosol profiles.

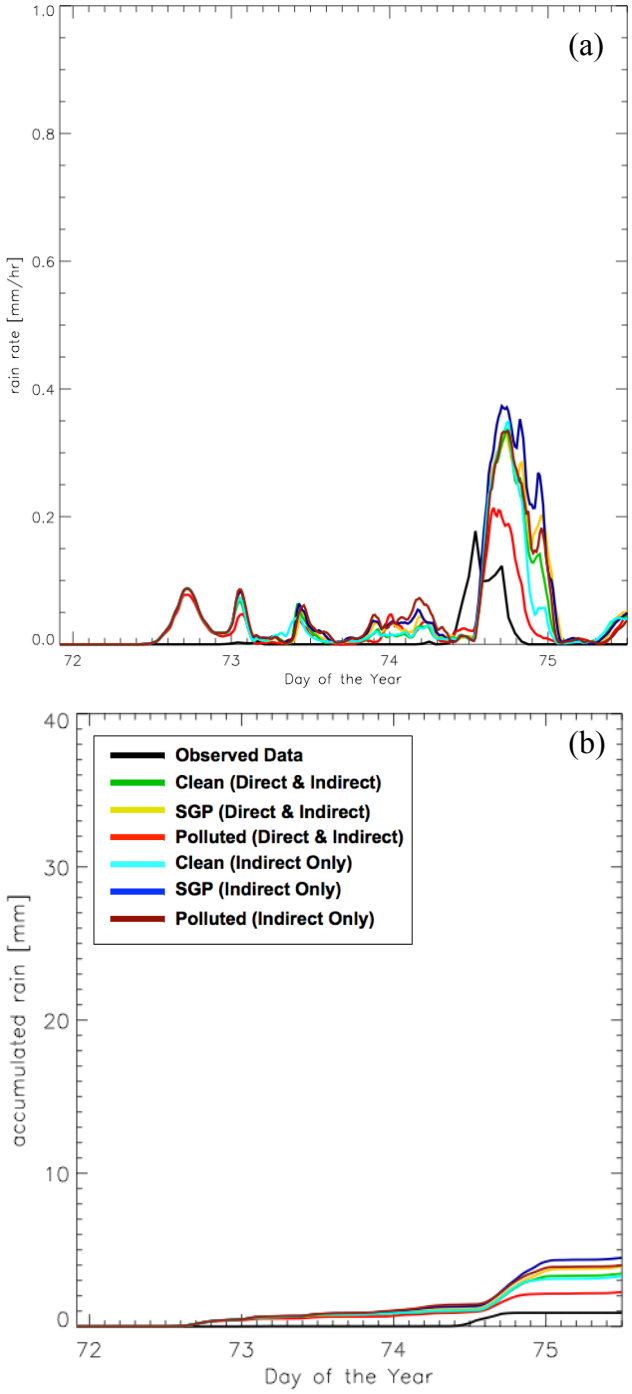

Figure 26. Domain average rainfall rates (a) and domain average accumulated rainfall (b) for Case D.

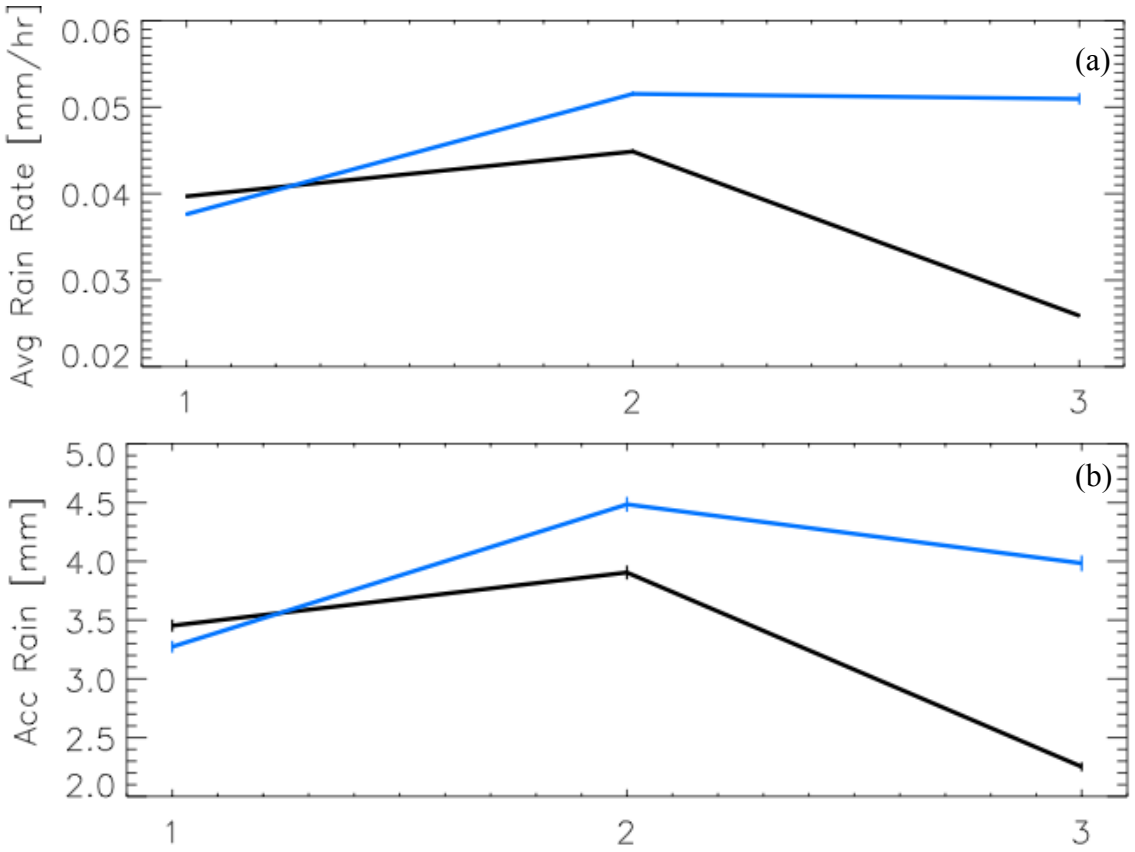

Figure 27. Average rainfall (a) and average accumulated rainfall (b) over the entire time period for Case D with 95% confidence intervals. The black lines are the DIE cases; the blue lines are the IEO cases. With 1, 2, and 3 coinciding with clean, SGP, and polluted aerosol profiles.

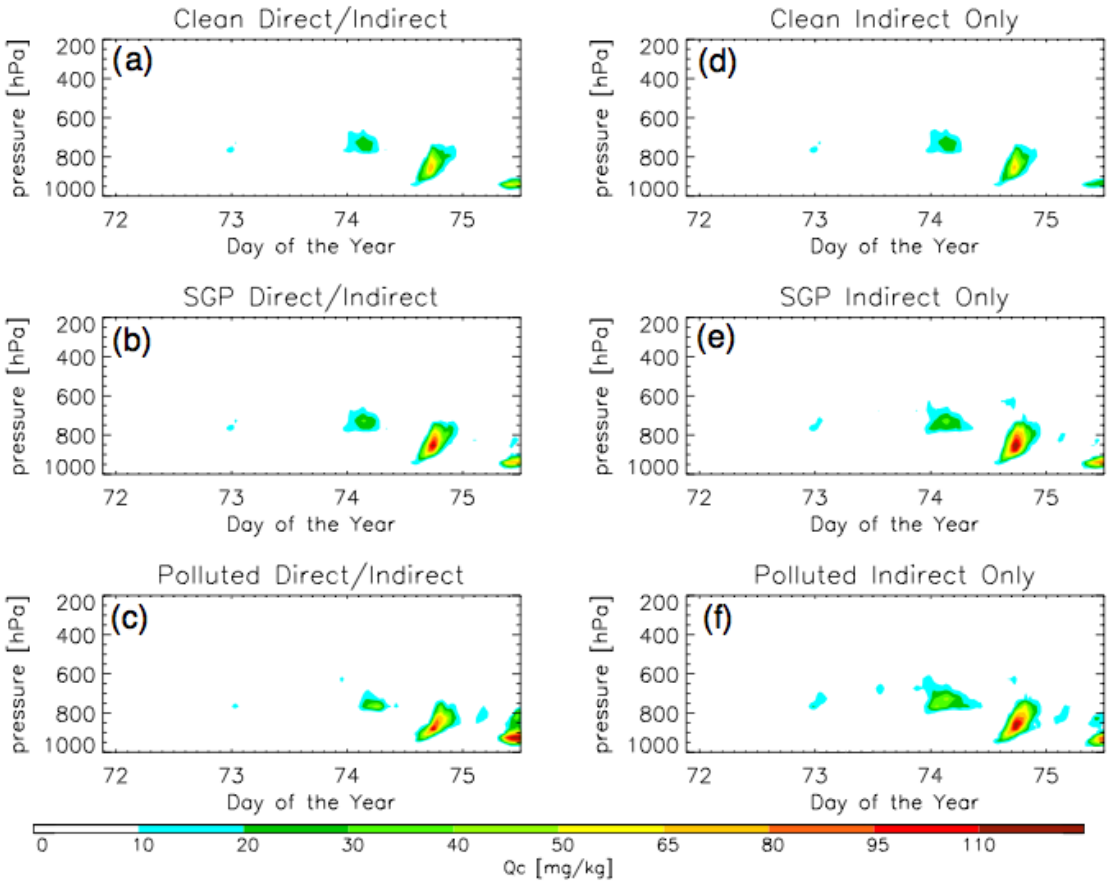

Figure 28. Domain average cloud water mixing ratio for Case D. The figures are for (a), (b), and (c) clean, SGP, and polluted DIE cases, respectively; (d), (e), and (f) clean, SGP, and polluted IEO cases, respectively.

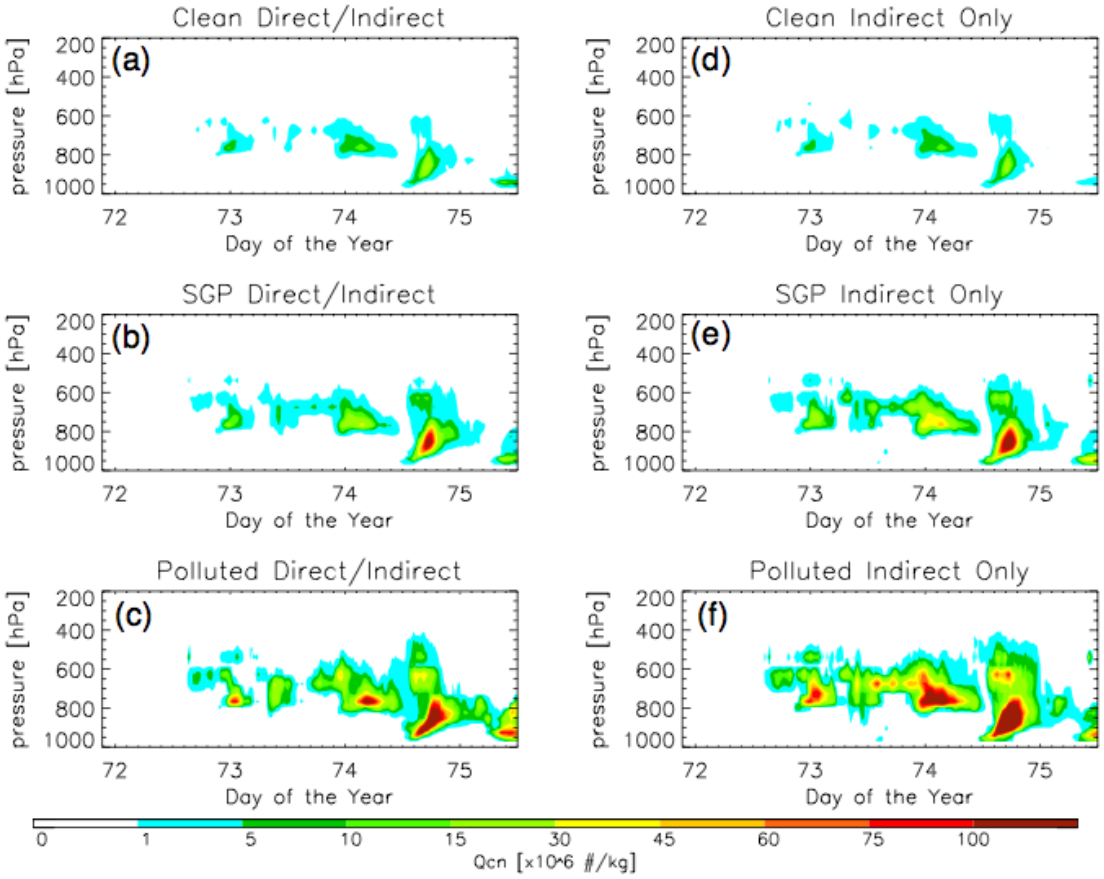

Figure 29. Domain average cloud droplet number concentration for Case D. The figures are for (a), (b), and (c) clean, SGP, and polluted DIE cases, respectively; (d), (e), and (f) clean, SGP, and polluted IEO cases, respectively.

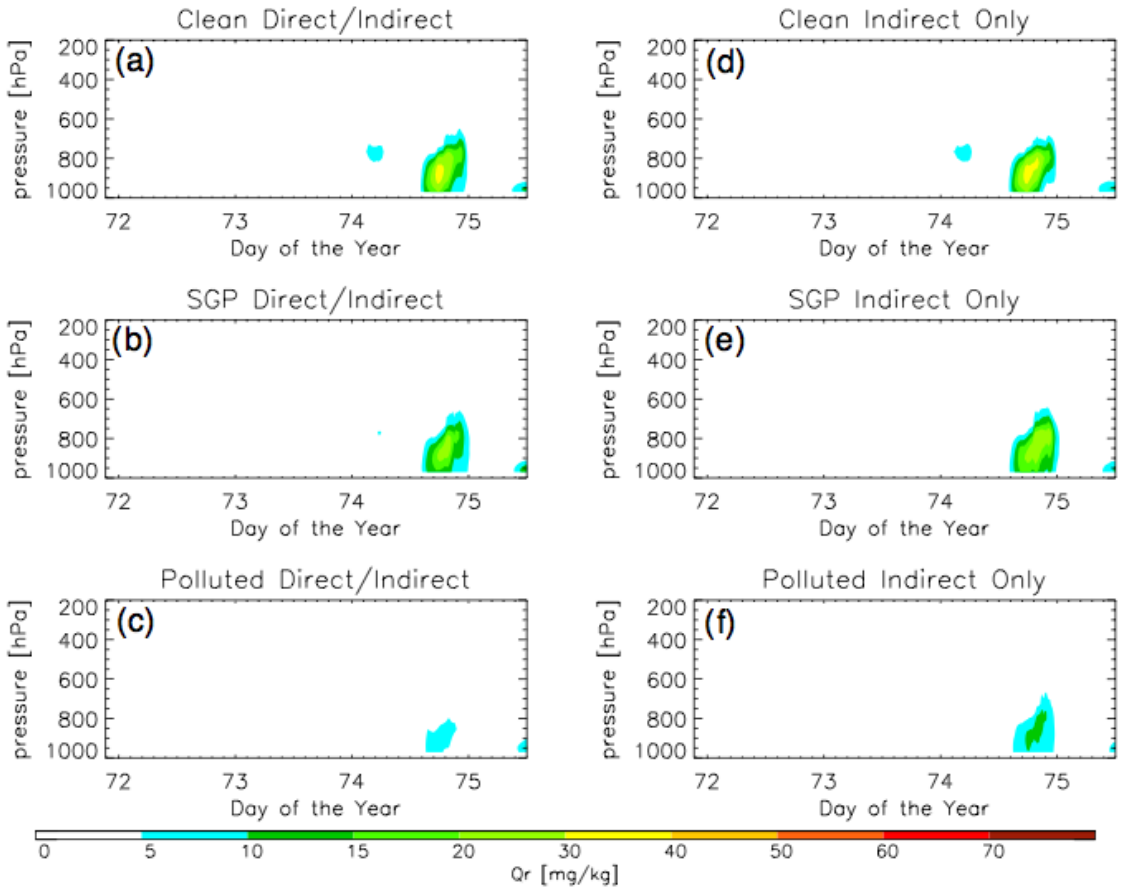

Figure 30. Domain average rain water mixing ratio for Case D. The figures are for (a), (b), and (c) clean, SGP, and polluted DIE cases, respectively; (d), (e), and (f) clean, SGP, and polluted IEO cases, respectively.

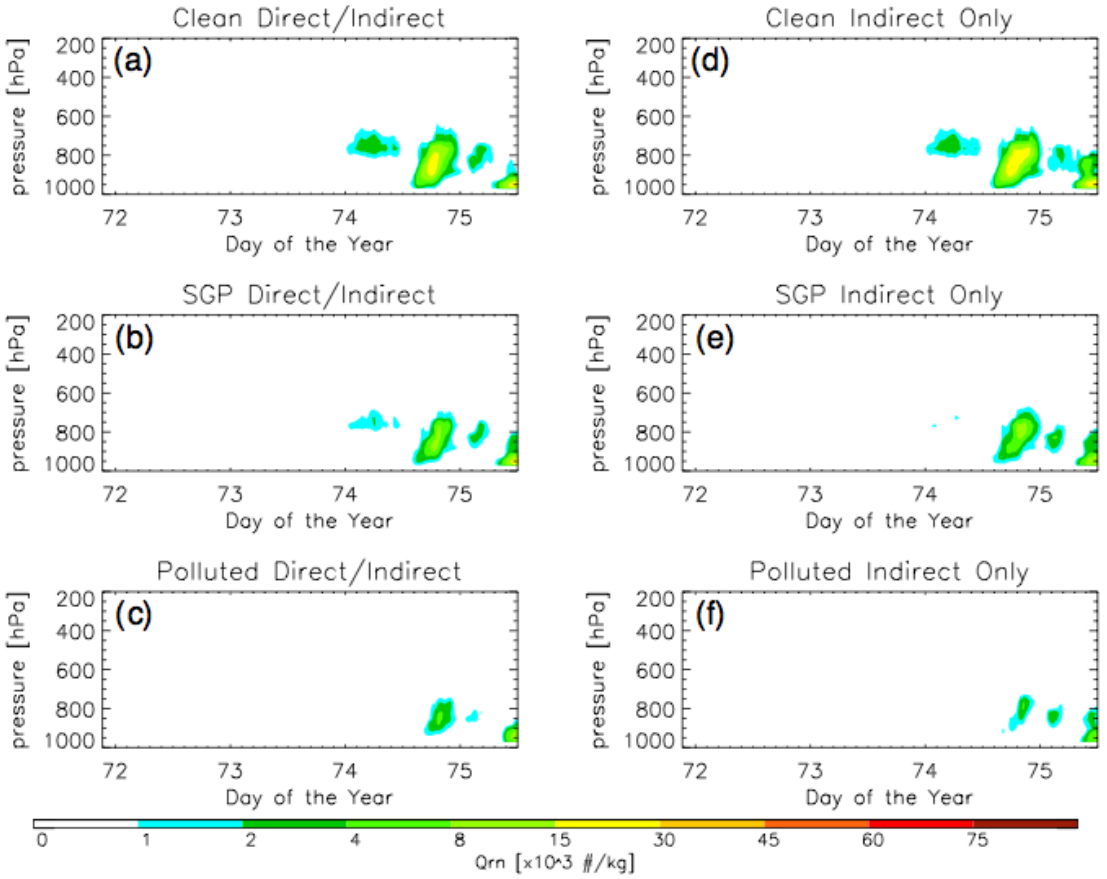

Figure 31. Domain average raindrop number concentration for Case D. The figures are for (a), (b), and (c) clean, SGP, and polluted DIE cases, respectively; (d), (e), and (f) clean, SGP, and polluted IEO cases, respectively.

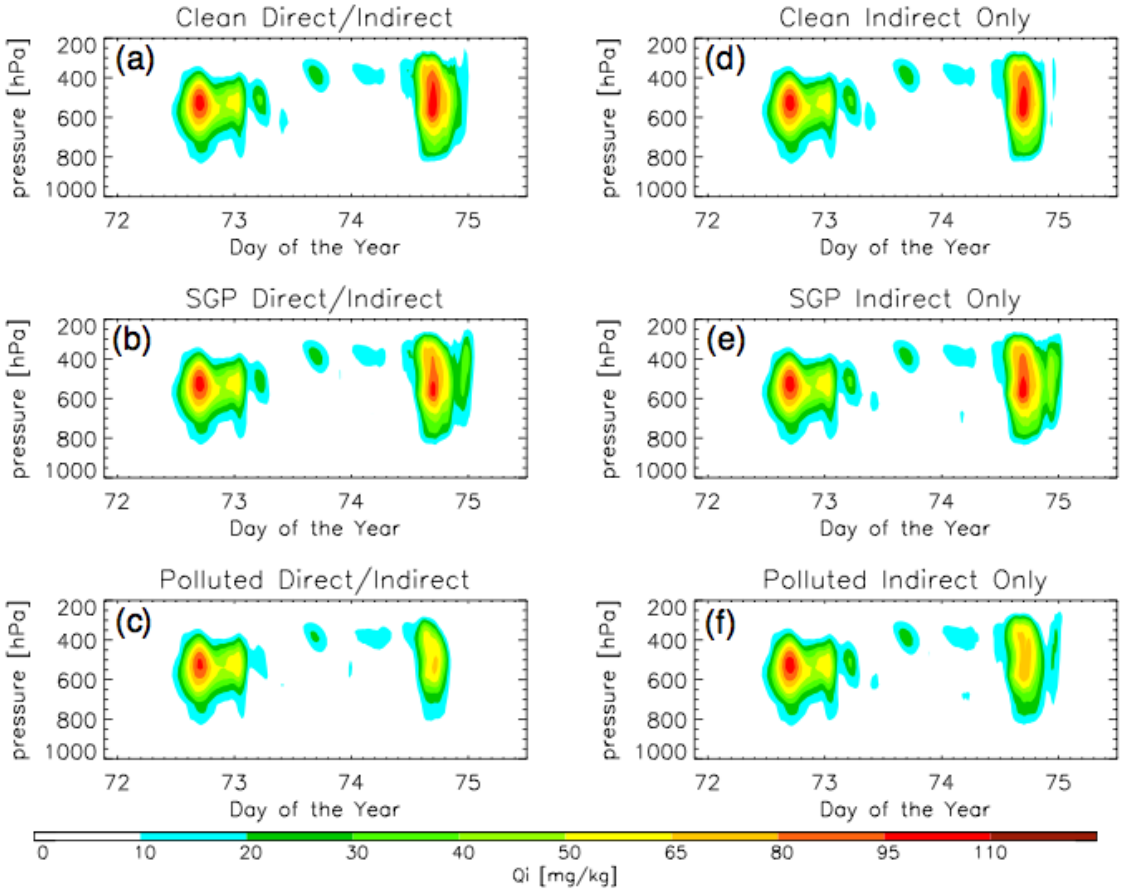

Figure 32. Domain average ice water mixing ratio for Case D. The figures are for (a), (b), and (c) clean, SGP, and polluted DIE cases, respectively; (d), (e), and (f) clean, SGP, and polluted IEO cases, respectively.

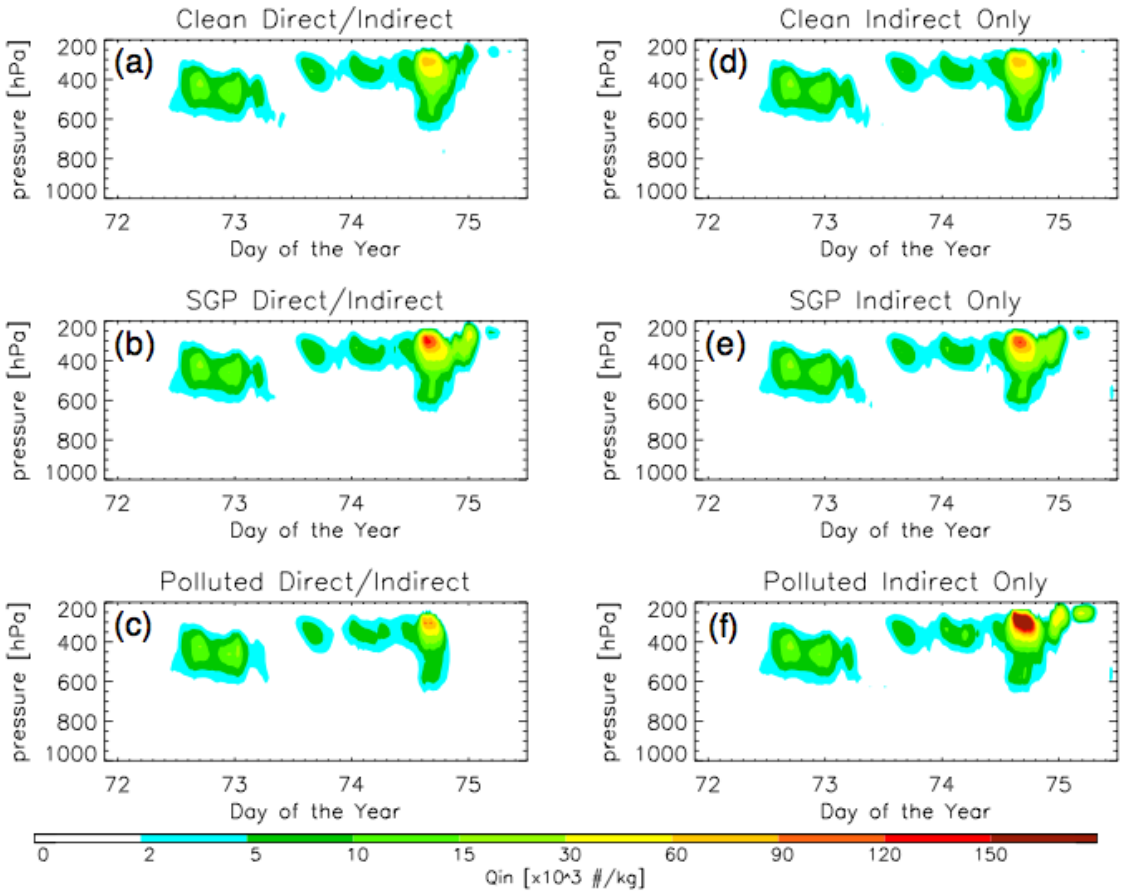

Figure 33. Domain average ice particle number concentration for Case D. The figures are for (a), (b), and (c) clean, SGP, and polluted DIE cases, respectively; (d), (e), and (f) clean, SGP, and polluted IEO cases, respectively.

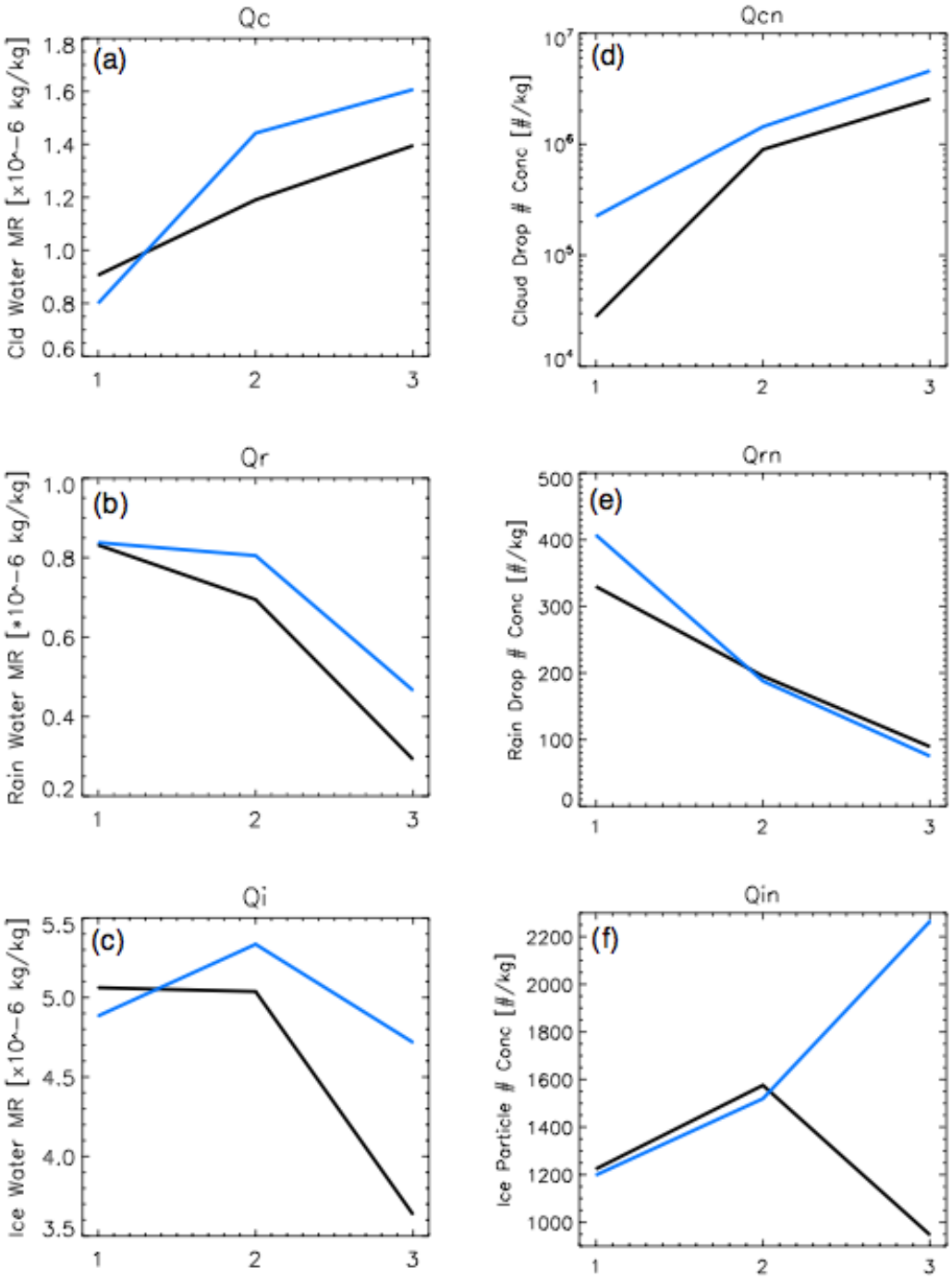

Figure 34. Average mixing ratio over the entire time period for Case D with 95% confidence intervals for cloud (a), rain (b), and ice (c) water. Average number concentration over the entire time period for Case D with 95% confidence intervals for cloud (d), rain (e), and ice (f) drops. The black lines are the DIE cases; the blue lines are the IEO cases. With 1, 2, and 3 coinciding with clean, SGP, and polluted aerosol profiles.

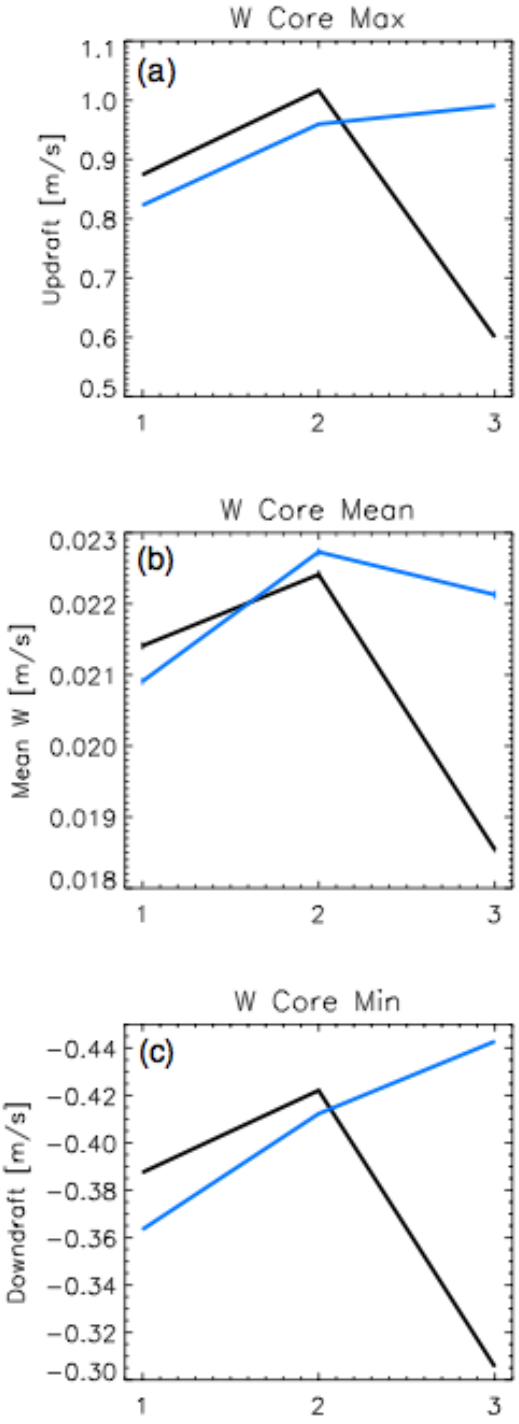

Figure 35. Average vertical velocity in cloudy regions over the entire time period for Case D with 95% confidence intervals for the strongest updraft (a), average velocity (b), and strongest downdraft (c). The black lines are the DIE cases; the blue lines are the IEO cases. With 1, 2, and 3 coinciding with clean, SGP, and polluted aerosol profiles.

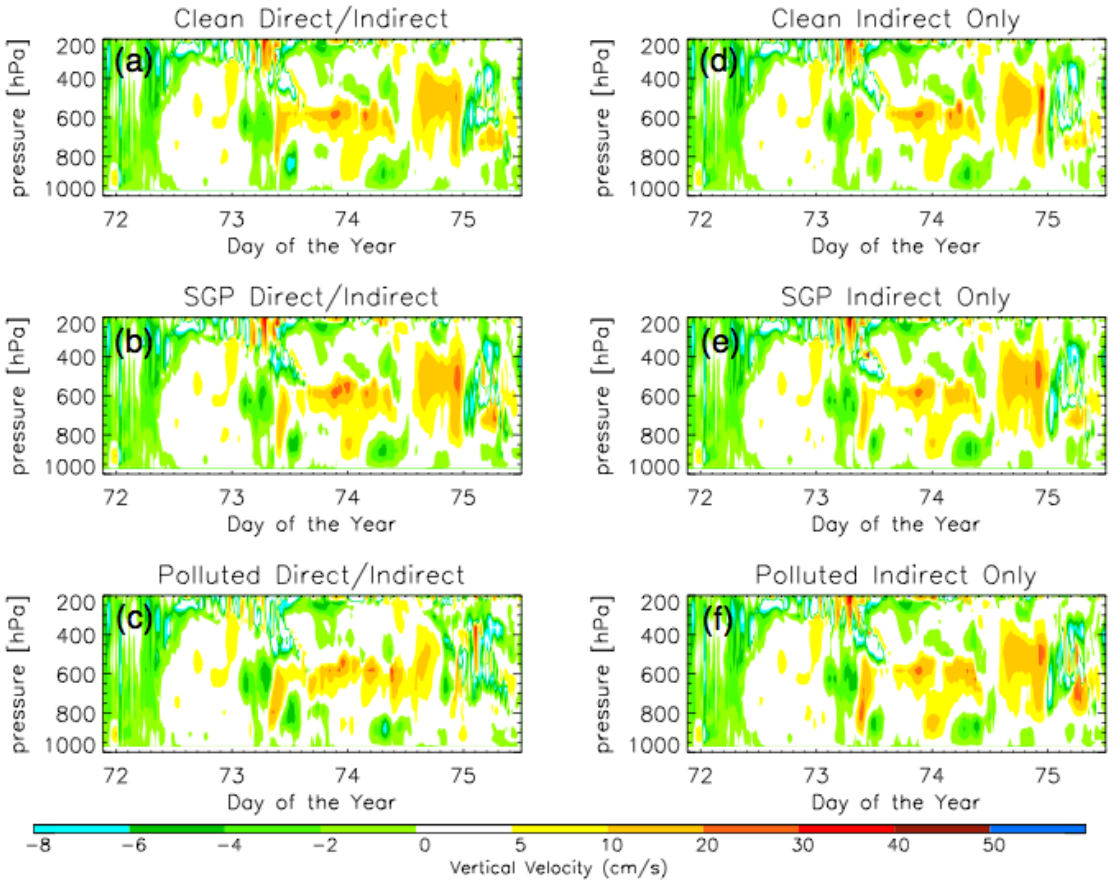

Figure 36. Average vertical velocity in cloudy regions for Case D. The figures are for (a), (b), and (c) clean, SGP, and polluted DIE cases, respectively; (d), (e), and (f) clean, SGP, and polluted IEO cases, respectively.

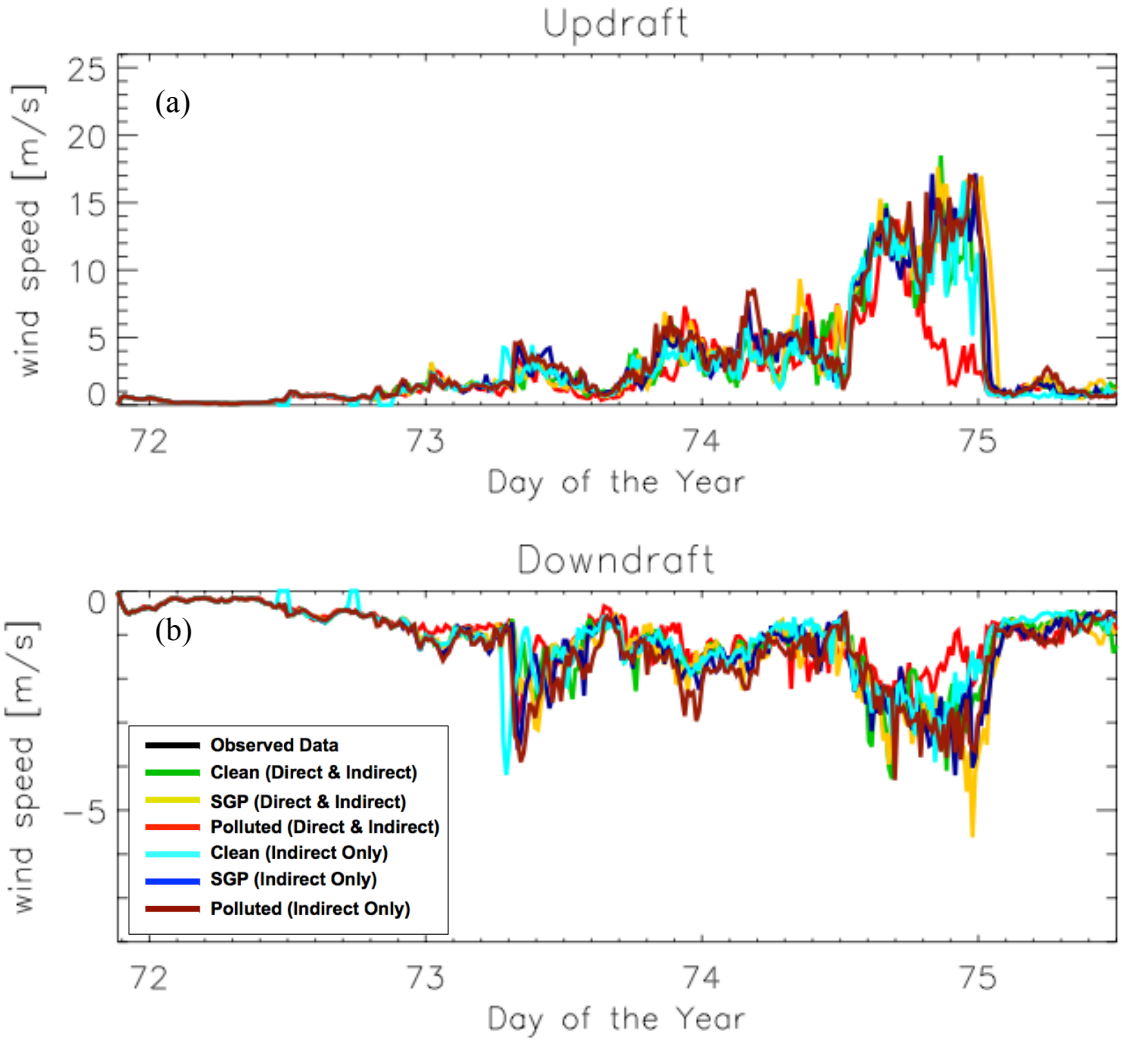

Figure 37. Time evolution of the maximum updrafts (a) and downdrafts (b) in the cloudy regions for Case D.

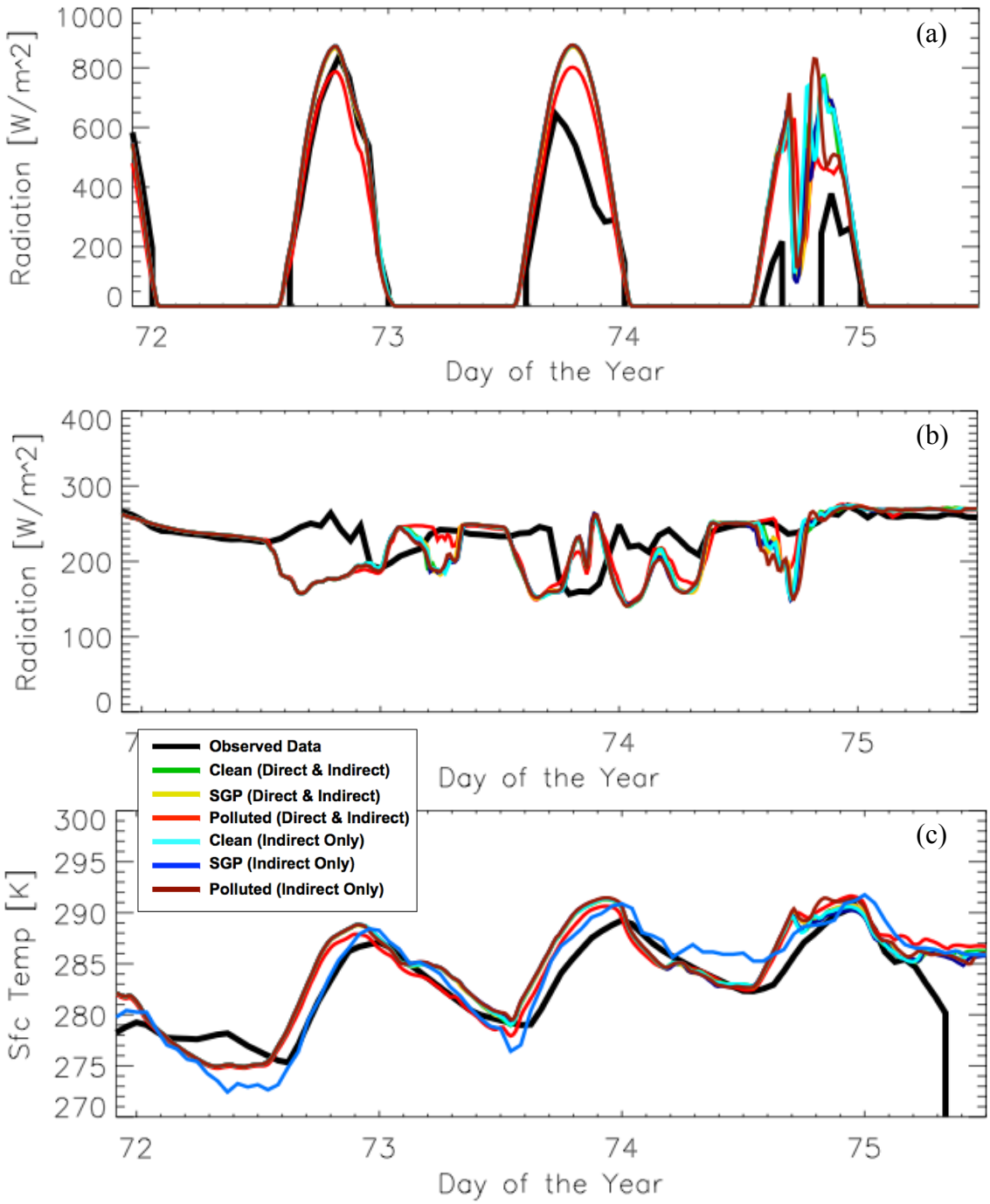

Figure 38. Averaged values of surface shortwave radiative fluxes (a), outgoing longwave radiative fluxes (b), and surface temperatures (c) for Case D.

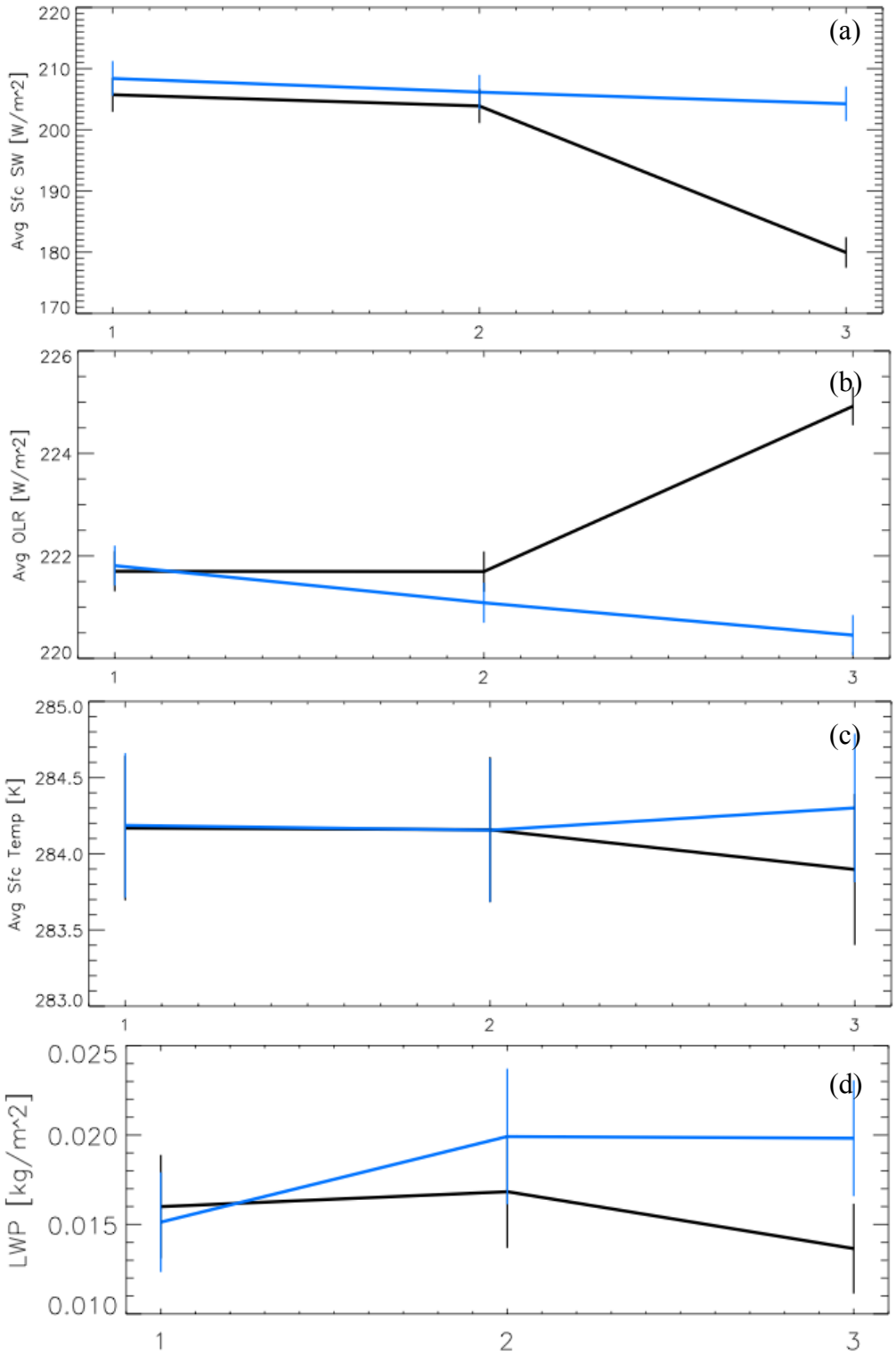

Figure 39. Time averaged values with 95% confidence intervals for Case D for surface shortwave radiative fluxes (a), outgoing longwave radiative fluxes (b), surface

temperatures (c), and domain averaged LWP (d). The black lines are the DIE cases; the blue lines are the IEO cases. With 1, 2, and 3 coinciding with clean, SGP, and polluted aerosol profiles.

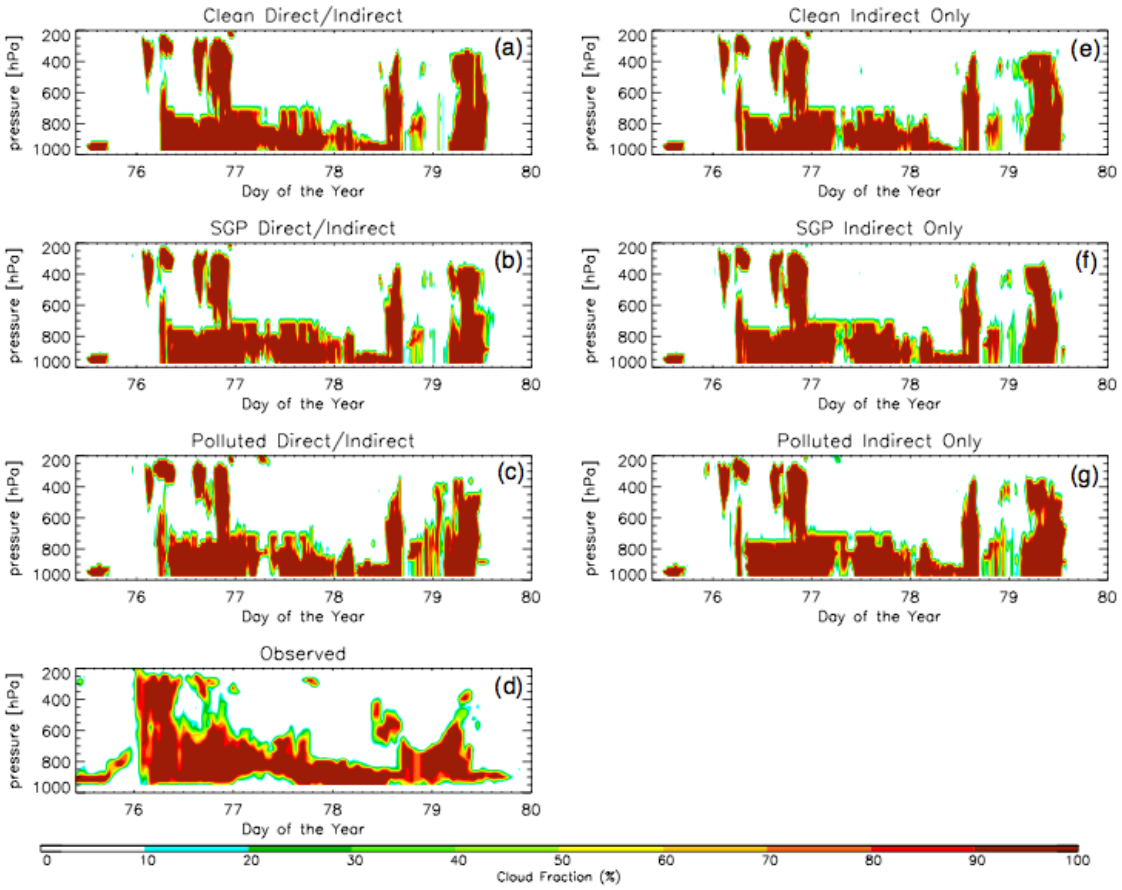

Figure 40. Cloud fraction values for Case E. The figures are for (a), (b), and (c) clean, SGP, and polluted DIE cases, respectively; (d) observations; (e), (f), and (g) clean, SGP, and polluted IEO cases, respectively.

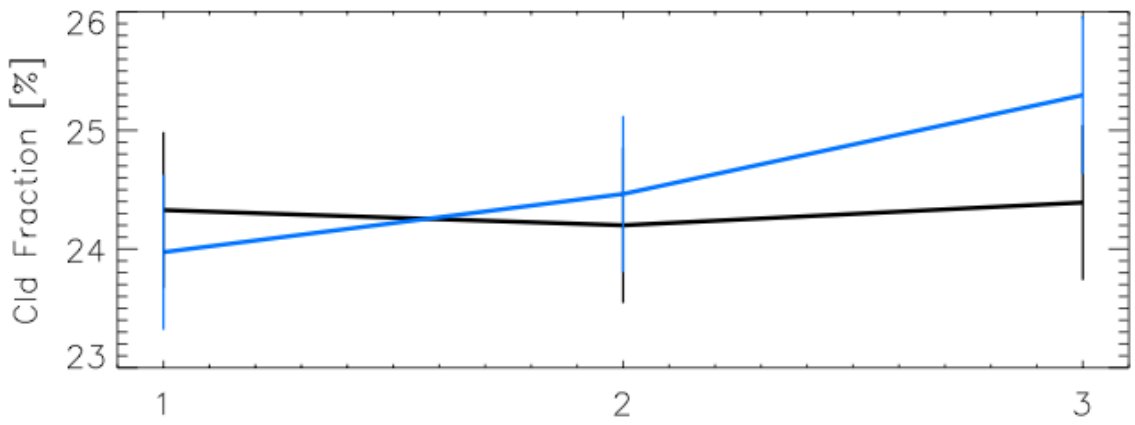

Figure 41. Average cloud fraction over the entire time period for Case E with 95% confidence intervals. The black line is the DIE cases; the blue line is the IEO cases. With 1, 2, and 3 coinciding with clean, SGP, and polluted aerosol profiles.

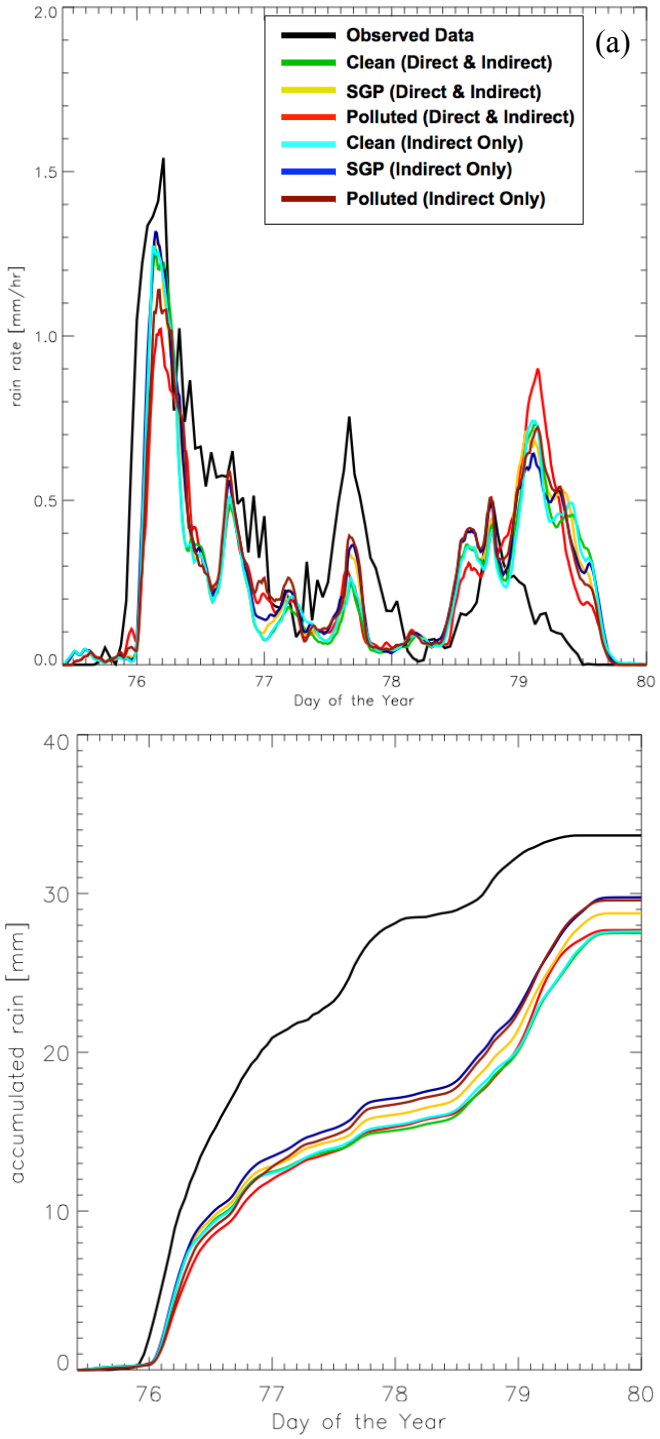

Figure 42. Domain average rainfall rates (a) and domain average accumulated rainfall (b) for Case E.

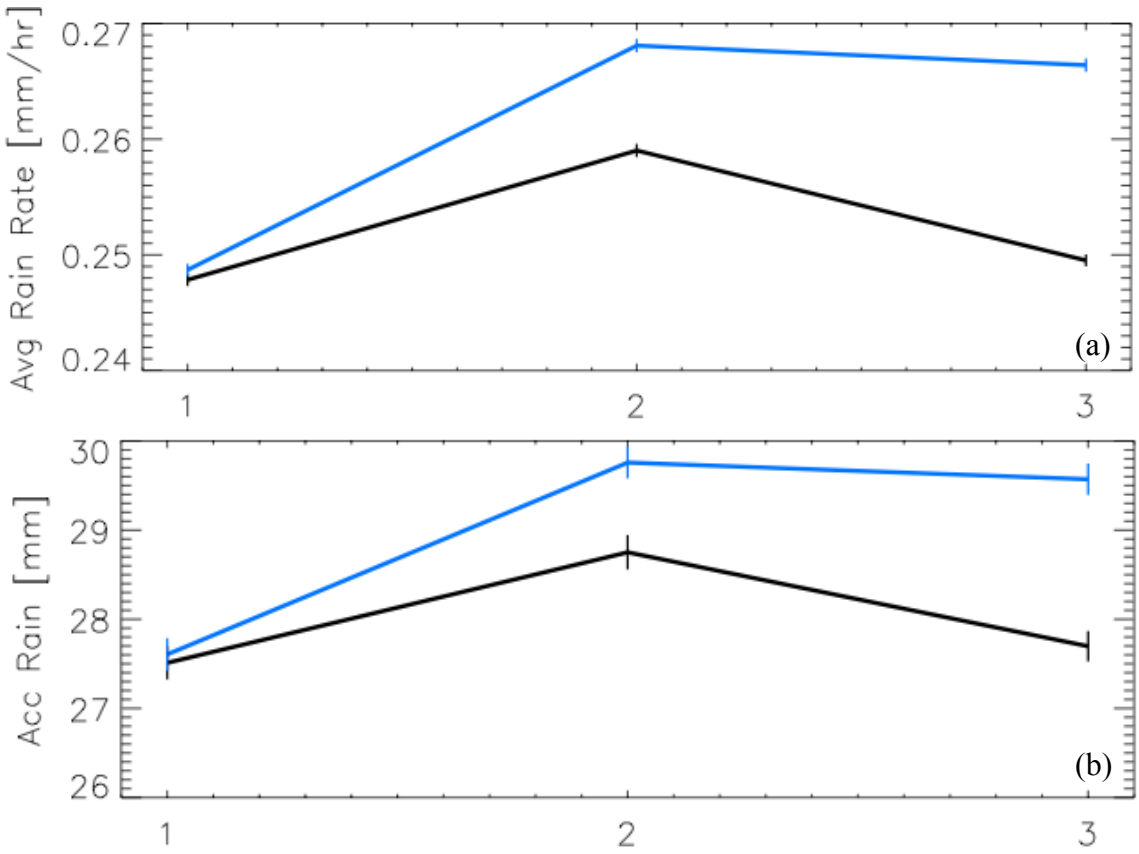

Figure 43. Average rainfall (a) and average accumulated rainfall (b) over the entire time period for Case E with 95% confidence intervals. The black lines are the DIE cases; the blue lines are the IEO cases. With 1, 2, and 3 coinciding with clean, SGP, and polluted aerosol profiles.

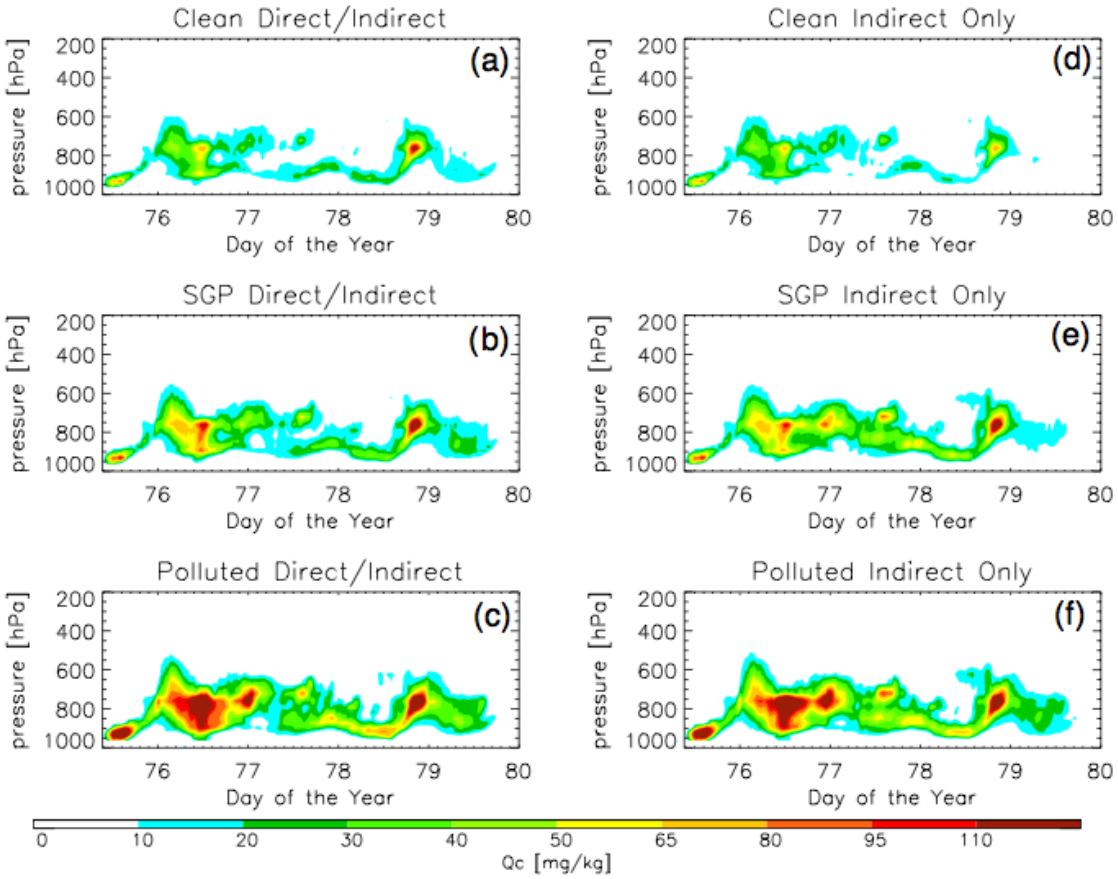

Figure 44. Domain average cloud water mixing ratio for Case E. The figures are for (a), (b), and (c) clean, SGP, and polluted DIE cases, respectively; (d), (e), and (f) clean, SGP, and polluted IEO cases, respectively.

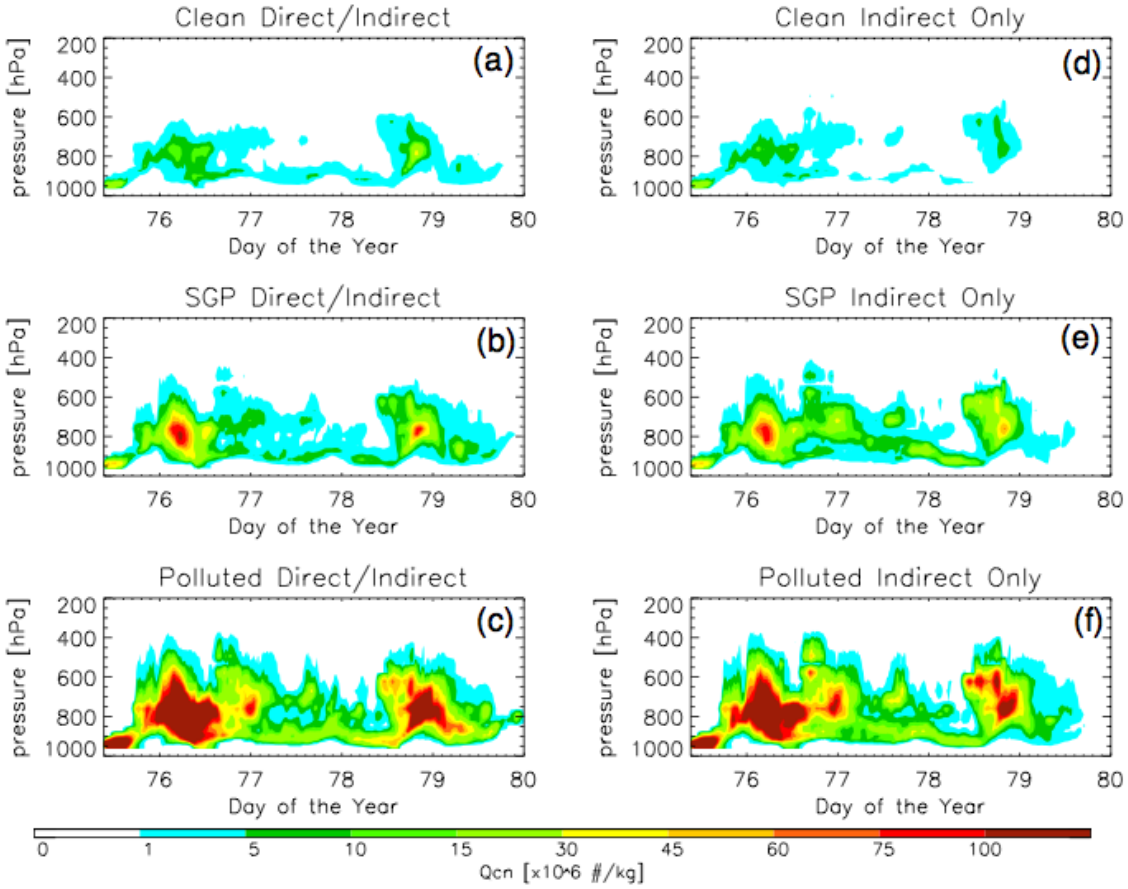

Figure 45. Domain average cloud droplet number concentration for Case E. The figures are for (a), (b), and (c) clean, SGP, and polluted DIE cases, respectively; (d), (e), and (f) clean, SGP, and polluted IEO cases, respectively.

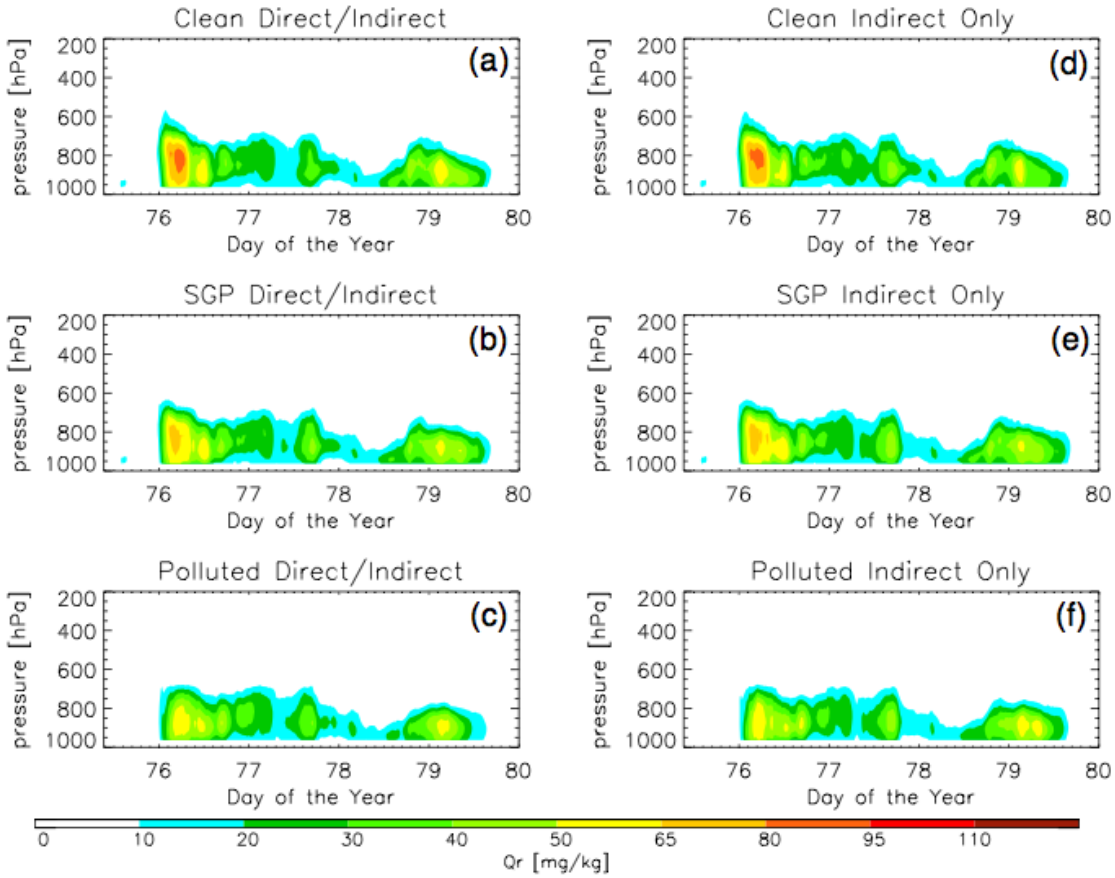

Figure 46. Domain average rain water mixing ratio for Case E. The figures are for (a), (b), and (c) clean, SGP, and polluted DIE cases, respectively; (d), (e), and (f) clean, SGP, and polluted IEO cases, respectively.

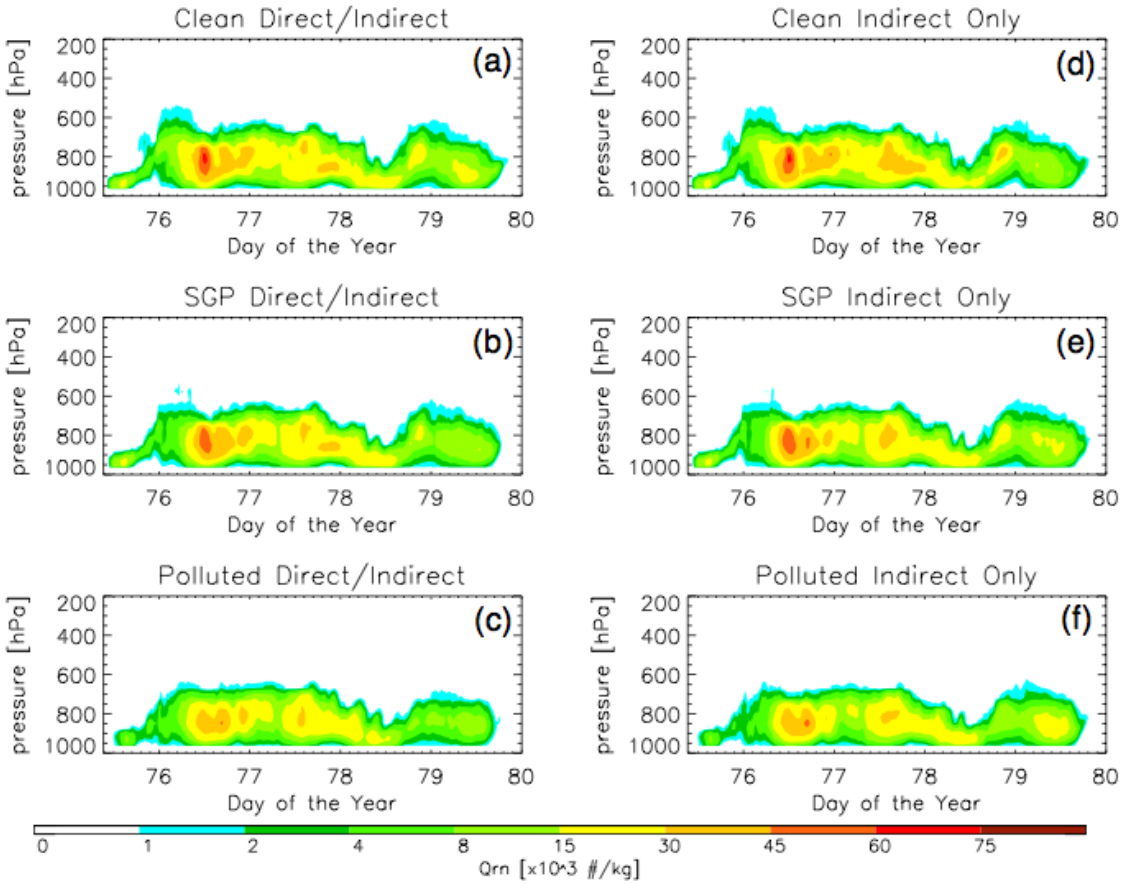

Figure 47. Domain average raindrop number concentration for Case E. The figures are for (a), (b), and (c) clean, SGP, and polluted DIE cases, respectively; (d), (e), and (f) clean, SGP, and polluted IEO cases, respectively.

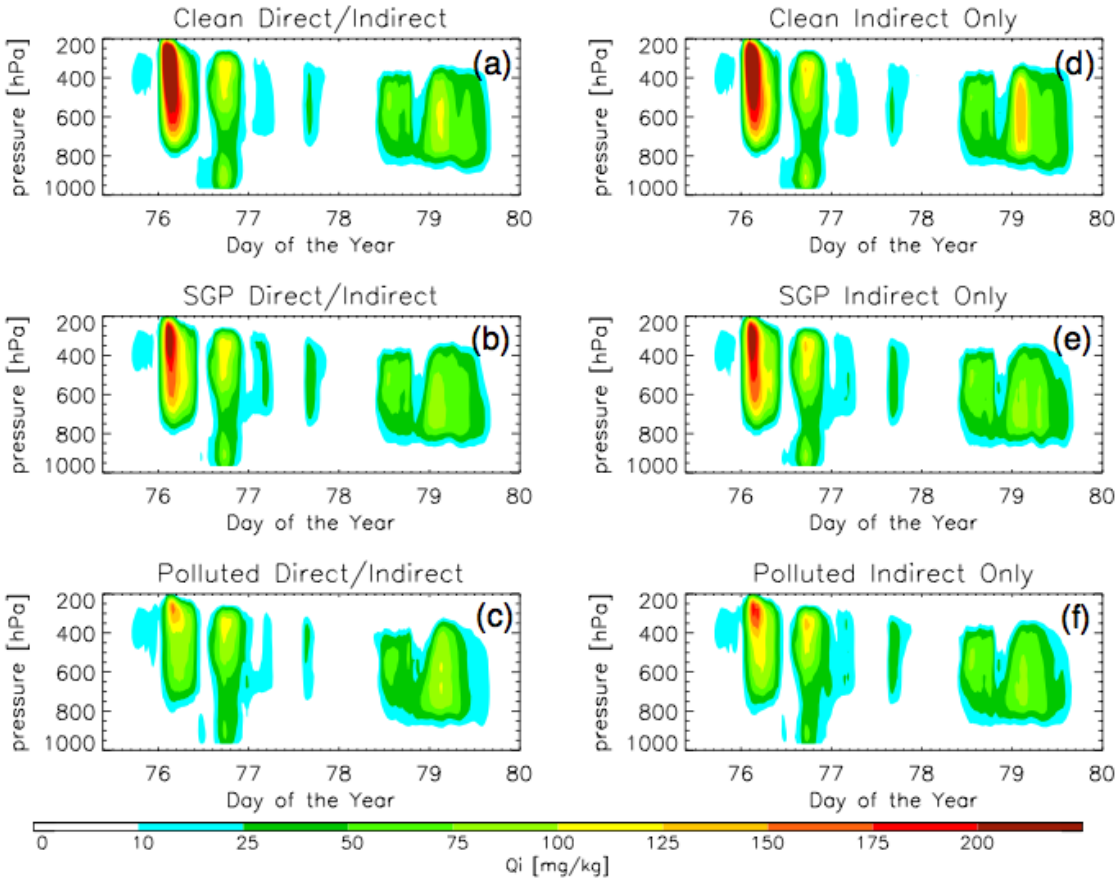

Figure 48. Domain average ice water mixing ratio for Case E. The figures are for (a), (b), and (c) clean, SGP, and polluted DIE cases, respectively; (d), (e), and (f) clean, SGP, and polluted IEO cases, respectively.

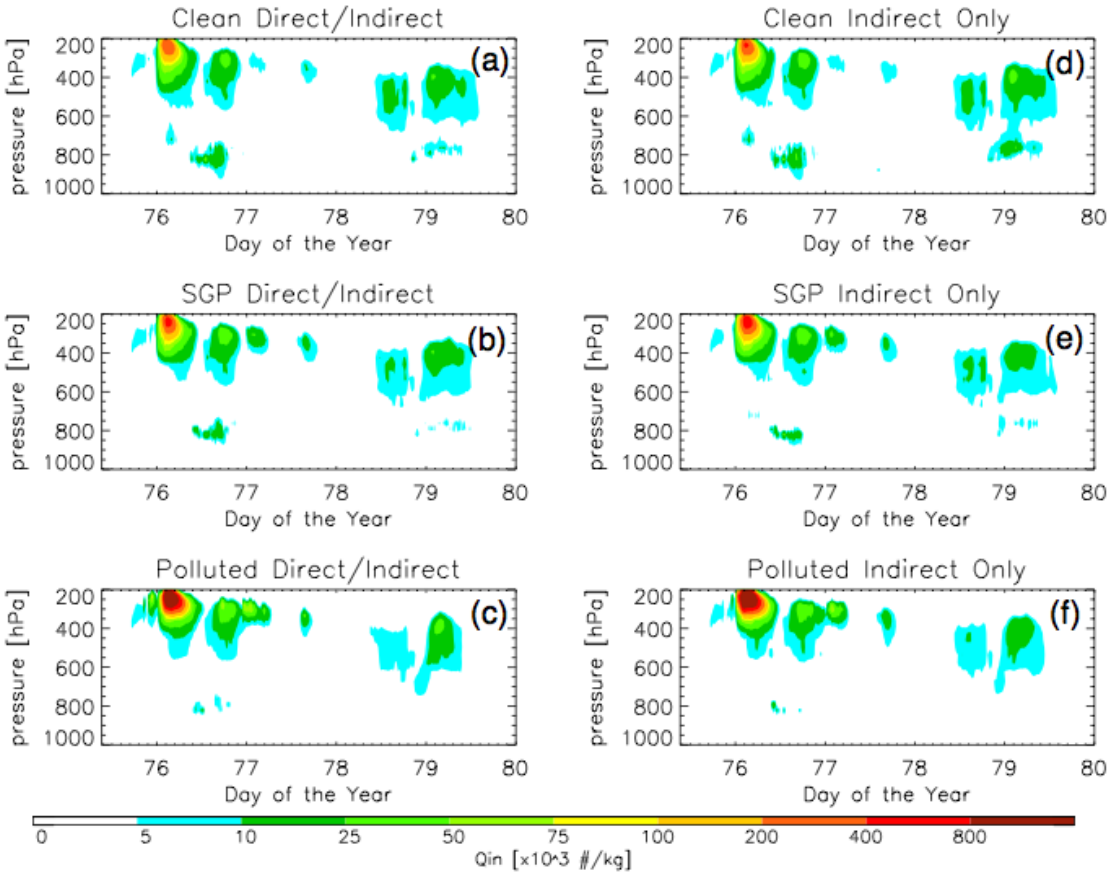

Figure 49. Domain average ice particle number concentration for Case E. The figures are for (a), (b), and (c) clean, SGP, and polluted DIE cases, respectively; (d), (e), and (f) clean, SGP, and polluted IEO cases, respectively.

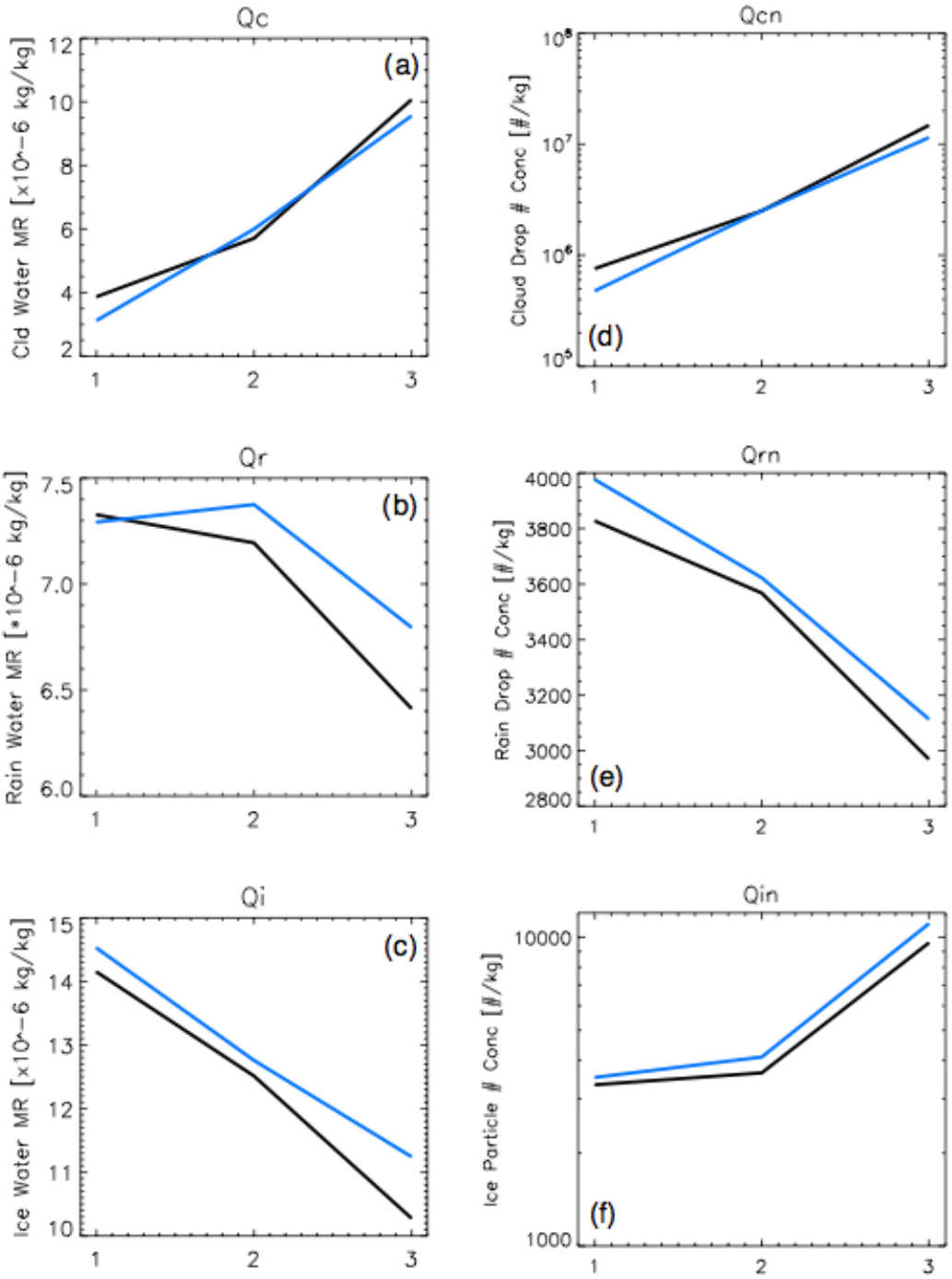

Figure 50. Average mixing ratio over the entire time period for Case E with 95% confidence intervals for cloud (a), rain (b), and ice (c) water. Average number concentration over the entire time period for Case E with 95% confidence intervals for cloud (d), rain (e), and ice (f) drops. The black lines are the DIE cases; the blue lines are the IEO cases. With 1, 2, and 3 coinciding with clean, SGP, and polluted aerosol profiles.

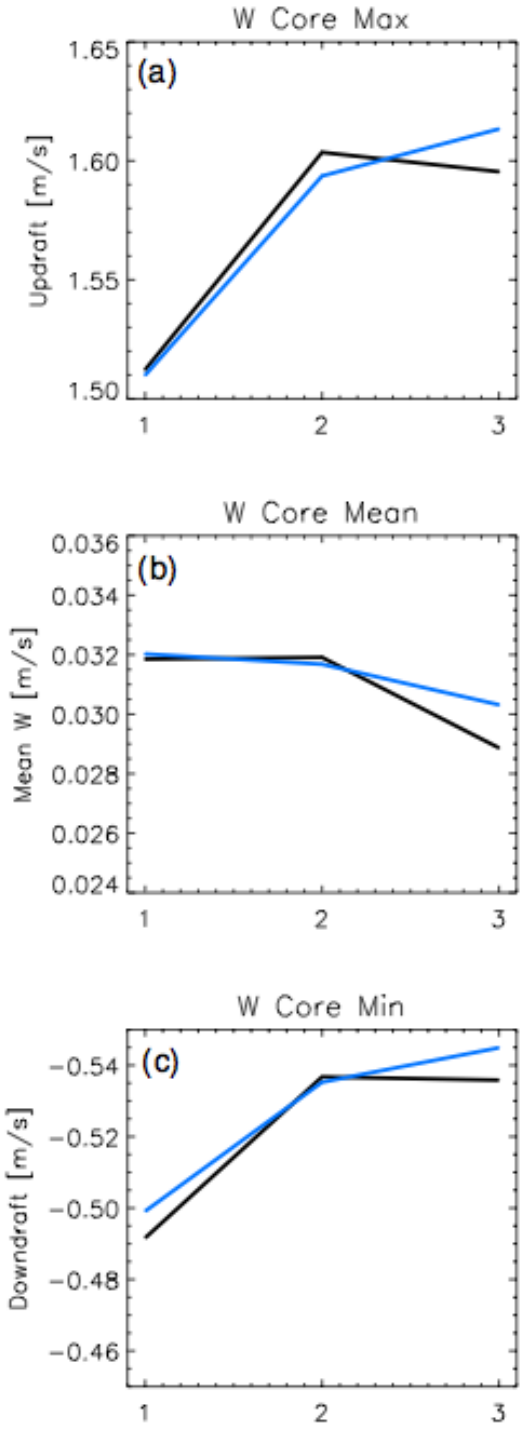

Figure 51. Average vertical velocity in cloudy regions over the entire time period for Case E with 95% confidence intervals for the strongest updraft (a), average velocity (b), and strongest downdraft (c). The black lines are the DIE cases; the blue lines are the IEO cases. With 1, 2, and 3 coinciding with clean, SGP, and polluted aerosol profiles.

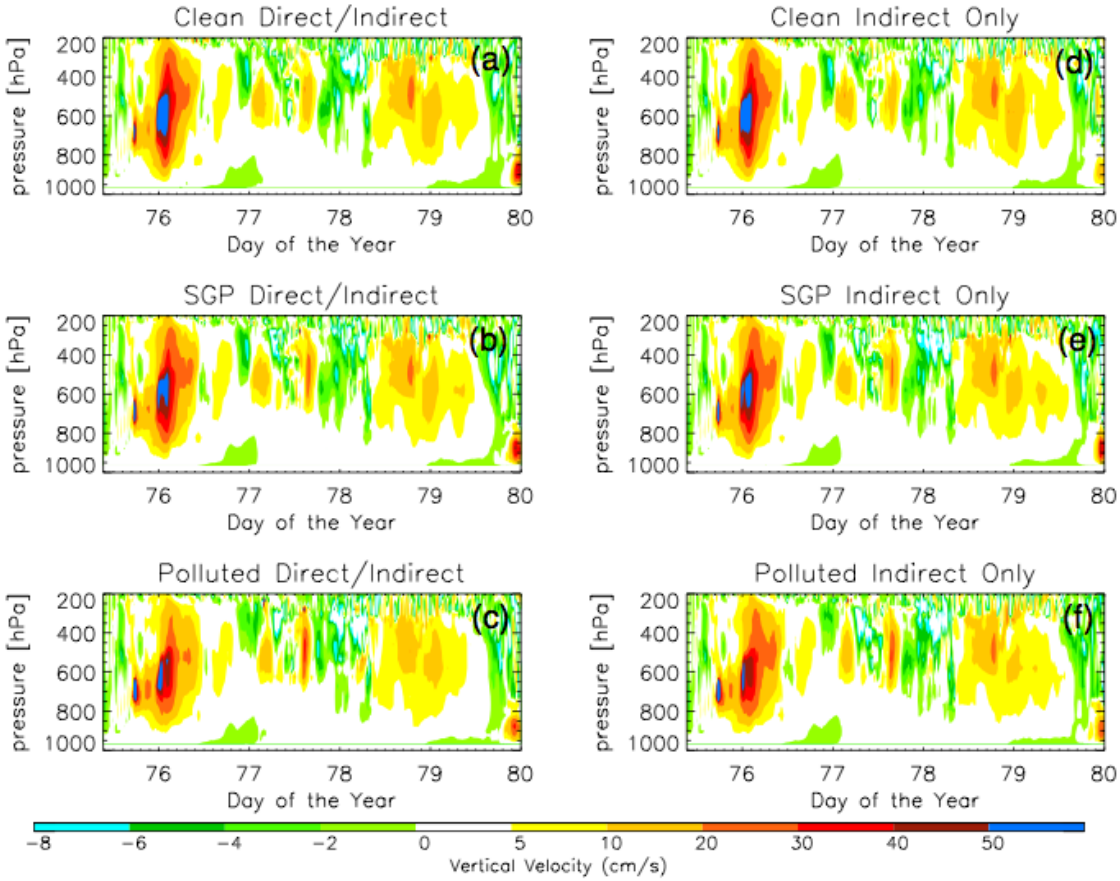

Figure 52. Average vertical velocity in cloudy regions for Case E. The figures are for (a), (b), and (c) clean, SGP, and polluted DIE cases, respectively; (d), (e), and (f) clean, SGP, and polluted IEO cases, respectively.

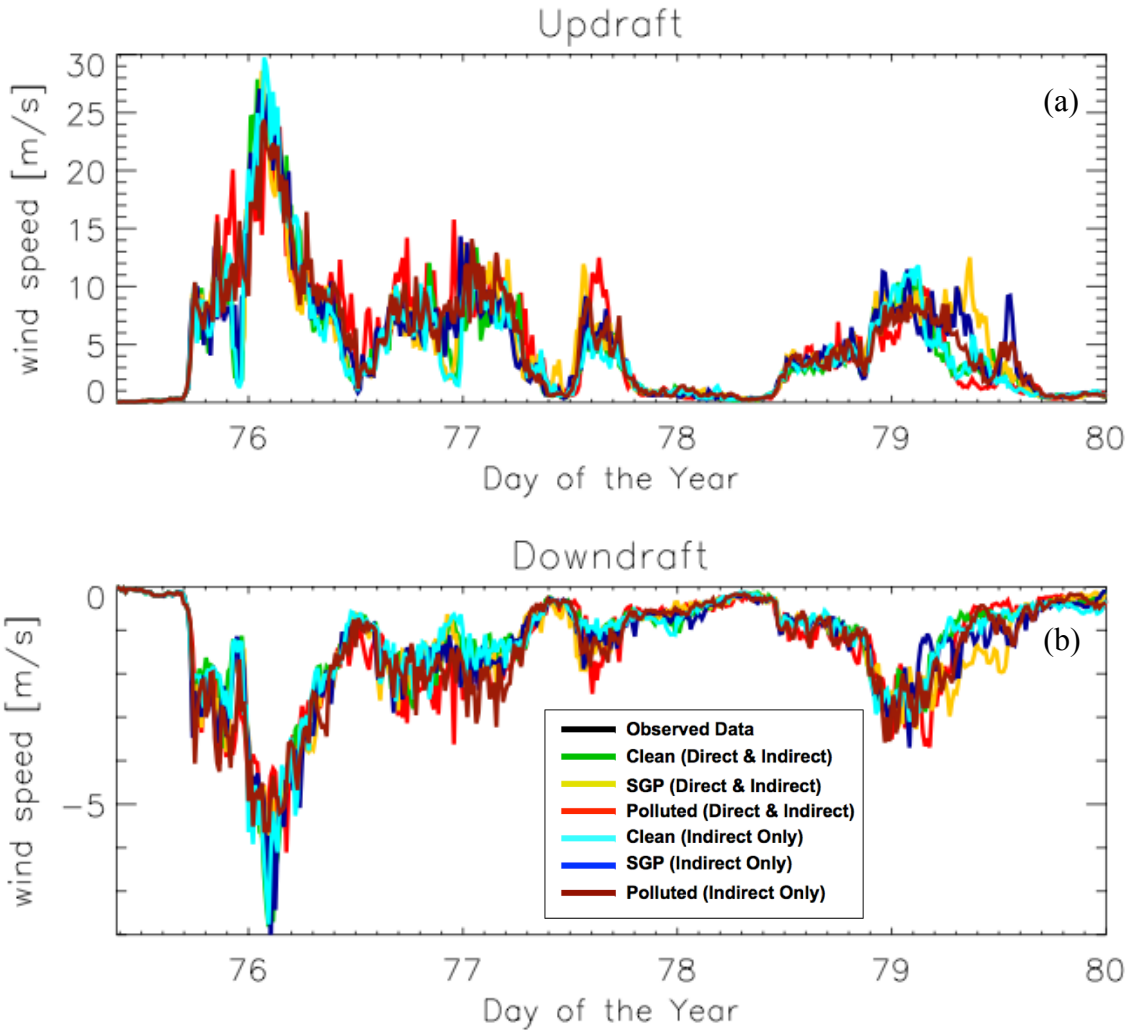

Figure 53. Time evolution of the maximum updrafts (a) and downdrafts (b) in the cloudy regions for Case E.

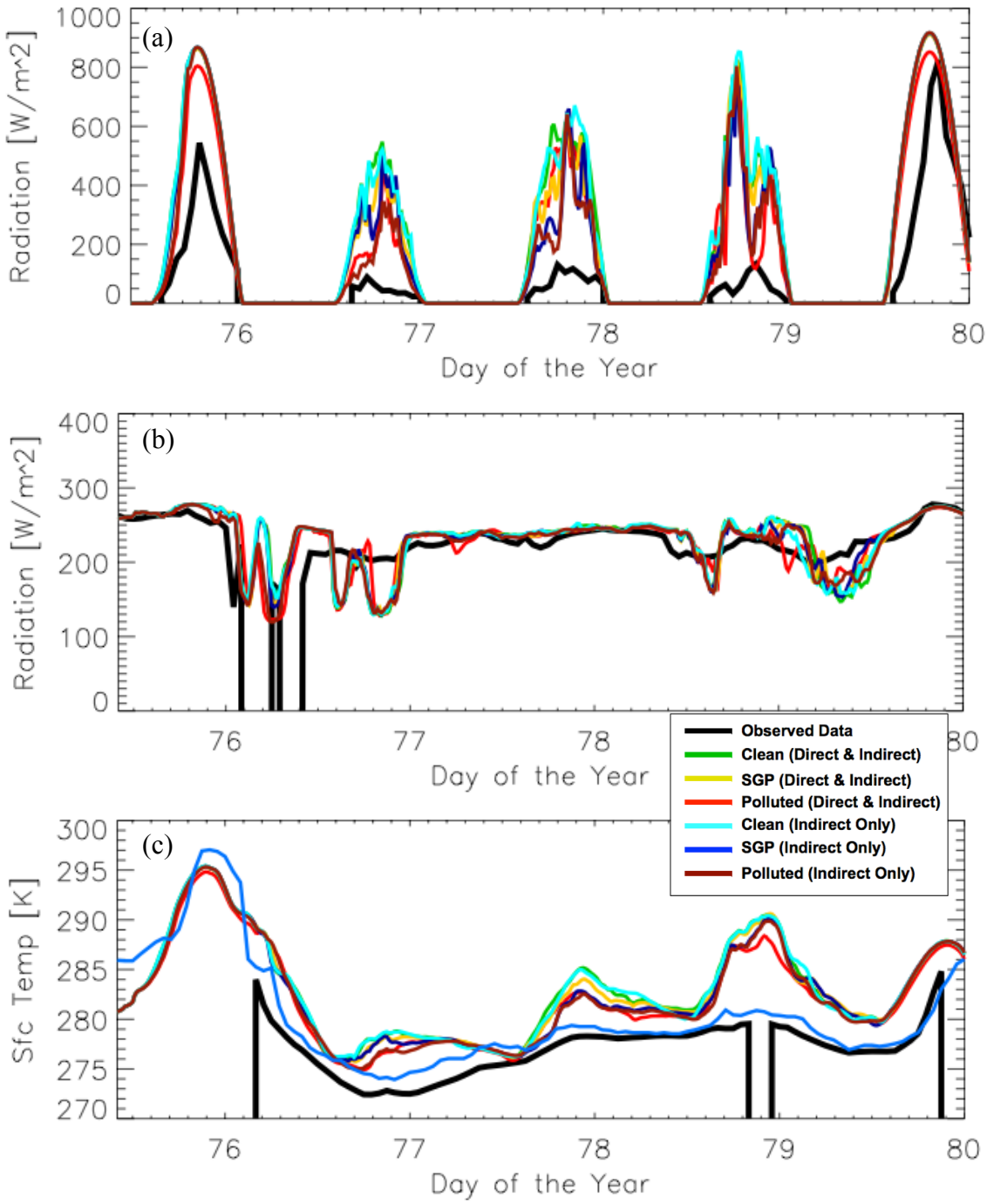

Figure 54. Averaged values of surface shortwave radiative fluxes (a), outgoing longwave radiative fluxes (b), and surface temperatures (c) for Case E.

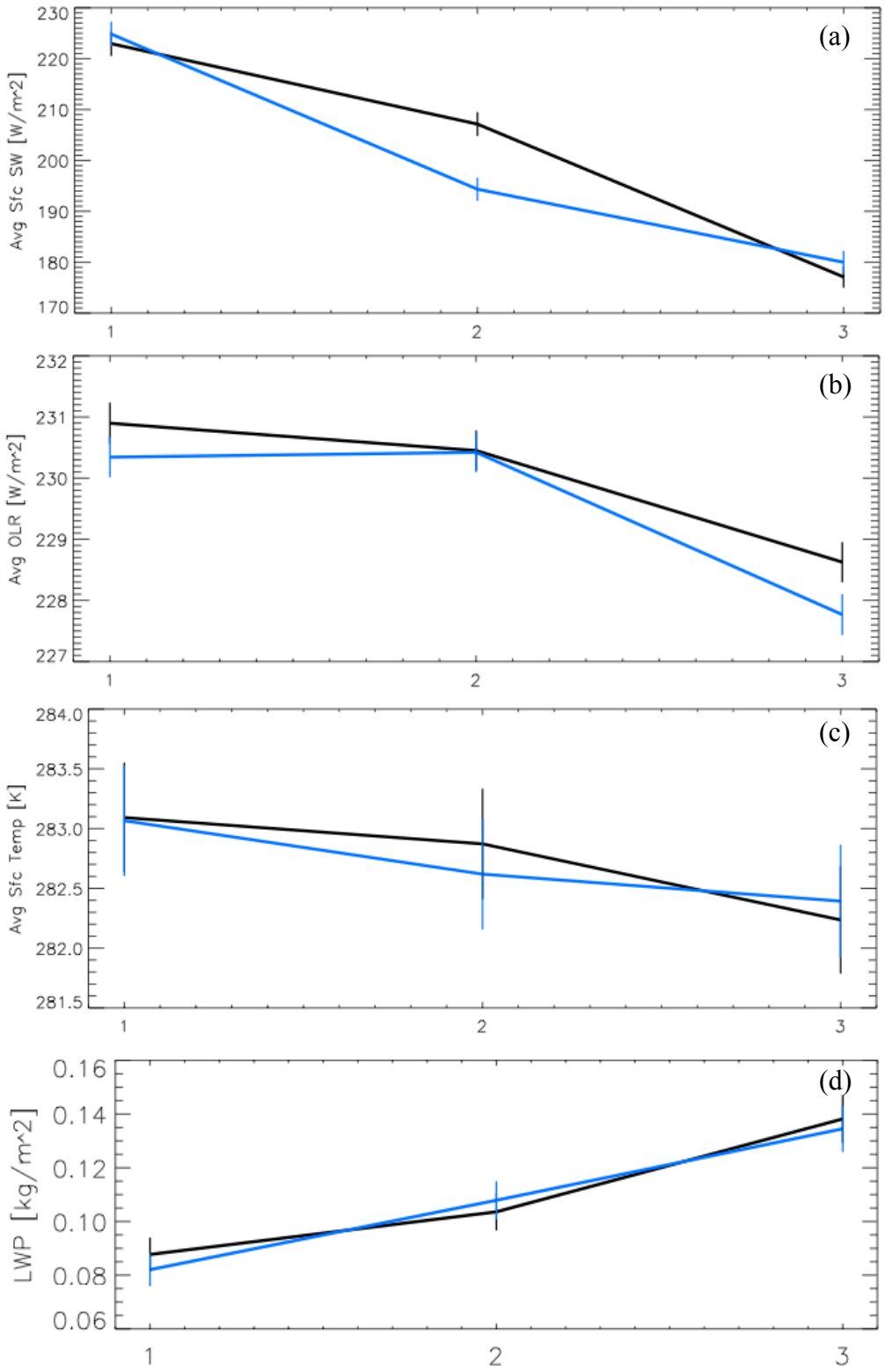

Figure 55. Time averaged values with 95% confidence intervals for Case E for surface

shortwave radiative fluxes (a), outgoing longwave radiative fluxes (b), surface temperatures (c), and domain averaged LWP (d). The black lines are the DIE cases; the blue lines are the IEO cases. With 1, 2, and 3 coinciding with clean, SGP, and polluted aerosol profiles.